Validation and Clinical Applications of the Four-Channel Point-of-Care Plasmonic Quantitative Polymerase Chain Reaction for Rapid Pathogen Detection

Joshua Hayes

Division of Experimental Medicine, Faculty of Medicine, McGill University, Montréal

Submitted April 2022

A thesis submitted to McGill University in partial fulfillment of the requirements of the degree of Master of Science

© Joshua Hayes, 2022

Abstract

Background: Current standard microbiological techniques are generally very time consuming, usually requiring 24 to 72 hours to establish a diagnosis. Consequentially, contemporary clinical practices implement broad spectrum antibiotic administration prior to pathogen detection, prompting the emergence of extremely dangerous antibiotic resistant bacteria. This thesis dedicates itself to the continued development and validation of a four-channel point-of-care (POC) plasmonic quantitative polymerase chain reaction (qPCR) machine. PCR is a molecular biology technique often used in the world of diagnostics to exponentially amplify low copy numbers of genetic material. It functions by transitioning between specified temperatures to achieve the desired steps of DNA amplification. Throughout the SARS-CoV-2 pandemic, PCR gained further relevancy as a diagnostic technique after having received emergency use authorization. The outstanding issues with traditional PCR devices are that they are time consuming and mainly kept in centralized laboratories, and as a result the wait time to receive results were long and testing was initially limited to those who presented themselves with symptoms. As a result, many infectious asymptomatic patients went undiagnosed or did not seek testing and therefore unknowingly contributed to the rapid rate of transmission.

The POC plasmonic PCR machine developed in our laboratory aims at tackling these issues. This device can achieve 30 cycles of PCR in under 10 minutes. Gold nanorods (GNRs) are used as nano heaters to cycle between desired temperatures and heat from within the sample. The GNRs are excited by VCSEL lasers and convert light to thermal energy with roughly 99% efficiency – allowing for instantaneous heating and cooling response times. Additionally, real

time quantitative DNA amplification monitoring is imbedded within the machine to provide valuable clinical and research information, as well as a near immediate test to result turnover. The device is designed to be portable and kept outside of centralized locations.

Objectives: The objective of this research is to demonstrate the effectiveness of the four-channel POC plasmonic qPCR device in the very challenging setting of sexually transmitted infections (STIs), in which clinics test dozens of patients daily. *Chlamydia trachomatis* is one of the few pathogens currently approved for PCR diagnosis and therefore provides a reasonable template to assess the machine's performance. The first aim of the research conducted is to develop an algorithm to analyze and interpret output amplicon signal to properly assess and differentiate between positive and negative data (i.e., primer dimerization). The second aim uses this generated analysis to describe the machine's limit of detection (LoD), limit of quantitation (LoQ), standard curve, efficiency, sensitivity, specificity, and ability to conduct clinical sample amplification.

Methodology: Firstly, an original python algorithm was designed to extract generated amplification data, graph multiple datasets simultaneously, and quickly return a threshold cycle (Ct) value, signal gain, goodness of curve fit, and PCR efficiency. Additionally, primers known to be prone to dimerization were analyzed by the same algorithm to understand the quantifiable characteristics that differentiate them from positive amplicon signal. Lastly, serial dilutions of *Chlamydia trachomatis* DNA were aliquoted in water and negative clinical urine specimens, and each dilution cycled through PCR four times. The lowest dilution demonstrating positive signal and the negative template control were repeated an additional 20 times to determine the aforementioned criteria.

Results: The generated algorithm uses a 5-parameter sigmoidal curve equation to accurately fit the output amplification data. Primer dimers of varying oligonucleotide sequences demonstrate fluorescent ceilings and slopes of the linear portion of their sigmoidal output half those of positive amplicon. Lastly, the LoD of the POC plasmonic PCR platform is shown to be $< 10^{1}$ starting DNA copies, efficiency levels surpass 85%, and the sensitivity and specificity values are both 100%.

Conclusion: The validation protocols used to assess this machine report very promising results for the detection of *C. trachomatis*, demonstrating the sensitivity and flexibility of this ultrarapid diagnostics device. The results aimed at highlighting the versatility of the POC plasmonic PCR machine and how it fares in the world of rapid diagnostics, as well as its potential in antimicrobial resistance mitigation.

Résumé

Contexte : Les techniques microbiologiques standard actuelles requièrent beaucoup de temps, un délai de 24 à 72 heures étant généralement nécessaire pour établir un diagnostic. Par conséquent, les pratiques cliniques actuelles privilégient l'administration d'antibiotiques à large spectre avant la détection d'agents pathogènes, ce qui suscite l'émergence de bactéries résistantes aux antibiotiques extrêmement dangereuses. Ce mémoire s'intéresse au développement et à la validation en cours d'un appareil de réaction en chaîne par polymérase quantitative plasmonique (qPCR) à quatre canaux au point d'intervention (PDI). La PCR est une technique de biologie moléculaire souvent utilisée en diagnostic pour amplifier de manière exponentielle un faible nombre de copies de matériel génétique. Elle fonctionne en effectuant la transition entre des températures spécifiées pour atteindre les étapes souhaitées d'amplification de l'ADN. Au cours de la pandémie de SRAS-CoV-2, la PCR a gagné en pertinence en tant que technique de diagnostic dès son approbation d'utilisation d'urgence. Toutefois, les dispositifs traditionnels de PCR prennent beaucoup de temps et sont conservés en grande majorité dans des laboratoires centralisés, ce qui a contribué à un long délai d'attente avant l'obtention des résultats et à la limitation initiale des tests à ceux et celles qui avaient des symptômes. Par conséquent, de nombreux patients infectieux asymptomatiques n'ont pas été diagnostiqués ou ne se sont pas fait tester, contribuant ainsi sans le savoir au taux de transmission rapide.

L'appareil de qPCR plasmonique PDI développé dans notre laboratoire vise à résoudre ces problèmes. Cet appareil peut réaliser 30 cycles de PCR en moins de 10 minutes. Les nanotiges d'or (GNR) sont utilisées comme nano-éléments chauffants pour alterner entre les

températures souhaitées et la chaleur provenant de l'intérieur de l'échantillon. Les GNR sont stimulés par des lasers VCSEL qui convertissent la lumière en énergie thermique avec une efficacité d'environ 99 %, ce qui permet des temps de réponse de chauffage et de refroidissement instantanés. De plus, le contrôle quantitatif en temps réel de l'amplification de l'ADN est intégré à l'appareil, ce qui fournit de précieuses informations cliniques et de recherche ainsi qu'un test presque immédiat pour la rotation des résultats. L'appareil est conçu de façon à être portable et à pouvoir être conservé hors des lieux centralisés.

Objectifs : Cette recherche a comme but de démontrer l'efficacité de l'appareil de qPCR plasmonique PDI dans le cadre particulièrement difficile des infections sexuellement transmissibles (ITS), et pour lesquelles des dizaines de patients sont testés quotidiennement dans des cliniques. La Chlamydia trachomatis est l'un des rares agents pathogènes actuellement approuvés pour le diagnostic par PCR, ce qui offre un modèle raisonnable pour évaluer les performances de l'appareil. Le premier objectif de la recherche consiste à développer un algorithme pour analyser et interpréter le signal de sortie de l'amplicon afin d'évaluer et de différencier correctement les données positives et négatives (c'est-à-dire la dimérisation des amorces). Le deuxième objectif vise à utiliser l'analyse générée pour déterminer la limite de détection (LoD) de l'appareil, la limite de quantification (LoQ), la courbe standard, l'efficacité, la sensibilité, la spécificité et la capacité à effectuer une amplification d'échantillon clinique. Méthodologie: D'abord, un algorithme Python a été concu pour extraire les données d'amplification générées, représenter graphiquement plusieurs ensembles de données simultanément et redonner rapidement une valeur de cycle de seuil (Ct), un gain de signaux, la qualité de l'ajustement de la courbe et l'efficacité de la PCR. Ensuite, les amorces connues pour être sujettes à la dimérisation ont été analysées avec le même algorithme afin de comprendre les

caractéristiques quantifiables qui les différencient du signal d'amplicon positif. Enfin, des dilutions en série d'ADN de la Chlamydia trachomatis ont été aliquotées dans de l'eau et des échantillons d'urine cliniques négatifs. Chaque dilution a subi quatre cycles de PCR. La dilution la plus faible montrant un signal positif et le modèle contrôle négatif ont été répétés 20 fois de plus afin de déterminer les critères susmentionnés.

Résultats: L'algorithme créé utilise une équation de courbe sigmoïde à 5 paramètres pour ajuster avec précision les données d'amplification de sortie. Les dimères d'amorces de différentes séquences d'oligonucléotides montrent des plafonds de la portion linéaire de leur signal sigmoïde, et des inclinaisons fluorescents, de la moitié de ceux de l'amplicon positif. Enfin, la limite de détection (LoD) de la plateforme qPCR plasmonique PDI est < 10¹ copies d'ADN de départ, les niveaux d'efficacité dépassent 85 % et les valeurs de sensibilité et de spécificité sont toutes deux de 100 %.

Conclusion: Les protocoles de validation utilisés pour évaluer cet appareil montrent des résultats très prometteurs en ce qui concerne la détection de la Chlamydia trachomatis, démontrant la sensibilité et la flexibilité de cet appareil de diagnostic ultra-rapide. Les résultats visaient à mettre en évidence la polyvalence de cet appareil et son fonctionnement dans le cadre des diagnostics rapides, ainsi que son potentiel d'atténuation de la résistance aux antimicrobiens.

Acknowledgments

I would firstly like to thank my supervisor, Dr. Miltiadis Paliouras, for his help, support, and guidance throughout my graduate studies. What you have done to oversee and ensure my success goes above and beyond what I could have expected from anybody. I am forever grateful for your help and for having given me the opportunity to be a part of this project. I would also like to thank Dr. Mark Trifiro, who constantly challenged me on an intellectual level and encouraged me to critically think about all aspects of my research. I truly appreciate all of your help and the late nights you spent helping me calibrate the machine! Additionally, I would like to thank Seung Lee, a wonderful friend I made along this journey. Our conversations were always intellectually stimulating, and you often engaged me in thought beyond the scope of my project. I have learned a tremendous amount from you, and I know you are going to go on to do great things. You are all incredibly kind and selfless people, and I could not have asked for a more supportive group throughout our two years together.

I would lastly like to thank my wonderful family for their devoted support throughout the entirety of my lengthy educational journey. Mom, Dad, Pam, and Rich, you have been supporters of my dreams since the moment I shared them with you, and I am so fortunate to have been blessed with four amazing parents. Erin, Lindsay, and Jilly, I love you three tremendously, and although this pandemic took me away from home for much more time than I would have liked, I know you are always rooting for me. I can't wait to bore you with the details of my thesis every time I come over!

Contribution of Authors

Joshua Hayes

- 1) Wrote and edited chapters 1 to 3 of this thesis, and realized contents within chapter 2
- 2) Designed and optimized plasmonic PCR amplification reactions
- 3) Designed biological reagents for quantitative analysis
- 4) Designed all experiments and research goals
- 5) Conducted all PCR reactions and gel electrophoresis assays
- 6) Conducted statistical quantitative analysis on generated results
- 7) Designed algorithm to analyze PCR amplification results

Miltiadis Paliouras

- 1) Supervision of the project
- 2) Assisted with experimental design
- 3) Editing/modifications of figures

Mark Trifiro

1) Assisted with experimental design

Nexless Healthcare

1) Manufactured and designed the point of care plasmonic qPCR machine

Table of Contents

Lis	ist of Figures	
Lis	ist of Tables	
Lis	ist of Abbreviations	
1.	Chapter 1	
	1.1 Fundamentals of Polymerase Chain Reaction	
	1.1.1 Biological Reagents	
	1.1.2 Polymerase Chain Reaction Mechanisms	
	1.1.3 Qualitative PCR	
	1.1.4 Quantitative PCR	
	1.2 DNA Amplification Techniques	22
	1.2.1 Isothermally Based Amplification	
	1.2.2 Thermocycle-Based Amplification	
	1.3 PCR Validation Protocols	
	1.3.1 Limit of Blank, Limit of Detection and Limit of Quantitation	
	1.3.3 Sensitivity and Specificity Testing	
	1.4 Plasmonic Nanoparticles	
	1.4.1 Plasmonic Particles Fundamentals	
	1.4.2 Photothermal Nanoparticles	51
	1.5 Photonic-Based PCR	54
	1.6 Research Objectives and Rationale	57
2.	Chapter 2	60
	2.1 Introduction	61
	2.2 Materials and Methods	
	2.3 Results and Discussion	
	2.3.1 SYTO-16 Optimization	
	2.3.2 Primer Design	
	2.3.3 Data Analysis Algorithm	
	2.3.5 Limit of Detection, Limit of Quantitation	
	2.3.6 PCR Efficiency	
	2.3.7 Sensitivity and Specificity	
	2.3.8 Clinical Sample Validation	

3. Chapter 3	
3.1 Diagnosis at the Point of Care	107
3.1.1 Defining Point of Care	107
3.1.2 Value of PCR as a Point of Care Tool	108
3.2 Point of Care Diagnostic Tests	109
3.3 Future of POC plasmonic qPCR	115
References	
Appendix I	

List of Figures

Figure 1.1: Three phases of one PCR cycle – denaturation, annealing, elongation	. 20
Figure 1.2: Schematic of the Peltier block in a thermocycler	. 24
Figure 1.3: Normalized Fluorescence vs. # PCR Cycles.	. 27
Figure 1.4: Fluorescence vs. Temperature graph demonstrating constant fluorescence measurements throughout PCR operating at 95°C, 60°C, 72°C for denaturation, annealing, and	
elongation, respectively.	. 28
Figure 1.5: Curve fitting raw fluorescence data with different fit models for comparative	
measures	
Figure 1.6: Illustrative diagram of the LAMP amplification process.	. 34
Figure 1.7: Basic graphic describing the RAM process, isolating the C-probe for simplicity	. 36
Figure 1.8: Graphical representation of the relationship between LoB, LoD, and LoQ	. 40
Figure 1.9: Standard curve (calibration curve) of Ct value vs. DNA copy number for qPCR	. 44
Figure 1.10: Cycle 'n' vs. starting DNA concentration 'qo' calibration curve	. 46
Figure 1.11: 2x2 table cross referencing the results from the gold standard reference test and the	ne
assay in question.	
Figure 1.12: Absorption, scattering, and extinction comparisons between gold nanoparticles of	f
different morphologies	. 53
Figure 1.13: The POC plasmonic qPCR machine.	. 58
Figure 2.1: Gel electrophoresis images showing PCR amplicon results of samples with varying final concentrations of SYTO-16 dye.	_
Figure 2.2: Thermocycling profile from one channel of the POC plasmonic qPCR machine	. 70
Figure 2.3: Hysteresis curves of fluorescence output vs. temperature across 5 PCR cycles	. 71
Figure 2.4: Hetero complementary primer dimerization scenarios for CTC-6 primers	. 74
Figure 2.5: Raw relative fluorescence vs. cycles data plot from the POC plasmonic qPCR	. 76
Figure 2.6: Normality assumption verification for fluorescence ceiling.	. 79
Figure 2.7: Boxplot of the relative fluorescence ceiling for positive samples and primer dimers	S .
	. 81
Figure 2.8: Normality assumption verification for the values of the slopes of the linear portion	of
the output sigmoid fluorescence curve.	. 84
Figure 2.9: Boxplot of the slopes of the linear portion of the output sigmoid fluorescence curve	
for positive samples and primer dimers.	. 85
Figure 2.10: Highest contributing hetero 3' complementarity binding sequences and the	
respective Gibb's free energy changes (ΔG) of primers (A) CTC-W, (B) CTC-1, (C) CTC-2, (
CTC-6, and (E , F) CTC-3	
Figure 2.11: Boxplot of the Ct values of 8 NTC samples for 4 separate primer sets	
Figure 2.12: 10-fold serial dilution of CTC DNA from 10,000 to < 10 starting DNA copies, an	
an NTC	
Figure 2.13: Gel electrophoresis image of the 4x repeats from the serial dilutions (NTC, 10e4	
10e0 initial DNA copies) in d2H2O, and 20x repeats of 10e1 and 10e0 dilutions	
Figure 2.14: Boxplots of ceiling fluorescence and Ct value	. 95

Figure 2.15: Standard curve of log10initial DNA concentration vs. Ct value generated on the	
POC plasmonic qPCR	96
Figure 2.16: Efficiency standard curve.	99
Figure 2.17: Relative fluorescence curves of 60 positive CTC DNA and 26 NTC samples in	
d2H2O _. 1	03
Figure 2.18: Relative fluorescence curves of 20 negative clinical urine samples spiked with 10-	
fold serial CTC DNA dilutions from 10e4 – 10e0 copies, 4 NTC samples, and their	
corresponding gel electrophoresis results1	04
Figure 2.19: Gel electrophoresis image of final urine concentration dilutions1	06
Figure 3.1: Graphic depicting fraction of clinical cases detected vs. LoD (genome copies/mL).	
	11
Figure 3.2: Antigen test decision matrix flowchart	13

List of Tables

Table 2.1: List of Reagents Used in POC Plasmonic qPCR Reaction	. 63
Table 2.2: List of Primers Used Throughout Experimentation	. 64
Table 2.3: Summary of LoD Results.	. 91
Table 2.4: Summary of Sensitivity and Specificity Results.	102

List of Abbreviations

A Adenosine

ATP Adenosine Triphosphate

BP Base Pairs

BST Bacillus stearothermophilus

C Cytosine

C-probe Circular Probe

cDNA Complementary Deoxyribonucleic Acid

Ct Threshold Cycle

CTC Chlamydia trachomatis Cryptic Plasmid

DNA Deoxyribonucleic Acid

dNTP Deoxynucleotide Triphosphates

dsDNA Double Stranded Deoxyribonucleic Acid

EtBr Ethidium Bromide

EUA Emergency Use Authorization

FN False Negative

FP False Positive

FVU Free Void Urine

G Guanine

HDA Helicase Dependent Amplification

HIV Human Immunodeficiency Virus

IR Infrared Radiation

LAMP Loop Mediated Isothermal Amplification

LCR Ligase Chain Reaction

LoB Limit of Blank

LoD Limit of Detection

LoQ Limit of Quantitation

LSPR Localized Surface Plasmon Resonance

MDA Multiple Displacement Amplification

mRNA Messenger Ribonucleic Acid

NASBA Nucleic Acid Sequence Based Amplification

NTC No Template Control

PCR Polymerase Chain Reaction

PID Proportional Integral Derivative

POC Point of Care

PPA Positive Percent Agreement

qPCR Quantitative Polymerase Chain Reaction

Q-Q Quantile-Quantile

RAM Ramification Amplification Method

RCA Rolling Circle Amplification

RNA Ribonucleic Acid

ROS Reactive Oxygen Species

RT Reverse Transcription

SD Standard Deviation

SDA Strand Displacement Amplification

SP Surface Plasmon

SPR Surface Plasmon Resonance

ssDNA Single Stranded Deoxyribonucleic Acid

STI Sexually Transmitted Infection

T Thymine

Ta Annealing Temperature

Taq Thermus aquaticus

Tm Melting Temperature

TN True Negative

TP True Positive

UV Ultraviolet

VCSEL Vertical-Cavity Surface-Emitting Laser

Chapter 1

1.1 Fundamentals of Polymerase Chain Reaction

1.1.1 Biological Reagents

Polymerase Chain Reaction (PCR), discovered by Kary Mullis in 1985, is a molecular biology technique used across an array of fields of study to exponentially amplify low copy numbers of target genetic material [1]. The basic principles behind the assay involve regulated and specified temperature fluctuations repeated multiple times to synthetically emulate DNA replication. PCR and its ability to confirm the existence of small traces of genetic material proved to be highly valuable within scientific research, and consequently gained substantial popularity as a diagnostics tool. As an inherently highly sensitive assay, clinical samples can be analyzed for infectious pathogens by amplifying specific sequences along their genome that are unique to their species. Before exploring the principal mechanisms behind this assay, it is firstly important to understand the biological components involved in this reaction and the roles they play in the amplification process:

Deoxynucleotide triphosphates (dNTPs) and Deoxyribonucleic Acid

Adenine (A), Thymine (T), Cytosine (C), Guanine (G) are the four nitrogen-containing nucleotide monomers that make up deoxyribonucleic acid (DNA). As free dNTPs, they are the building blocks of synthesized DNA strands. Adenine and Thymine are complementary nucleotides because they share two hydrogen bonds, and Cytoside and Guanine are complementary because they share three [2].

DNA is a helically shaped molecule composed of two complementary strands of nucleic acid polymers (polynucleotides). Imbedded within this molecule is the genetic material of all

forms of life, and its role is to control and initiate the synthesis of proteins. This process, referred to as the central dogma of molecular biology, was detailed by Francis Crick in 1957 as DNA acting as a template to transcribe messenger ribonucleic acid (mRNA), which then then gets translated into proteins in ribosomes [3]. DNA is composed of a sugar (deoxyribose) and a phosphate group (sugar-phosphate backbone), and one of four dNTPs (the variable region). Each nucleic acid monomer along a singular strand is linked together through covalent bonding between the sugar and phosphate groups, and the helical structure forms due to the hydrogen bonding between the complementary dNTPs [4]. Each DNA strand has a 3' and 5' end, referring to the 3rd and 5th carbon atoms in the deoxyribose sugar rings at each end, where the 3' carbon is bound to a free hydroxyl (-OH) group and the 5' carbon is bound to a free phosphate group [4].

Polymerase

The polymerase is an enzyme that is responsible for synthesizing the complementary DNA strand along a template strand in DNA replication. This enzyme is crucial to PCR as it is the catalyst for amplification. The polymerases found in human somatic cells are not the same used in PCR, since they will denature and lose utility at high temperatures. In the 1960s, biological organisms in hot springs were studied for their unique ability to survive in high temperatures, although it was thought that thermophilic bacteria could not survive in temperatures above 55°C [5]. In 1969, Thomas D. Brock and Hudson Freeze discovered a species of said bacteria, *Thermus aquaticus (Taq)*, that could thrive in temperatures nearing 80°C [5]. This allowed for the isolation and extraction of its 'Taq' polymerase in 1976 [6], which proved to survive in extreme temperatures required for PCR (95°C) and optimal for DNA synthesis (72°C) [7].

Primers

Primers are oligonucleotides, meaning they are short polymers made up of dNTPs.

Oligonucleotides are composed of 13-25 nucleotides [8], and they are single stranded. Primers play an important role in DNA replication during mitosis of establishing a starting point for the polymerase to begin synthesizing a complementary DNA strand along the template strand. When the strands begin to separate from one another, the polymerase will extend along the leading strand with the use of one primer, although multiple primers are required along the lagging strand to form Okazaki fragments. In PCR, the primers have a similar function, however their importance extends beyond this. Primer design is crucial to successful PCR, as they denote amplicon length and are highly specific to the gene of interest that is unique to a species (i.e., highly discriminatory against non-specific binding).

1.1.2 Polymerase Chain Reaction Mechanisms

DNA Amplification

The amplification process aims at manipulating temperature to synthetically achieve three phases required for DNA replication: denaturation, annealing, and elongation [9]. After the completion of each of these phases, one PCR cycle has been conducted. As seen in **figure 1.1**, denaturation usually occurs at temperatures nearing 95 °C, and is the first step in the cycle involving the separation of double stranded DNA (dsDNA) into two single stranded DNAs (ssDNA). This step is held for a varying amount of time – usually requiring 10-60 seconds in most cases, although this may dependent on the template's G-C content [10]. After the dsDNA has denatured, the temperature is dropped to its lowest point to allow the primers to anneal to the ssDNA. The annealing temperature (T_a) used for this step is highly dependent on the melting temperature (T_m) of the primers which can be estimated from the empirically deduced equation:

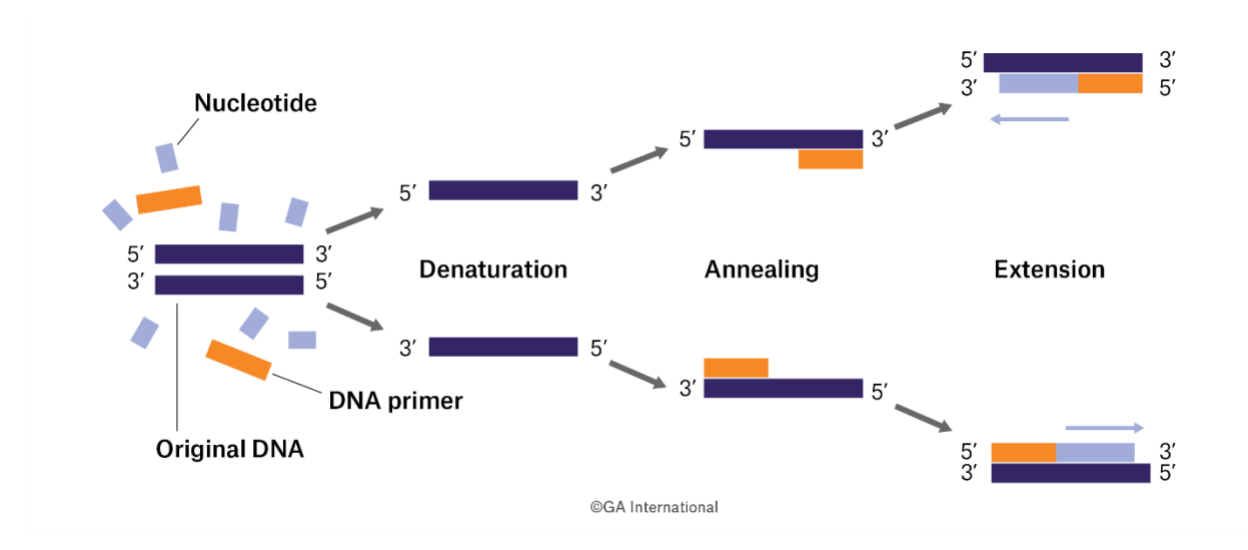


Figure 1.1: Three phases of one PCR cycle – denaturation, annealing, elongation.

Light blue, orange and dark blue rectangles refer to dNTPs, DNA primers, and ssDNA template, respectively.

This figure is derived from "A Brief History of PCR and Its Derivatives" [11].

$$T_a^{opt} = 0.3 T_m^{primer} - 0.7 T_m^{template}$$

(1.1)

where T_m^{primer} and $T_m^{template}$ refer to the melting temperatures of the least stable primer and DNA template, respectively [12]. Once this temperature is achieved, it is again held for a platform dependent timeframe, although empirical results suggest 30 seconds suffice [10]. Lastly, when the primers have annealed to the template DNA, the temperature is raised to roughly 72 °C (polymerase dependent) to allow the polymerase to construct a secondary complementary strand along the ssDNA template. The elongation hold time is also polymerase dependent and is based on the enzyme's processivity and speed. Taq DNA polymerase, for example, requires 1 minutes to elongate 2kb and an extra minute for each additional 1kb extension [10]. Once the hold at the desired temperature is complete, one full cycle of PCR has been finalized [9].

One cycle of PCR alone is not enough to complete the assay, and the total theoretical number of amplicons generated depends on the total number of cycles conducted. Assuming 100% amplification efficiency, we can estimate the amount of expected DNA copies after 'n' cycles of PCR by:

$$Q = q_0 * (2^n - 2n)$$

(1.2)

where Q, q_0 , and n are final DNA copy number, initial DNA copy number, and cycle number, respectively. This formula is comprised of two parts describing the theoretically expected replication: amplified product with determinant and indeterminant product lengths. The ' 2^n ' portion of the expression refers to the exponential replication of the segments of the PCR template amplified with known length (as governed by the chosen primers), while the '2n' portion refers to the linear replication of the original DNA strands that are outside the bounds of

the primer-driven replication (i.e., product with unknown length) [13]. Based on the DNA detection assay, its limit of detection, and the theoretical amplicon yield, PCR is commonly run for a minimum of 30 cycles to satisfy the conditions to generate an amplification signal.

Ribonucleic Acid Amplification

When ribonucleic acid (RNA) is the template of analysis, it cannot be amplified in the same manner as DNA due to the fact that Taq polymerase cannot extend along it [14]. In order to "amplify" RNA, it must first undergo a preliminary step preceding denaturation. As explained by *Haddad and Baldwin (2010)* [15], PCR is an assay solely for DNA amplification, and therefore the desired target RNA must first be converted to DNA through a process known as reverse transcription (RT). The RT process is carried out by a retroviral DNA polymerase enzyme called reverse transcriptase and it works in tandem with a primer designed against the RNA to synthesize a single stranded complementary DNA (cDNA). This enzyme is multipurpose as it acts as a weak DNA polymerase without exonuclease activity and exhibits an RNase H function to degrade the RNA from the transcribed RNA/DNA hybrid strands.

1.1.3 Qualitative PCR

The first PCR machines were not quantitative in nature and mainly focused on amplicon generation. Before the discovery of the Taq enzyme, the three stages of PCR were conducted manually in separate water baths held at the desired temperatures. Since the enzyme would denature at high temperatures, they would have to be replaced after each cycle. The discovery of Taq polymerase and its ability to withstand temperatures at which DNA denatures redirected this cumbersome process towards an automated thermocycler device, changing the face of molecular biology [16]. This device employed Peltier-effect thermoelectric heating and cooling which uses a thermoelectric module (TE module) made up of n-type and p-type semiconductors to transfer

heat to and from the sample block shown in **figure 1.2** [17, 18], allowing for complete control over temperature manipulation. The Peltier effect, realized in 1834 by Jean Peltier, was directly based upon the Seebeck effect and stated that if an electrically conductive metal is connected at two points with differing temperatures, they will have different voltage potentials. Alternatively, Peltier discovered the opposite to be true as well – two points on an electrically conductive metal will have different temperatures. Both methods relate electrical current and temperature, as confirmed by the definition of the Peltier constant stating it is the "ratio of the generated heat current to the applied charge current", and therefore semiconductive materials were used as a method of heat transfer within thermocyclers [19-21].

Sample heating and cooling in a conventional platform occurs through conductive heat transfer, where the sample block will heat the outside of the tube, in turn heating the sample. The temperature requirements for PCR are crucial and must be as accurate as possible to ensure efficient and reproducible results. It is therefore understood that proper temperature management is of utmost importance. This commonly occurs through the Proportional-Integral-Derivative (PID) control system, although more complex hybrid systems utilizing various other controllers such as feedforward, feedback, and bang-bang controllers have been implemented to attempt to improve ramping speeds without compromising accuracy [17]. While these machines are generally very efficient, their control algorithms have optimization ceilings considering their hardware limitations (i.e., heating block with low thermal conductivity).

Gel Electrophoresis and Ethidium Bromide

In conventional PCR, there is no real-time monitoring system to verify whether the genetic material amplified, therefore gel electrophoresis is used. This molecular technique uses an agarose-based hydrogel and an electric current to separate DNA by size.

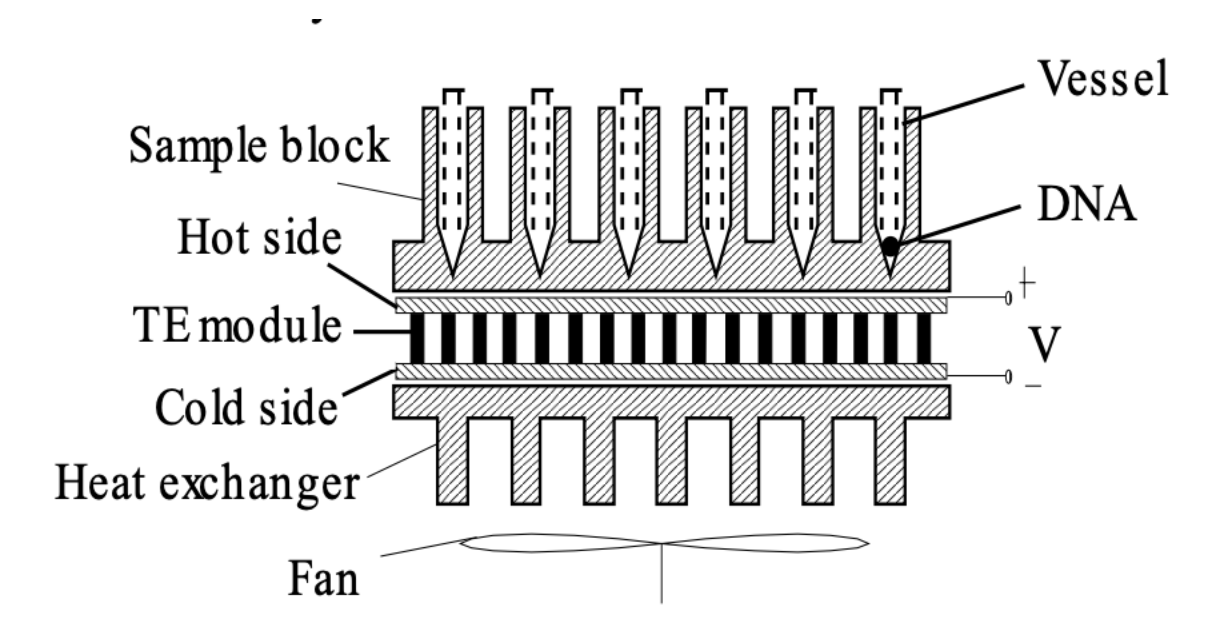


Figure 1.2: Schematic of the Peltier block in a thermocycler.

Multidirectional current is run through the semiconductive TE module between the heat exchanger and the sample block to deliver to and expel heat from the DNA containing vessel via conduction. A fan is incorporated underneath the heat exchanger fins to increase convectional heat transfer to the environment. This figure is derived from "Temperature control for PCR thermocyclers based on peltier-effect thermoelectric" [17].

The process relies on the inherent polarity of DNA and therefore its attraction towards the positive pole in an electric field [22]. Before the separation process, the gel is mixed with a fluorescent tag/label (often ethidium bromide (EtBr) [23]) and will later serve as the indicator of DNA amplification.

EtBr is an aromatic DNA intercalating fluorescent tag that, when mixed in an aqueous solution, has ultraviolet (UV) light absorption peaks at 210 and 285 nm. When excited, it omits an orange light wavelength of 605 nm [24]. On its own in an aqueous solution the emission intensity is unobservable, however once intercalated in DNA, it is hypothesized that the hydrophobic environment between the strands removes any EtBr bound water molecules and omits a strong fluorescent signal. The rationale behind this idea is that water is naturally a fluorescence quencher and impedes on the inherent emissions of the EtBr [25, 26].

1.1.4 Quantitative PCR

Quantitative PCR (qPCR) uses identical heating mechanisms seen in qualitative PCR but introduces a quantitative aspect to the assay. These machines allow the end user to monitor DNA amplification in real time using fluorophore molecules. While these machines don't necessarily offer an advantage over conventional platforms regarding sensitivity or speed, the quantitative aspect is incredibly desirable from a research and clinical diagnostic standpoint [27].

Real Time Fluorescent Labels

qPCR allows for real time monitoring via photodetectors and excitation LEDs. This allows the end user to sidestep gel electrophoresis and instead just require the interpretation of an output fluorescence signal. Some commonly used and commercially available PCR dyes are SYBR Green and PicoGreen, which are similar to ethidium bromide in the sense that they are DNA binding, although their excitation and emission peaks are different. SYBR Green, for

example, has excitation and emission wavelengths of 497 and 520 nm, respectively, when bound to DNA. These dyes provide the real-time sigmoidal signal seen in **figure 1.3**. While many of the binding mechanisms involving commercially available dyes are proprietary information, *Dragan et. al.* (2012) [28] proposed a model for SYBR Green/DNA complex formation. The overall complex formation energy gains contributions from the SYBR molecule's phenyl-quinilinium and benzo-thiazole aromatic ring systems. Considering the favourable interaction between aromatics and DNA [29], it is assumed that they intercalate between base pairs. The motility of the molecule is severely reduced when these interactions are couples with the van der waal forces formed with the individual nucleotides. As a result, the quinilinium-thiazole rings are forced into a conformational state that is depicted by a large increase in fluorescence.

With each cycle of PCR, DNA copies are exponentially amplified and therefore bind more dye molecules. The result of a positive PCR demonstrated on a qPCR machine takes the mathematical form of a sigmoid curve as seen in **figure 1.3**. For a true intercalating dye, such as SYBR green, fluorescence is usually monitored at either annealing or elongation temperatures. **Figure 1.4** demonstrates a graph produced by constant fluorescence monitoring throughout multiple PCR cycles, and their ensuing relative values as a function of temperature [30]. From this figure, it can be deduced that either annealing or elongation are appropriate fluorescence measuring points. The discrepancy between values at both stages is unknown, although can potentially be attributed to polymerase activity throughout the hold time at annealing.

There are several pieces of information that one can infer from **figure 1.3**, as described by *Brunstein (2015)* [31], beginning with the most critical – the cycle threshold (Ct) value. Though its definition varies, the consensus is that it is the first indication of deviation from the

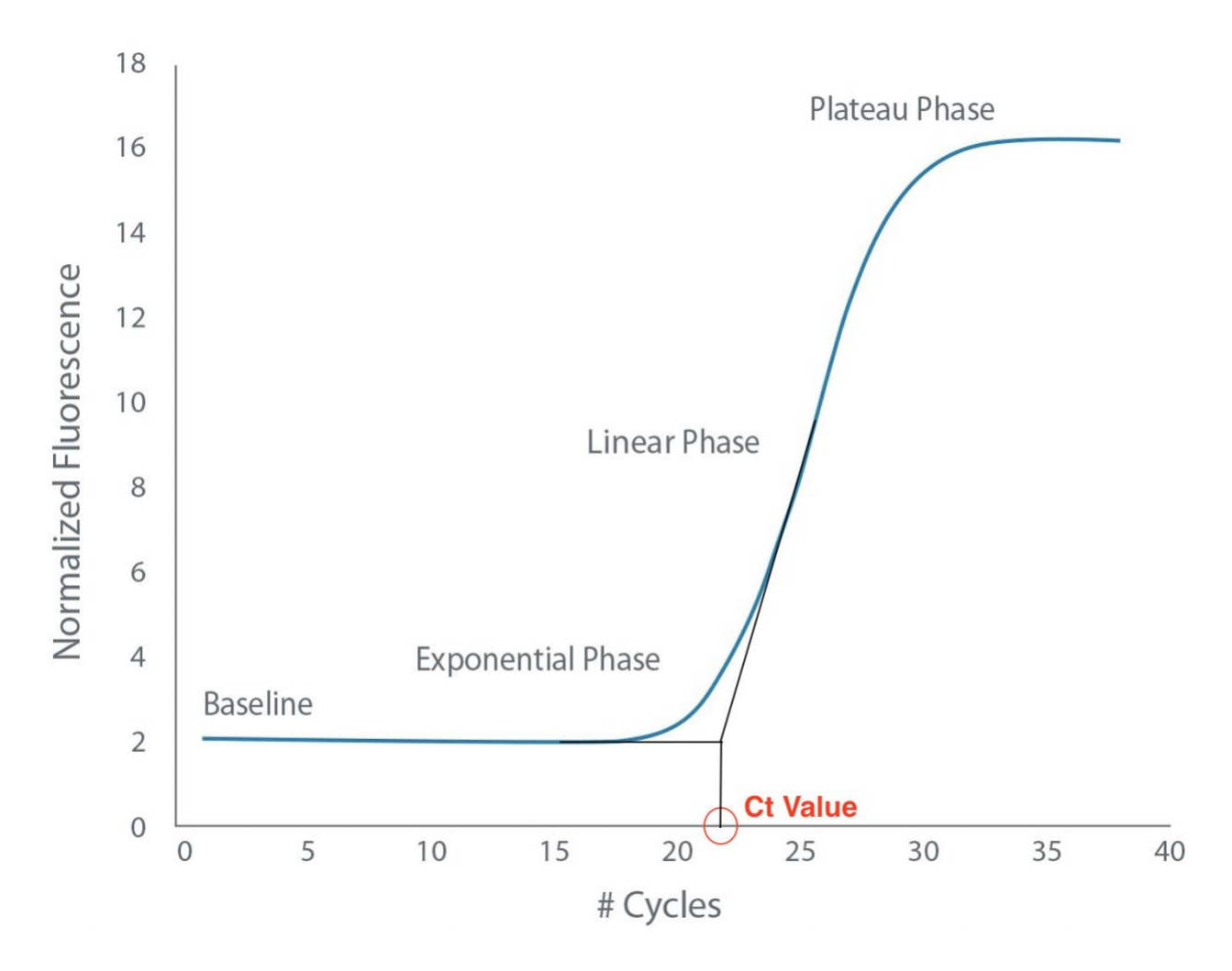


Figure 1.3: Normalized Fluorescence vs. #PCR Cycles.

The relationship between these variables takes the mathematical form of a sigmoid curve, denoted be a linear baseline, exponential phase, linear phase, and logarithmic plateau phase. This figure is derived from "qPCR Checklist: Steps to Better Results" [32] and modified to include the Ct Value.

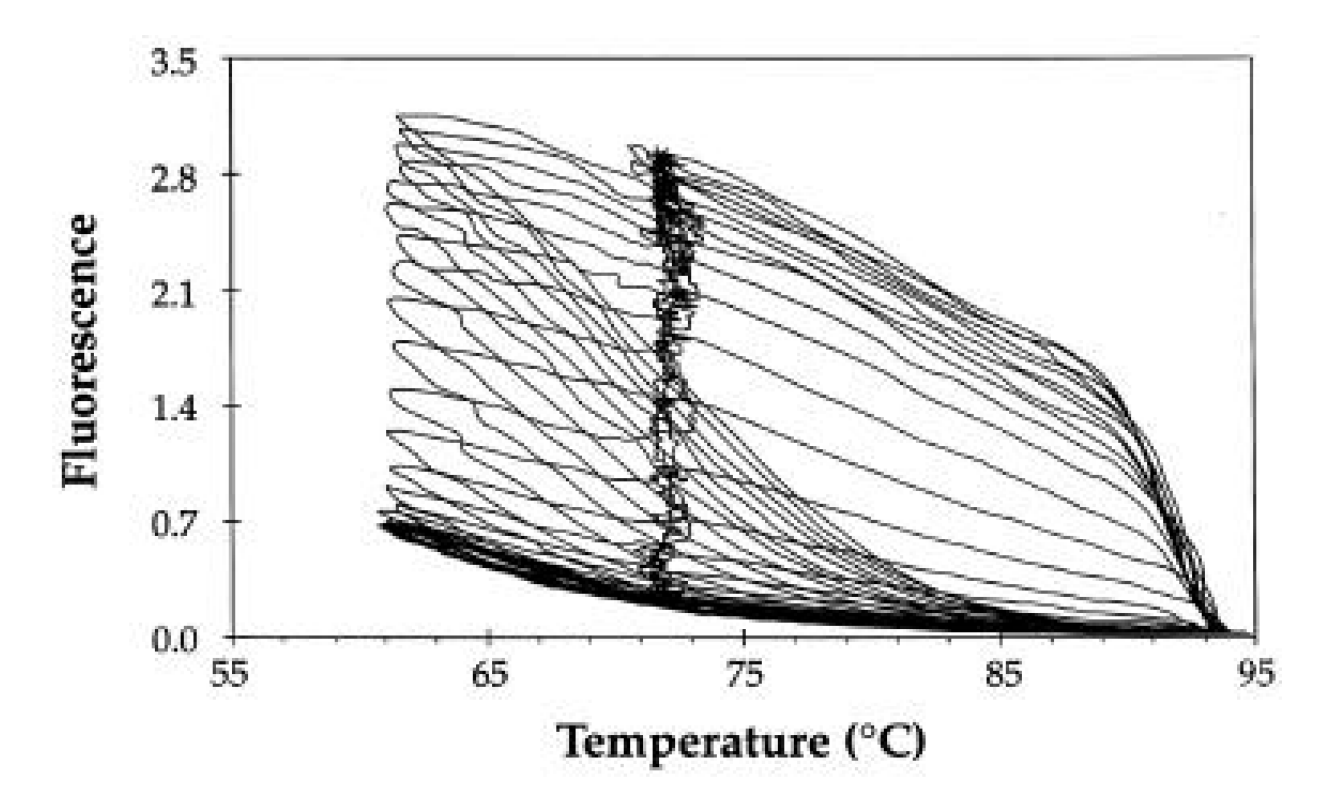


Figure 1.4: Fluorescence vs. Temperature graph demonstrating constant fluorescence measurements throughout PCR operating at 95°C, 60°C, 72°C for denaturation, annealing, and elongation, respectively. SYBR Green intercalating dye was used as the reporter dye molecule. Fluorescence values are highest at annealing throughout each cycle, similarly intense at elongation, and lowest at denaturation. This figure is derived from "Continuous fluorescence monitoring of rapid cycle DNA amplification" [30].

linear baseline into the exponential phase of the sigmoid curve to a statistically significant degree [31]. This value indicates the instance of measurable DNA amplicon, essentially the limit of detection of the monitoring system. The cycle at which this occurs can also be used to deduce a quantitation of the starting DNA copy number. The second piece of information that can be observed is what is called the inflection point, located halfway through the linear phase. This point creates a divide between the exponential and logarithmic portions of the sigmoid, indicating the instance at which there will begin a decline in observed amplification. It is important to consider that this is assay dependent and does not necessarily mean that amplification rate is slowing down, as this could be due to unforeseen confounding factors such as low fluorophore concentration, although a study conducted by Jansson and Hedman (2019) [33] reported that the plateau phase is mainly caused by primer depletion. **Figure 1.4**, however, gives interesting insight into the molecular kinetics within a reaction, and demonstrates that during the later cycles of PCR, target DNA strands begin to hybridize well before the annealing temperature is reached. Wittwer et. al. (1997) suggested that based on this finding, that the rapid hybridization of amplicon in later PCR cycles is perhaps entirely responsible for the plateau phase [30].

TaqMan Assay

Fluorescent labelling is an effective method of quantifying DNA amplification, however another commonly used method for qPCR is the TaqMan assay. As described by ThermoFisher [34], rather than using dye molecules that fluoresce with DNA-binding dependency, the TaqMan assay utilizes two (forward and reverse) primers and an oligonucleotide probe binding a fluorophore and quencher molecule in close proximity. The primers and probe are designed to be complementary against a desired target, and the polymerase will begin extension along the

template at the primer's location. Once the polymerase reaches the probe, its exonuclease activity cleaves the fluorophore, furthering its distance from the quencher and emitting a fluorescence signal. With each round of amplification, more fluorophores are cleaved and the signal increases accordingly. As a quantitative method, the TaqMan assay is comparably on par with binding dyes and should be viewed as an alternative. Its greatest advantage mainly lies within the fact that they bind more discriminately to target template, preventing instances of false positive signals, and reassuring that achieved signal is true amplicon generation. As for its disadvantages, it is generally more costly, and the probes often have to be redesigned for each instance of varied application [35].

Raw Sigmoidal Data Curve Fitting

The raw data produced by the photodetectors within a qPCR machine does not appear as eloquent as shown in **figure 1.3** due to disruptive electrical and background noise. These signals can be attenuated to a certain degree; however, curve fitting algorithms are often used to smooth out the datapoints and fit them with a mathematical relationship. Many algorithms define four function parameters to fit a sigmoid curve, however a study conducted by *Spiess et al. (2008)* suggests adding an additional asymmetry parameter to later infer information (i.e., PCR efficiency, starting DNA copy quantitation) with the accuracy and precision of non-sigmoidal quantification methods [36]. **Figure 1.5** demonstrates a curve fit precision comparison between exponential, 4-parameter sigmoid and 5-parameter sigmoid models over the exponential portion of the raw fluorescence vs. cycles data. The 5-parameter model closely resembles the precision of the exponential model over the exponential portion of the sigmoid curve, demonstrating that it is a more precise than the 4-parameter fit. The equation for a sigmoid curve using five function parameters is:

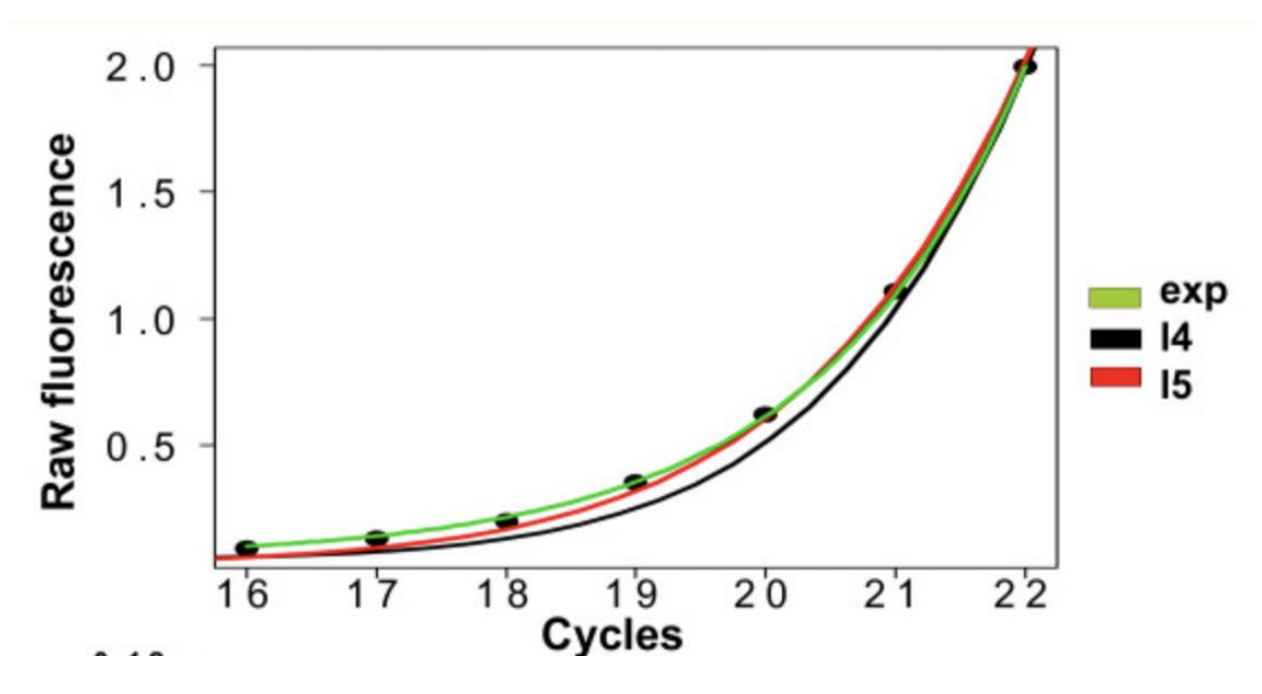


Figure 1.5: Curve fitting raw fluorescence data with different fit models for comparative measures.

The exponential data is a magnified segment of a sigmoid curve. The green, black, and red curves correspond to exponential, 4-parameter, and 5-parameter models, respectively. The black dots refer to the raw fluorescence vs. cycles data. This figure is derived from "Highly accurate sigmoidal fitting of real-time PCR data by introducing a parameter for asymmetry" [36].

$$f(x,b,c,d,e,f) = c + \frac{d-c}{(1+e^{(-b(x-e))})^f}$$
(1.3)

Where: 'b' is the slope, 'c' is the baseline asymptote, 'd' is the plateau asymptote, 'e' is the inflection point, and 'f' is the novel asymmetry parameter [36]. A four-parameter fit does not include the asymmetry variable 'f'.

Ultraviolet Light Monitoring

Another DNA detection alternative to using fluorescence is UV monitoring. dNTPs inherently absorb UV light at 260 nm as a result of the resonance structures of their purine and pyrimidine bases [37], and this property can be used to monitor amplicon in real time or post PCR. At the beginning of the assay, the starting amounts of DNA are composed of dNTPs, oligonucleotide primers, and initial template. The beer-lambert law denotes the extinction coefficient relating the amount of light absorbed to the concentration of the light absorbing molecule [38]. Since UV light is absorbed differently for DNA forming duplexes than ssDNA, oligonucleotides and single dNTPs, UV transmissions are differentiable [39]. With each cycle, as more dNTPs are being converted into dsDNA and more primers are depleted, the change of transmission at 260 nm can be monitored via photodetector [26].

1.2 DNA Amplification Techniques

As previously discussed, PCR is one of the more common DNA amplification methodologies involving fluctuating temperatures to satisfy genomic and enzymatic conditions. It is very commonly used in the worlds of research and diagnostics; however, it is worth discussing other relevant amplification assays that exist as alternatives to PCR that aim at achieving the same goals.

1.2.1 Isothermally Based Amplification

Isothermal amplification assays are alternatives to PCR that operate at a constant temperature rather than thermally cycle between desired temperatures. The following methodologies are the most relevant to (point of care) diagnostics as discussed by *Fakruddin et. al. (2013)* [40], although there are a variety of others in existence, such as nucleic acid sequence based amplification (NASBA), strand displacement amplification (SDA), multiple displacement amplification (MDA), and rolling circle amplification (RCA).

Loop Mediated Isothermal Amplification

One common alternative to traditional PCR is the loop mediated isothermal amplification (LAMP) assay. The objective of this technique is to amplify genetic material, but contrary to PCR, it does so isothermally at roughly 60 - 65 °C for 45 to 60 minutes. The biological reagents used are similar to PCR, which include a polymerase, dNTPs, 4 primers, and template DNA. The polymerase used for LAMP is derived from the *Bacillus stearothermophylus* (BST) bacterium to operate at the desired temperature and incorporate its high strand displacement activity. The assay mechanisms can be seen in **figure 1.6**, which include three main steps: starting material generation, amplification and elongation, and recycling [41].

There are several advantages to using LAMP over PCR, and the most outstanding ones are the setup simplicity and cost effectiveness without compromising precision. Since there is no need to cycle between temperatures, the required expensive equipment used for traditional PCR is not needed. Additionally, this technique is less sensitive to the inhibitory substances found in clinical samples, in turn not requiring time consuming DNA purification preparations [42].

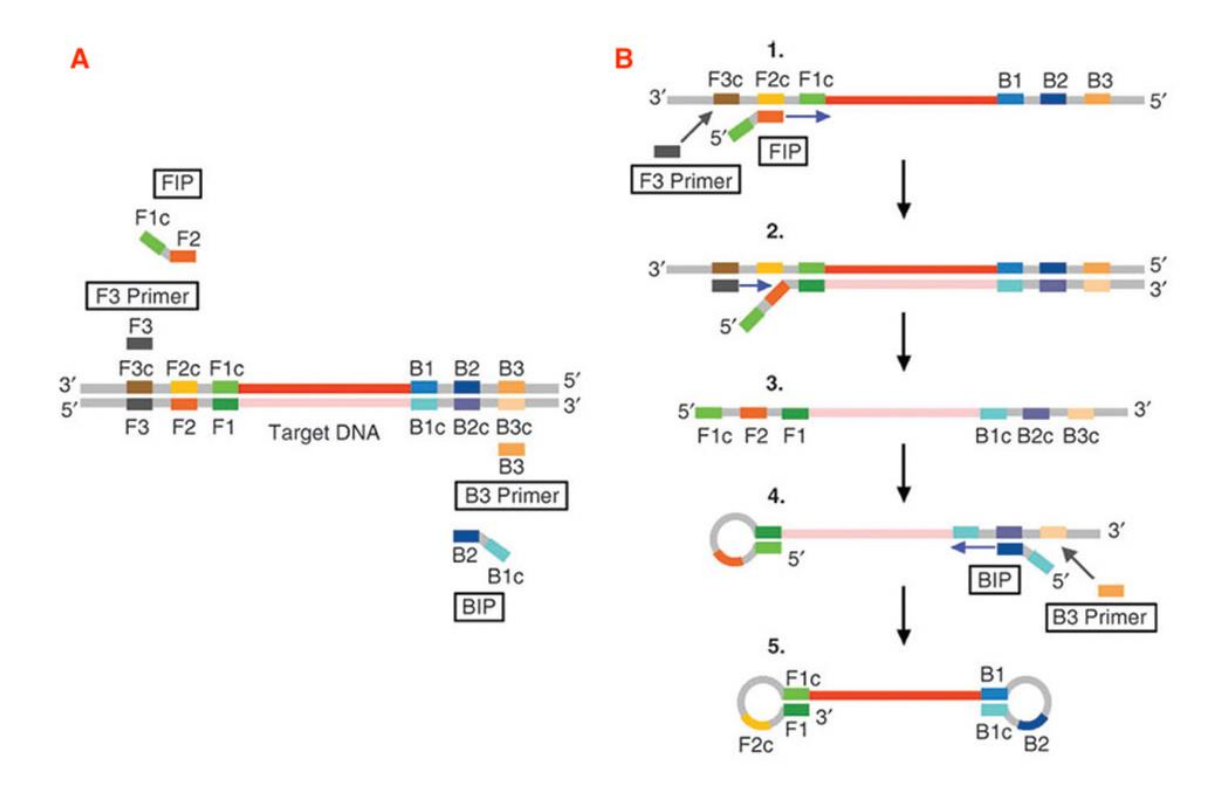


Figure 1.6: Illustrative diagram of the LAMP amplification process.

(A) 'F', 'B', and 'c' denote forward, backwards, and complementary, respectively. Primers required for LAMP amplification: forward inner primer (FIP), forward 3' primer (F3 Primer), backwards inner primer (BIP), and backwards 3' primer (B3 Primer). Coloured bands along target DNA denote complementary primer targets.

(B) 1. FIP binds to F2c and polymerase extends along the template strand. FIP contains a hanging F1 segment.

2. F3 primer binds to F3c and extends along the template using its strand displacement ability to separate the template from the strand formed from the FIP. 3. The strand formed in step 1 is separated. 4. F1c and F1 segments on the strand in step 3 hybridize forming a loop structure. On the 3' end, BIP binds to the B2c segment, and extends along the strand. BIP contains a hanging B1c segment. The B3 Primer binds to the B3c segment for the purpose of strand displacement. 5. The final form of the separated strand, where F1 and B1 bind to their complements, resulting in a double loop "dumbbell" structure. This is the strand that is continuously amplified, as all primers can bind to their complementary parts. Additional loop primers are often used to enhance amplification. As a result of multi-primer usage, the final products are of different lengths and conformations. This figure is derived from "Nucleic acid amplification: Alternative methods of polymerase chain reaction" [40].

On the other hand, there are certain shortcomings to LAMP such as the complexity of designing multiple primers against different locations along a genome, the complex conformations of the final amplicon, and lack of commercial availability [43].

Helicase Dependent Amplification

In the somatic DNA replication process, helicase enzymes are tasked with separating dsDNA duplex into two ssDNA in the presence of adenosine triphosphate (ATP) [44], forming a replication fork structure. Helicase dependent amplification (HDA) synthetically replicates this process and does so at a constant temperature [45], rather than using high temperatures as a means to denature dsDNA. The rest of the process is very similar to that of PCR, as it requires template specific primer binding at the 3' end and exonuclease-deficient polymerase extension to exponentially amplify genetic material.

There are several advantages to using HDA over other isothermal amplification methods, namely its simplicity, synthesis speed (100 base pairs [bp]/second), and processivity (10 kilobase pairs [kb]/binding) [46]. These qualities offer obvious benefits as a competitive point of care diagnostic tool.

Ramification Amplification Method

Ramification amplification method (RAM) is an isothermal method that takes advantage of the principals of RCA, whereby a circular oligonucleotide probe is the amplification target. The inventors of RAM, *Zhang et. al. (1998)* [47], understood that the probe-target bonding strength contributes greatly to the overall assay sensitivity and specificity (namely as a result of bond breaking after the washing step), and therefore suggested the incorporation of circular probes (C-probe) to circumvent the issue of weaker hydrogen bonding between linearized probes and target. This method, as demonstrated in **figure 1.7**, is described by *Zhang et. al.* as follows:

Ramification: primer extension and strand displacement

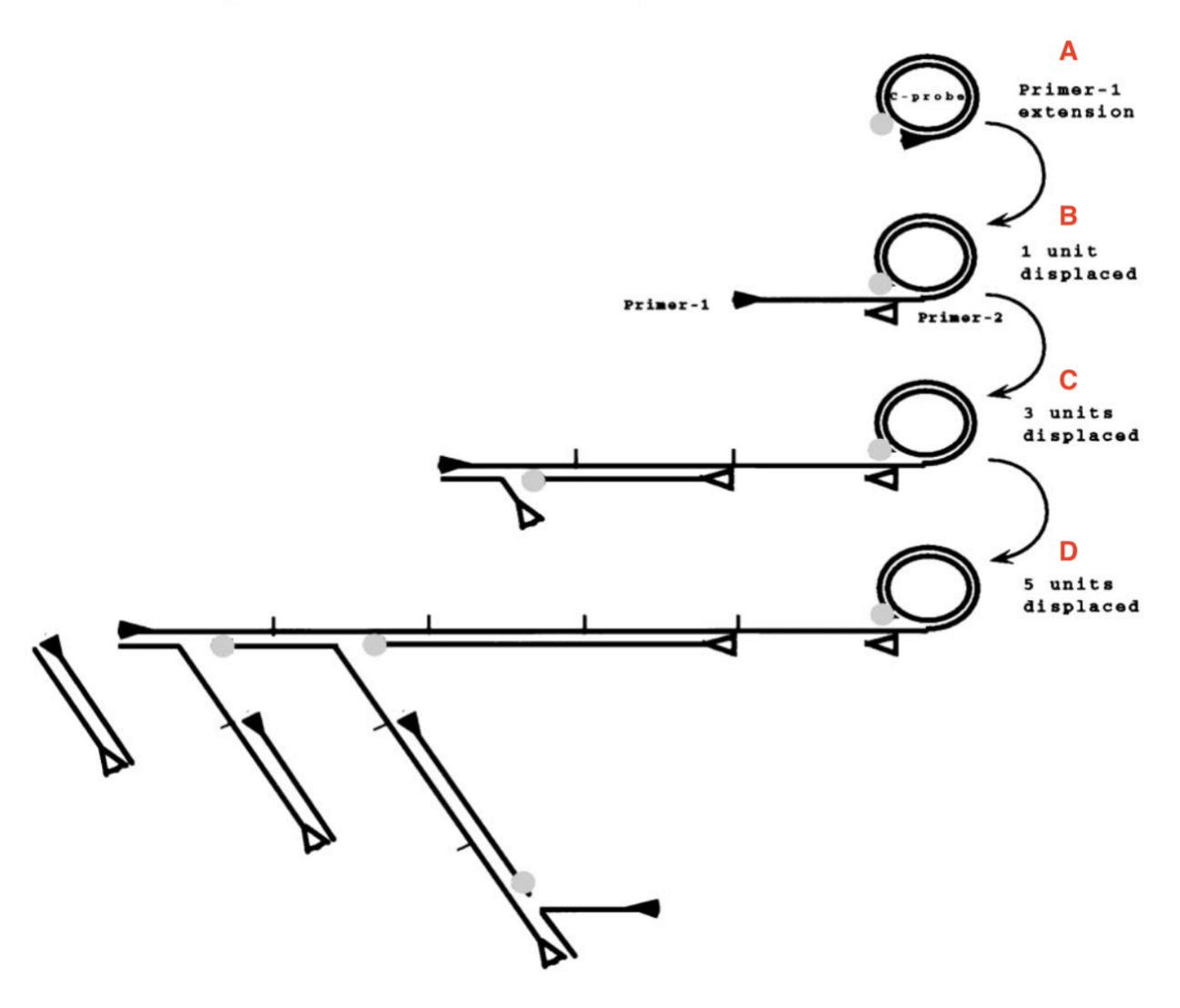


Figure 1.7: Basic graphic describing the RAM process, isolating the C-probe for simplicity.

Black and white arrows represent primer-1 and primer-2, respectively. Grey dot represents the polymerase. (A) Primer-1 anneals to C-probe and polymerase extends. (B) Extension around probe is continuous. The polymerase displaces the previously formed strand from the C-probe and continues to elongate. Primer-2 binds to its target on the displaced unit. (C) Process continues and reveals 3 displaced fully replicated segments forming a multimeric DNA polymer. (D) Multimeric polymer composed of 5 displaced units with 5 primer-2 binding sites. Each polymerase elongating from primer-2 displaces the strand downstream from it, resulting in varying amplicon sizes. This figure is derived from "Amplification of target-specific, ligation-dependent circular probe" [47].

Step 1: The 3' and 5' ends of the C-probe hybridize with specificity to the target DNA strand, and the circle is target-dependently and covalently linked via ligase enzyme. An ensuing helix formation develops between the probe and the target which causes them to intertwine with a strength much greater than that of classical hydrogen bonding. Capture probes are used to isolate the target DNA/C-probe complexes, and the excess reagents washed from the solution.

Step 2: A primer is designed to hybridize to the C-probe, and a polymerase extends alongside it.

This extension is continuous because of its ligated nature, and this results in the formation of a

This extension is continuous because of its ligated nature, and this results in the formation of a multimeric DNA polymer. As this strand grows, it develops multiple sites for a secondarily designed primer to bind to.

<u>Step 3:</u> Polymerases simultaneously extend along the multimeric strand at the various secondary primer sites and displace extended strands downstream from one another. These displacements result in amplicon production of various lengths, each beginning with the target sequence for the secondary primer to bind to.

There are several advantages to using RAM, one of which is its high processivity. Using the bacteriophage Ø29 DNA polymerase, the assay can be complete within an hour at a temperature of 35 °C [48]. The multimeric aspect of this assay allows for simultaneous polymerase extension, further increasing the overall amplification power [47]. Additionally, the C-Probe terminals can be ligated regardless of whether the target genetic material is RNA or DNA, and since the final product relies solely on the amplification of the probe, there is no need for an RT step [49].

Lastly, this method is highly specific as ligation can only occur if there is an exact pairing between the probe's terminals and the target template. As a result of its simplicity, accuracy, and

isothermal functionality, it is a legitimate candidate for a point of care diagnostics technique, however its total run time falls short to its competition.

1.2.2 Thermocycle-Based Amplification

PCR is the most widely used thermocycle-based nucleic acid amplification technique used today. As previously discussed in great lengths, it relies on stringent temperature manipulation to replicate genetic material. Interestingly, it is not the only amplification technique that uses thermal fluctuations.

Ligase Chain Reaction

Ligase chain reaction (LCR) is an amplification method similar to PCR in that it requires controlled fluctuation between desired temperatures. Its mechanisms are also analogous, the difference being that the amplification target is a probe rather than the template itself. The process, as described by *Barany (1991)* [50], involves designing two probes in close proximity to one another against both ssDNA templates. Assuming there is a perfect match between the template and probes, the gap between the probes will be covalently bound via a ligase enzyme. The length of the ligated probes will be the target for amplification.

If the probes are not perfect matches to the template, the ligation reaction and ensuing amplification reaction will not occur. This makes LCR highly specific, even more so than PCR [51]. While this may make LCR more attractive as an option, it requires an extra enzyme that PCR does not, and should be considered an alternative method rather than a preferable substitution.

1.3 PCR Validation Protocols

1.3.1 Limit of Blank, Limit of Detection and Limit of Quantitation

In analytical chemistry, there are various terms used to describe the overall sensitivity of an assay and define the limits at which it can work with a desired confidence. Since PCR has developed into a quantitative tool used to detect analyte, these terms are often used to assess and validate its performance. As a collectivity, the limit of blank (LoB), limit of detection (LoD) and limit of quantitation (LoQ) are used to define the smallest amount of measurand that can be measured with statistical confidence by an analytical assay [52]. While their definitions are inherently different, **figure 1.8** shows their conceptual relationship. The following information is characterized by *Armbruster & Pry* (2008) [52]:

Limit of Blank

The LoB is used to determine a baseline signal from which the first instance of a positive result can be distinguished. Many instruments, for example, use electronics to acquire, interpret, and demonstrate analog signals. It can then be assumed that there is going to be unwanted electrical background noise due to the imperfection within the instruments themselves, or from surrounding objects that omit readable signals. For this reason, it is important to distinguish the background signals acquired when a negative result is expected and determine the expected spectrum/value range distribution. The equation to estimate the LoB is:

$$LoB = \mu_{blank} + 1.645 \, \sigma_{blank}$$

(1.2)

Where μ_{blank} is the mean blank signal value, and σ_{blank} is the blank signal standard deviation (SD). The 1.645 value represents the t-statistic or z-statistic depending on the test being used.

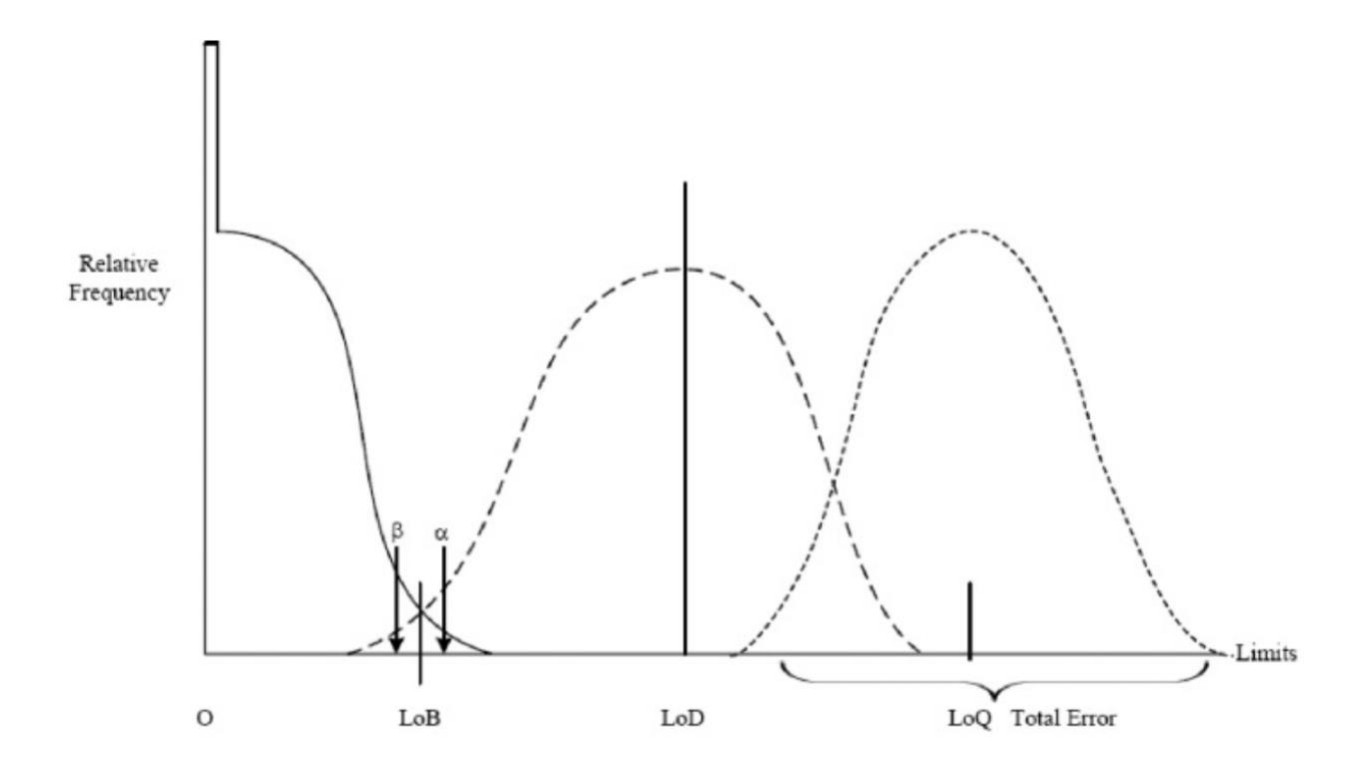


Figure 1.8: Graphical representation of the relationship between LoB, LoD, and LoQ.

Plotted on a 2-D axis demonstrating relative frequency vs. limits. Solid, dashed, and dotted lines denote the LoB, LoD, and LoQ frequency distributions, respectively. Modern analyses do not usually report limits less than 0, therefore the left half of the LoB distribution was replaced by an increased frequency at 0. This figure is derived from "Protocols for Determination of Limits of Detection and Limits of Quantitation, Approved

Guideline" [53].

This estimation equation assumes a normally distributed dataset in the scenarios containing a linear relationship between analyte concentration and assay signal production (known as the calibration curve).

To experimentally deduce the LoB, numerous true negative samples must be analyzed via the assay of interest and their output signals collected. When determined experimentally, the appropriate statistical value should be used instead of 1.645 depending on the study's degrees of freedom and desired confidence [54]. Under a normal distribution, this equation covers 95% of the dataset, with the type I error α (5%) crossing into the LoD range as seen in **figure 1.8**. This error constitutes the datapoints that generated signal similar to that produced by the lowest true positive samples used to determine the LoD and it can be attributed to false positive results (i.e. analyte contamination) or maximal background noise.

Limit of Detection

The LoD is a measure of the lowest amount or concentration of analyte that the assay in question can detect (with a desired probability) that is distinguishable from the LoB. There are different methods of calculating this:

- 1) The first method involves measuring a blank sample (without analyte) twenty times, obtaining the mean value, and the LoD is calculated as the mean signal value + 2 SDs. The number of SDs can be modified to remain more conservative. The outlying issue with this method is that it is purely theoretical and does not take into consideration whether the assay can sufficiently produce distinguishable signals from the LoB.
- 2) The second method involves conducting the assay with small known starting numbers of analyte and developing a signal distribution for various dilutions. The benefit of this

method is that it validates and quantifies the change in signal between a true negative and positive result.

For validation purposes, the 2^{nd} method will be further discussed. Similar to the LoB, a predetermined maximum allowable type II error (β) percentage is used (i.e., false negative), and the goal is to ensure that the portion of the LoD distribution that crosses into the LoB distribution does exceed that value. While continuously reducing the analyte concentration, twenty repeats of each are conducted and the lowest concentration value that satisfies the statistical limits becomes the LoD. To estimate the LoD, the following equation is used:

$$LoD = LoB + 1.645 \sigma_{lowest analyte concentration}$$

(1.3)

Where LoB is the previously obtained limit of blank, 1.645 is a rough t-statistic estimate, and $\sigma_{lowest\ analyte\ concentration}$ is the standard deviation of the distribution of the signals obtained by the lowest known analyte concentration. Once again, this equation assumes a linear calibration curve and by association normality in the distribution of signal outputs at individual concentration levels.

Limit of Quantitation

The LoQ is similar to the LoD in the sense that it is also aiming to extrapolate a minimal concentration value. While the definitions seem to vary, the LoQ takes into consideration application dependent fitness of purpose, as well as some previously defined bias and imprecision, and is described as "the lowest concentration at which the performance of a method or measurement system is acceptable for a specified use" [55]. It can also be interpreted as the lowest analyte concentration that can be detected with any degree of certainty for a specified use. The LoQ therefore cannot be lower than the LoD, only equivalent or higher, as seen in **figure**

Non-Linear Calibration Curves

The estimation calculations for LoB, LoD and LoQ are only possible if the calibration curve is linear to render the data normally distributed. qPCR uses the Ct value of the output fluorescence signal as a benchmark for positive amplicon, however its relationship with concentration is logarithmic [54]. As a result, its calibration curve is therefore non-linear, and the Ct values obtained at each concentration cannot be assumed normal. This occurs because the change in concentration/analyte amount by serial dilution is orders of magnitude higher than the change of Ct values. To account for the non-linearization (and therefore inability to assume statistical normality), it is convention to linearize the function by using a logarithmic scale as seen in **figure 1.9**.

Empirically, the PCR LoD is found by using the 2^{nd} aforementioned method. Serial dilutions of the known control DNA are made, and each is run through the assay twenty times over. The lowest dilution that tests positive 19/20 (95%) times is deemed the experimental LoD [56]. A recent study conducted by *Fung et. al.* (2020) [56] compared various PCR platforms and their LoD concerning Sars-CoV-2 and found the Roche Cobas platform to be the most sensitive with an LoD \leq 10 DNA copies, while most other platforms can detect 100 or more copies.

1.3.2 PCR Efficiency

PCR efficiency refers to how effectively a PCR machine can amplify DNA within a PCR cycle, denoting the fraction of copied genetic material [57, 58]. When the efficiency levels are higher, the assay itself becomes more quantifiable. In general, an efficiency of 90% or higher is an indication of a properly designed assay conducted by a robust system [59, 60]. Lacklustre efficiencies could be due to numerous reasons which may not be machine dependent, such as biological reagent performance, unwanted inter and intra-molecular interactions, and the

Standard Curve Ct vs Log DNA dilution

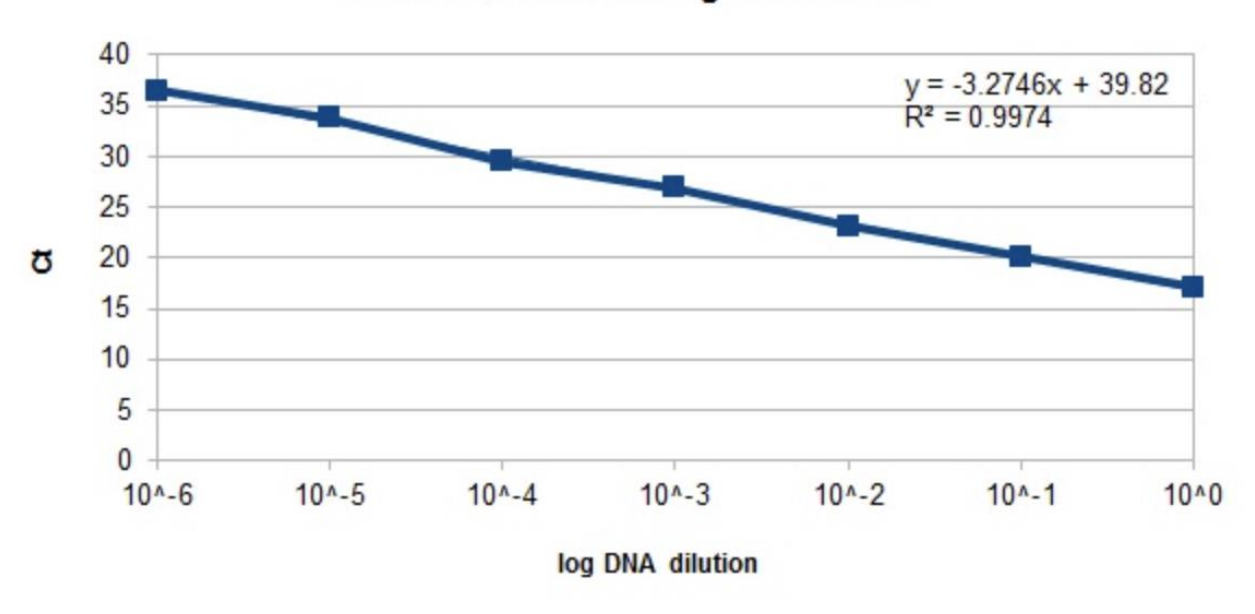


Figure 1.9: Standard curve (calibration curve) of Ct value vs. DNA copy number for qPCR.

Curve is linearized through logarithmic scaling. This figure is derived from "Generating Standard Curve to analyse the reaction optimization - Real Time qPCR, Calculating PCR Efficiency" [61].

presence of reaction inhibitors and clinical organic material [59, 62]. The following method to estimate PCR efficiency is derived through the methodology outlined by *Evrard et. al* (2009) [63].

To calculate efficiency, it is firstly important to derive a standard curve relating starting DNA material and the corresponding cycle of an arbitrarily chosen fluorescence value in the linear portion of the sigmoid output curve, as seen in **figure 1.10**. Assuming 100% amplification efficiency, it is known that PCR amplicon generation can be represented by:

$$Q = q_o 2^n \tag{1.4}$$

Where 'n' is the cycle number, 'Q' is the final amplicon generated at cycle 'n', and q_o is the known starting DNA copy number. Under realistic conditions PCR is never truly 100% efficient and equation 1.9 can be rewritten as:

$$Q = q_o (1+\rho)^n \tag{1.5}$$

Where ρ represents the efficiency variable. Values of 1 and 0 represent 100% and 0% efficiency, respectively. As previously discussed, to linearize the calibration curve, the starting DNA copy amounts are represented on a logarithmic scale rather than a linear one, and equation 1.10 can be rewritten as:

$$\log Q = \log q_o + n \log(1+\rho) \tag{1.6}$$

This equation takes a linear form and describes the regression lines seen in **figure 1.10 (b)**. The slopes of these lines are represented by $\log(1 + \rho)$, which indicates their relationship with efficiency ρ .

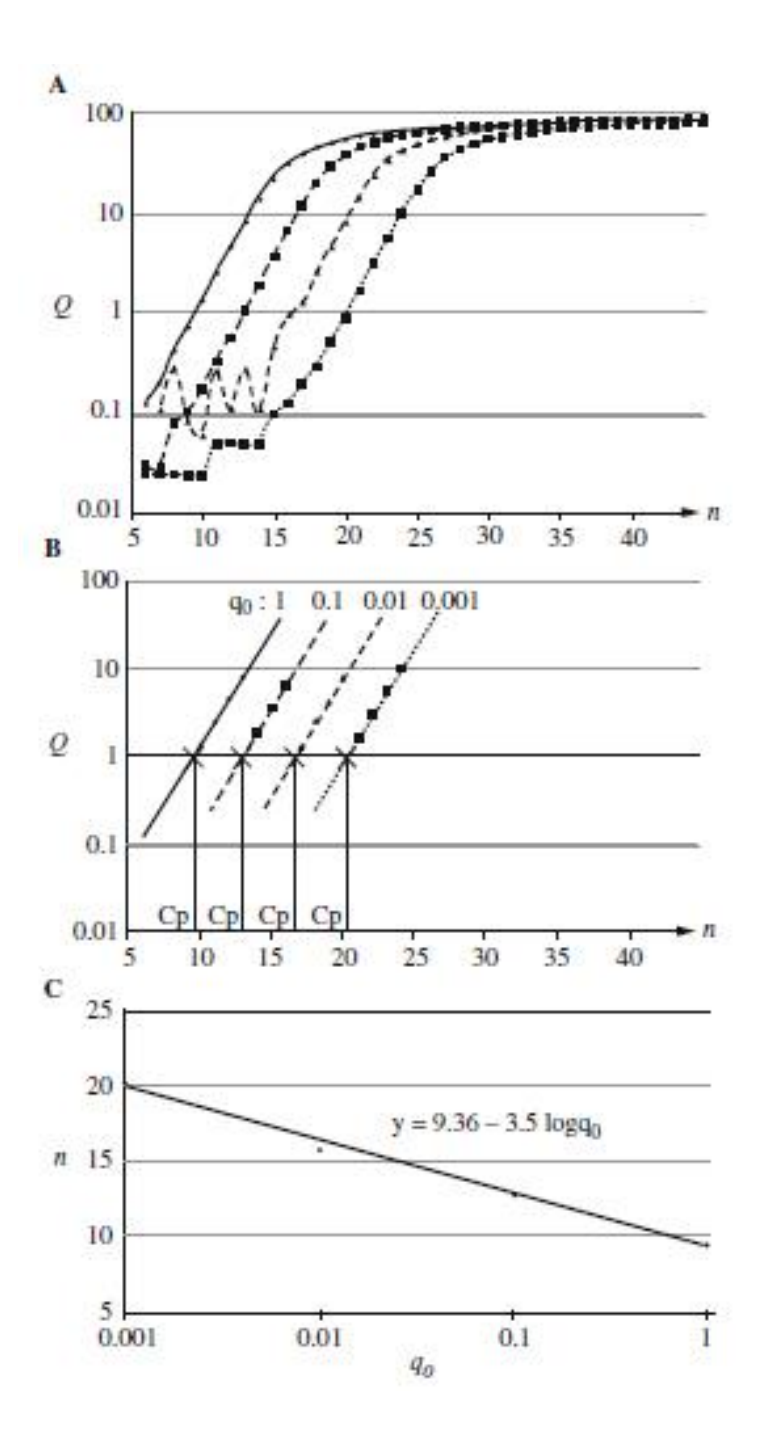


Figure 1.10: Cycle 'n' vs. starting DNA concentration ' $q_{\rm o}$ ' calibration curve.

(A) Four serial 1/10 dilutions amplified by PCR with results plotted on a fluorescence vs. cycles graph. Fluorescence is denoted by Q (indicating amplicon number at cycle 'n') because they increase proportionally. (B) An arbitrary value of $\log (Q) = 1$ is selected across the linear portions of the dilutions. (C) Cycles 'n' vs. $\log (\text{starting DNA concentration})$ ' $\log (q_o)$ ' at $\log (Q) = 1$ linearized calibration curve. The slope of this line is -3.5. This figure is derived from "Nanoscience: Nanobiotechnology and Nanobiology" [63].

An arbitrary value of $\log Q = 1$ is selected at each regression line, and further plotted against their respective cycle number 'n' to create the calibration curve as seen in **figure 1.10 (c)**. To match this graphical representation and demonstrate the relationship between 'n' and ' q_o ' for a given 'Q', equation 1.11 can be rearranged as:

$$n = \frac{\log Q}{\log (1+\rho)} - \frac{\log q_o}{\log (1+\rho)}$$
(1.7)

The slope of this equation is represented by $\frac{1}{\log{(1+\rho)}}$ and can be equated to the slope of the calibration curve to solve for efficiency ρ . A slope value of -3.32 will equate to $\rho = 1$ which means 100% efficiency.

1.3.3 Sensitivity and Specificity Testing

The sensitivity and specificity of a diagnostic tool are crucial benchmarks of an assay's reliability in a clinical setting. They simply determine how well a diagnostic test can diagnose the presence of the pathogen of interest, and whether it can distinguish a negative from a positive result. The assessment begins with ensuring that there is a commonly used robust and reliable test to firstly conduct clinical testing on a predetermined number of positive and negative samples, referred to as the 'gold standard' reference test [64]. Once the reference results are complete, the same samples are tested by the assay in question and their results compared. After the results are gathered, they are categorized into four groups as seen and explained in **figure**1.11: True positive (TP), false positive (FP), false negative (FN), and true negative (TN). *Parikh et. al.* (2008) [64] describe the definitions of sensitivity and specificity as follows:

	Gold standard disease present	Gold standard disease absent	
Test positive	True positives (TP)	False positives (FP)	Total test positives:
	a	b	a+b
Test negative	False negative (FN)	True negatives (TN)	Total test negatives:
	C	d	c+d
	Total diseased:	Total normal:	Total population:
	a+c	b+d	a+b+c+d

Figure 1.11: 2x2 table cross referencing the results from the gold standard reference test and the assay in question.

(a) True positive: the number of reference test positive results detected as positive by the assay. (b) False positive: the number of reference test negative results detected as positive by the assay. (c) False negative: the number of reference test positive results detected as negative by the assay. (d) True negative: the number of reference test negative results detected as negative by the assay. This figure is derived from "Understand and using sensitivity, specificity and predictive values" [64].

Sensitivity

The sensitivity of a diagnostic test refers specifically to the test's ability to properly diagnose a positive sample when the pathogen of interest is present. Clinically speaking, it is the probability of a patient testing positive when they truly are infectious. The sensitivity is calculated by assessing how many positive samples it can detect from a lot of samples deemed positive from the reference test. It can be mathematically calculated by [65]:

$$sensitivity = \frac{TP}{TP + FN}$$
(1.8)

The total summation of positive reference tests is represented by the denominator in equation 1.13 and it includes false negative results. This type of error can be a result of assay malfunction, or an insufficient LoD wherein the clinical sample contains pathogen analyte concentrations smaller than the detection capabilities of the test.

Specificity

The specificity of a diagnostic test refers specifically to the test's ability to properly recognize and report a negative sample when it truly is devoid of the pathogen of interest. Clinically speaking, it is the probability of testing negative when the patient is negative.

To calculate an assay's specificity, the samples deemed negative by the reference test are tested by the assay and its ability to recognize them as true negatives is assessed. The following equation is used to calculate specificity [65]:

$$specificity = \frac{TN}{TN + FP}$$
(1.9)

The total summation of negative reference tests is represented by the denominator in equation 1.14 and it includes false positive results. This type of error can be a result of assay limitations concerning unwanted secondary effects from reagents or hardware, or analyte contamination.

1.4 Plasmonic Nanoparticles

1.4.1 Plasmonic Particles Fundamentals

Plasmonic materials are unique in the sense that they can couple with electromagnetic radiation to exhibit optical properties that cannot be found inherently in nature. They do so by exploiting surface plasmon resonance, which needs to be well understood to further discuss plasmonic PCR.

Surface Plasmon Resonance

Surface plasmon resonance (SPR) is a phenomenon that occurs at the interface of a metallic and dielectric material. The concept can be broken down into 2 definitions:

- Resonance is a concept often discussed in classical physics describing the instance at which an object is met with an external periodic force operating at a frequency that matches its natural frequency. The natural frequency of an object is the frequency at which it will oscillate if disturbed without any constant external influence. The amplitude of the object's oscillations will be highest at resonance [66].
- <u>Surface Plasmons (SPs)</u> are oscillations of delocalized electrons at the metal-dielectric interface that occur as a result of the electromagnetic wave induced material dipole. To further elaborate, the dipole causes restoring forces between the separated charges, in turn causing back-and-forth oscillations of the free electrons [67, 68].

Surface plasmon resonance is an occurrence that combines these definitions and denotes the moment at which the frequency of the external periodic force (electromagnetic radiation, i.e.,

light) matches the plasma (electron cloud) frequency at the interface to create resonant conditions and an electric field extending roughly 300 nm from the metal-dielectric interface [69] – the point at which plasmonic properties occur [70].

Plasmonic particles are those that exhibit unique optical properties as a result of localized SPR (LSPR [71]) such as photoluminescence [72], light scattering [73], and heat release [74]. The incident electromagnetic radiation wavelengths are much larger than the particles themselves and introduce what is known as the confinement effect – the spatial restrictions of the oscillating free electrons at the interface [67]. In the resonant condition, the LSPs will either decay radiatively and emit photons at the incidence frequency (i.e., light scattering), or non-radiatively and emit phonons (i.e., absorption). Since LSP concerns the electrons within the metallic material, the conditions to achieve LSPR and its resulting optical properties are highly dependent on the physical dimensions and properties of the metal, such as size, shape, and material composition [67, 75, 76].

1.4.2 Photothermal Nanoparticles

The unique optical properties of plasmonic particles are used for various applications; their light scattering capabilities are used in Raman spectroscopy [77, 78], metal-enhanced fluorescence [79], and optical imaging [80, 81], and they are also used photothermally for biosensing, therapeutics, drug delivery, and *in vivo* imaging [73]. As previously mentioned, morphology and size are important indicators of the particle's plasmonic properties, and this determines which are most appropriate for heating. According to Gans theory, this relationship is mathematically derived through the following equations describing absorption, scattering, and extinction cross-sections [67, 82]:

$$C_{abs} = \frac{2\pi}{3\lambda} \varepsilon_m^{\frac{3}{2}} V \sum_{i} \frac{\varepsilon_2/(n^i)^2}{(\varepsilon_1 + [\frac{1-n^i}{n^i}]\varepsilon_m)^2 + \varepsilon_2^2}$$

(1.10)

$$C_{sca} = \frac{8\pi^3}{9\lambda^4} \varepsilon_m^2 V^2 \sum_i \frac{(\varepsilon_1 - \varepsilon_m)^2 + \varepsilon_2^2/(n^i)^2}{(\varepsilon_1 + [(1 - n^i)/n^i)]\varepsilon_m)^2 + \varepsilon_2^2}$$

(1.11)

$$C_{ext} = C_{abs} + C_{sca}$$

(1.12)

Where λ is the incident light wavelength, ε_m is the dielectric constant of the medium joined at the interface, ε_1 and ε_2 are the real and imaginary parts of the dielectric constant, respectively, and n^i is the depolarization factor. As seen in equations 1.4 and 1.5, there is a proportionality between the volumetric absorption and scattering coefficients with V and V^2 , respectively, indicating that the larger sized particles have higher scattering effects. **Figure 1.12** denotes experimental results further validating this theory.

The results seen in (a) demonstrate that smaller nanoparticles have near negligible incident light scattering effects, yet the larger they get, the more scattering there is. The results in (b, c, d) clearly demonstrate that the ratio of the scattering to absorption cross sections increases with diameters for three different nanoparticle shapes, reaffirming that the scattering effect is greater on larger nanoparticles.

Photothermal nanoparticles generate heat from LSPR via the Joule effect, which states than an electric current passing through a conductor will generate heat [83, 84]. While light scattering is useful for a variety of applications, absorption is required for heat generation and therefore it can be deduced that smaller gold nanoparticles are better for this application.

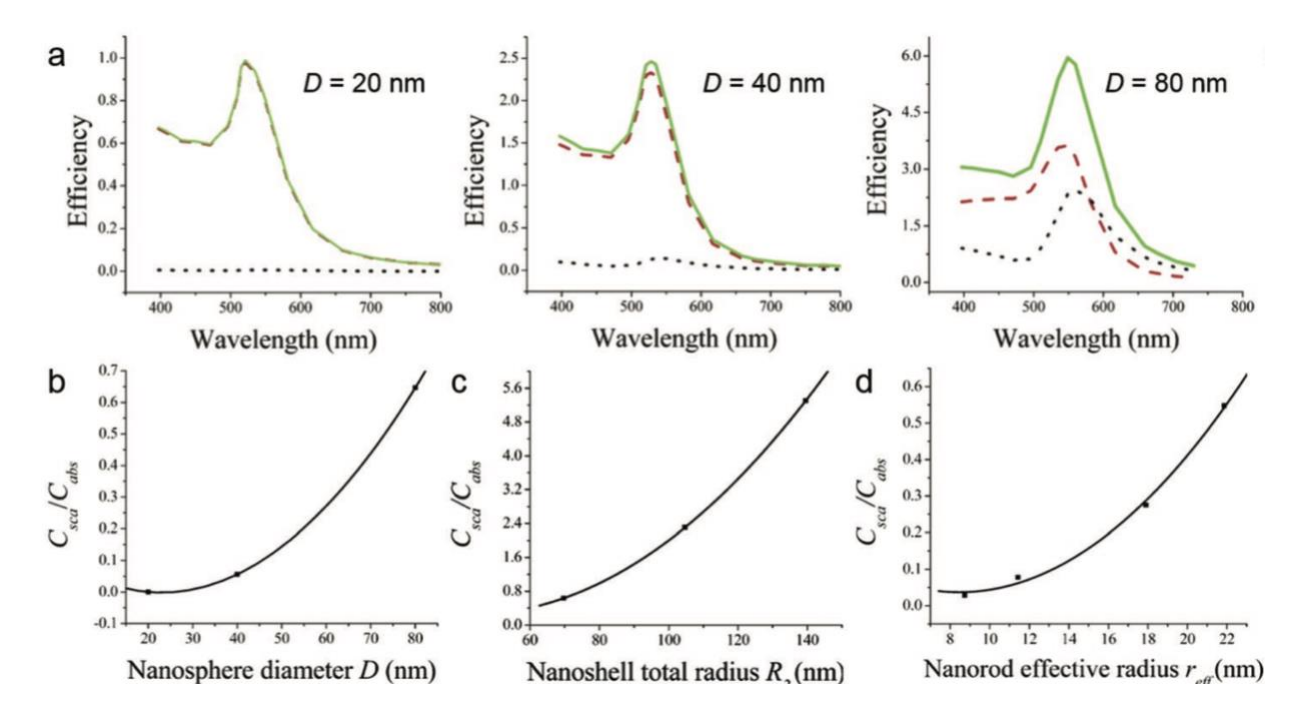


Figure 1.12: Absorption, scattering, and extinction comparisons between gold nanoparticles of different morphologies.

(a) Absorption, scattering, and extinction of nanospheres with varying diameters (D = 20, 40, 80 nm). Red (dotted), black (dotted), and green lines indicate absorption, scattering, and extinction efficiencies, respectively. (b) Ratio of scattering to absorption cross-sections vs. *nanosphere* diameter. (c) Ratio of scattering to absorption cross-sections vs. *nanoshell* radius. (d) Ratio of scattering to absorption cross-sections vs. *nanorod* effective radius. This figure is derived from "Calculated absorption and scattering properties of gold nanoparticles of different size, shape, and composition: applications in biological imaging and biomedicine" [85].

As for the optimal shape to use, it has been found that gold nanorods exhibited volumetric coefficients of absorption and scattering significantly beyond those of other shapes [73].

1.5 Photonic-Based PCR

Photonic-based PCR is an alternative method of thermocycling between the three stages of DNA amplification. Instead of using Peltier-based heating, photonic-based PCR uses light as an energy source to be converted into thermal energy. This amplification method can be further broken down into intrinsic and extrinsic heating, as discussed by *Mohammadyoussef et. al.* (2020) [86]:

Intrinsic Heating

Intrinsic heating involves using a broadband (large frequency spectrum) infrared light source to irradiate water within a PCR solution. Water highly absorbs light in the infrared region at 2660 nm, 2780 nm, and 620-850 nm range, and when irradiated, the excitation energy releases in the form of heat. One example of intrinsically heated photonic-based PCR is a concept proposed by *Huhmer and Landers (2000)* [87] where a 160 nL PCR sample in a fused-silica capillary is irradiated by a 50 W tungsten filament lamp. Both the water and capillary greatly absorb in the infrared range and produce compounded heating. The ensuing result demonstrated heating and cooling rates 30 and 15 times faster than conventional thermo cycling PCR machines, respectively. Various iterations to improve upon this have been done, such as reducing the solution volume, implementing faster cooling mechanisms, concentrating light, and altering the sample and machine chamber materials.

Another important example to discuss is the laser-excited nanodroplet PCR. This PCR requires a smaller sample volume, which in turn results in much faster assay times considering the small amount of water to irradiate. For such applications, lasers are desirable considering

their beam's narrow diameter and monochromatic (wavelength specific) nature, contrary to the tungsten lamp that emits a wide infrared light spectrum. Having the laser's power concentrate at a specific wavelength can maximize the efficiency of the conversion from optical to thermal energy. The laser-based nanodroplet PCR conceptualized by *Pak, Saunders, Phaneuf, and Forest (2012)* [88] used an 820 nL reaction volume powered by a 580 mW 1450 nm laser diode and demonstrated a 500 bp amplification in 10 minutes with repeatability.

Extrinsic Heating

The principles of extrinsic heating differ from intrinsic heating in that they involve irradiating nanoparticles and making use of their plasmonic properties, rather than heating the solvent itself. As discussed in the section prior, a laser excites the particles and causes surface plasmon resonance to occur, ultimately releasing heat as a result. The presence of nanoparticles inside PCR reactions has been shown to include inherent benefits, such as increased sensitivity and specificity (with reduced non-specific binding) [89-92], and lower PCR limits of detection [93]. In addition to this, the photothermal properties of metallic nanoparticles offer a much higher optical absorption than water in intrinsically heated platforms (approximately 10^6 times higher), in turn increasing the efficiency of optical to thermal energy conversion. As a result, less incident light power is required to achieve the desired PCR heating rates.

The plasmonic PCR is one of said extrinsic heating platforms, and it has the same goals as conventional systems in that it targets specific genomic sequences bound by specifically designed primers and amplifies them exponentially through heat fluctuation. The first instance of using nanoparticles for thermal cycling was introduced by *Roche et. al. (2012)* [94], where 60 nm citrated capped gold nanospheres were added to the reaction mixture and excited via a 532 nm laser with 2.7 W optical power output. With the use of a fan for rapid cooling, they achieved

30 cycles of PCR in less than 10 minutes. This protocol was later adapted to use pegylated gold nanorods (GNRs) as the preferred nanoparticle to be excited by a laser in the infrared light spectrum (808 nm). The gold particles act as the nano heaters that convert optical energy to heat with near instantaneity, allowing for precise control of heating and cooling. The mode of heating is therefore from within the sample, as opposed to conventional machines that heat them conductively from the exterior.

The benefits of the plasmonic PCR are evidently centered around the incredible heating speed capabilities. These machines can function on low optical power (\sim 2 Watts) and have been shown to achieve heating rates of up to 72.7 °*C*/second for sample volumes of roughly 25 μ L [94-98], having even achieved overall speeds of 30 PCR cycles in 54 seconds with detectable product [96]. In addition to cycling speed, the plasmonic PCR started to demonstrate candidacy for point of care (POC) diagnostics with the implementation of vertical-cavity surface-emitting lasers (VCSELs) as an alternative to large class IV lasers to allow for a light weight and ergonomic device shape [86]. VCSELs are small-scale devices that emit light with a high coupling efficiency and beam precision. The small nature of these devices enables them to be placed close to the bottom of the PCR tubes to couple light without extra optical equipment. In turn, the laser-like capabilities and low space consumption allow for a lightweight and powerful device.

With the implementation of the VCSEL came the POC plasmonic qPCR machine. This device has four channels that fit classical PCR tubes, and each channel is heated by its own individual VCSEL. Each channel's temperature monitoring is conducted optically using a small-scale imbedded infrared radiation (IR) thermometer, and a separate optical system to monitor fluorescence in real time is included as well. To contribute to the rapid nature of this device, a

fan is implemented to assist with reaction cooling. The device operates within a 3-D printed housing, making it lightweight and portable. The ergonomic design (as seen in **figure 1.13**) and benefits of the application of the plasmonic concepts seen above, this PCR format is an excellent candidate for POC diagnostics as it can offer an incredibly rapid test-to-result turnover time at the site where clinical care is delivered.

1.6 Research Objectives and Rationale

The SARS-CoV-2 pandemic has shed light on the importance of POC testing. The PCR test received emergency use authorization (EUA) during the pandemic, and while they are reliable and precise assays, they are time consuming and often located outside testing centers in centralized laboratories. In turn, the demand for testing could not be kept up with, causing a cascading effect that contributed to the rapid spread of the virus. In addition to the pandemic, the lengthy test-to-result turnover time affects other domains of medical diagnostics, such as in the field of sexually transmitted infections (STIs). It is common practice for physicians to prescribe broad spectrum antibiotics before receiving confirmation of a positive STI test, and this is greatly contributing to antimicrobial resistance. Both of these problems can benefit from rapid and on-the-spot testing that POC devices offer.

The POC plasmonic qPCR is a novel device designed in our laboratory that requires validation and performance testing to verify its viability as a diagnostics device. The literature review within this thesis discusses plasmonic PCR and its incorporation of gold nanorods as internal heating sources, and the POC plasmonic qPCR incorporates the novelty of testing at the point of care. A device that includes the sensitivity and precision of classical nucleic acid amplification assays with rapid result generation and easy accessibility is highly appealing for a variety of applications within the world of diagnostics, and therefore the research is merited.



Figure 1.13: The POC plasmonic qPCR machine.

Commonly conducted validation tests for diagnostic equipment are conducted in the subsequent chapter, namely LoD, LoQ, efficiency, sensitivity, specificity, and precision. These assessments are crucial into understand how this device fares against other POC assays and whether it has the potential to translate well into clinical settings. A POC device that offers high sensitivity and efficiency will certainly address endless issues in medical diagnostics.

Chapter 2

Abstract

Background: The research conducted within this thesis dedicates itself to the validation and performance testing of the POC plasmonic qPCR machine. This chapter expands on the analysis of relative fluorescence output signals and further using these results to validate the device's performance and capabilities. The time and temperature conditions under which the machine operates are described, and a uniquely developed python algorithm is used to define important characteristics of the output sigmoidal fluorescence curves, such as fluorescence ceiling gain, the slope of the linear portion of the sigmoid, and Ct value. These metrics are used to differentiate between true and false positive signals, and later implemented to assess the LoB, LoD, LoQ, PCR efficiency, sensitivity, specificity, and clinical translation of the machine. Findings: Using SYTO-16 as a DNA monitoring dye, generated hysteresis curves demonstrated that annealing was the most effective step to record fluorescence output values. Relative fluorescence ceiling values, the slope of the linear portion of the sigmoid output curve, and the Ct value all proved to be parameters that can be used to differentiate between true and false positive signals with 95% confidence. The LoD and LoQ were found to be 10⁰ and 10¹. respectively, and the PCR efficiencies of each of the 4 channels were 91.90%, 93.37%, 81.4%, and 86.5%. The sensitivity and specificity of the device were both 100%, and PCR serial dilutions were possible in 2% diluted negative CT urine spiked with CTC. Conclusions: The POC plasmonic qPCR is a highly sensitive and efficient device that has great potential as a point of care diagnostics tool. STI clinics can benefit from the rapid test-to-result

turnover time and quantitative signal output, and its translation into clinical settings looks promising.

2.1 Introduction

The test to result turnover time for most diagnostic assays are generally very time consuming, particularly within the setting of STI diagnostics. Additionally, testing is often done in centralized laboratories outside of the clinics where patients present themselves, further compounding the issue of delayed result generation. As a result, broad spectrum antibiotics are often administered before confirmation of infection as a preventative measure. These antibiotics contribute to the vast majority of antimicrobial resistance [99], and they have shown to be erroneously prescribed in 50% of cases [100]. STI clinics can therefore greatly benefit from rapid and sensitive testing to assist physicians in making proper diagnoses and providing appropriate care. *Chlamydia trachomatis* (CT) is one of the sexually transmitted pathogens for which PCR testing has been approved by the FDA, and through rapid testing, broad spectrum antibiotics can be completely eliminated as a treatment plan [101]. A device that is designed to be used at the point of care can increase diagnostic result generation speed and volume, and eliminate the need for centralized testing locations – and the four-channel POC plasmonic qPCR machine has the qualities to address these requests.

The POC plasmonic PCR machine developed in our laboratory can achieve 30 cycles of PCR in under 10 minutes using optically excited GNRs as nano heaters to cycle between desired temperatures and heat from within the sample. The device uses a 1.1 mm x 1.11 mm VCSEL [86] to excite the nanoparticles, which emit light at powers equivalent to those of class IV lasers, allowing for a lightweight, compact system. In addition to its embedded real time fluorescence monitoring system and small 20 μ L reaction volumes, the overall portability and speed of the

device make it a prime candidate for POC diagnostics. The subsequent research will use CT as a template to validate the capabilities and limitations of this machine.

2.2 Materials and Methods

The biological reagent formulation for the POC plasmonic qPCR was previously developed in the laboratory and used as a starting reference point. One 20 μ L reaction mixture is composed of the reagents listed in **table 2.1**. The overall formulation remained the same throughout the subsequent experiments, however optimization assessments were required to conduct the validation assays. The formulation was therefore slightly altered, namely affecting the primers (as listed in **table 2.2**) and reporter dye. Considering the small reaction volume, 20 μ L of mineral oil was layered on top of the reaction to prevent evaporation.

Statistical assessments conducted within this chapter were done using RStudio.

Confidence intervals and hypothesis testing were required to validate the experimental data, and they were conducted in accordance with the normalized nature of the data. Considering the smaller data sample sizes, t-tests were selected. The null and alternative hypotheses of a 2-sided t-test are as follows:

$$H_0: \mu_1 = \mu_2$$

$$H_a$$
: $\mu_1 \neq \mu_2$

Where μ_1 and μ_2 are the population mean values for the compared sample groups (1 and 2). Under the assumption of equal variance, the study's degrees of freedom are calculated by:

$$df = n1 + n2 - 2$$

Where n1 is the sample size for group 1, and n2 is the sample size for group 1. The degrees of freedom are then used to calculate pooled and differences standard deviations:

Table 2.1: List of Reagents Used in POC Plasmonic qPCR Reaction.

Reagent	Manufacturer	Initial Concentration	Volume/Reaction (µL)
Hemo Klentaq Buffer	New England Biolabs	5X	4
Reaction Mix	(NEB)		
Hemo Klentaq DNA	New England Biolabs	1 Unit	1
Polymerase	(NEB)		
GNRs	Nanopartz	50 nM	1
SYTO-16	Thermofisher	1000 mM	0.08
Purified Genomic	American Type	$> 10^5$ copies/ μL	1
Cryptic DNA	Culture Collection		
Plasmid of	(ATCC)		
Chlamydia			
trachomatis (CTC)			
Forward Primer	Integrated DNA	10 μΜ	0.6
	Technologies (IDT)		
Reverse Primer	Integrated DNA	10 μΜ	0.6
	Technologies (IDT)		
dNTPs	Fisher Scientific	10 mM	0.5
d_2H_2O	N/A	N/A	11.22

List of reagents and their corresponding manufacturers and concentrations. Volume per reaction is listed to achieve desired final concentrations. It is recommended to pre-mix 10 μ L of SYTO-16 with 490 μ L Hemo Klentaq Buffer Reaction Mix and aliquot 4 μ L of this stock to the reaction due to the inherently high concentration of SYTO-16.

Table 2.2: List of Primers Used Throughout Experimentation.

Primer	Primer Sequence	Melting Temperature (°C)	Amplicon Length (bp)	
CTC-1F	TCCGGAGCGAGTTACGAAGA	57.8	241	
CTC-1R	AATCAATGCCCGGGATTGGT	57.4	241	
CTC-2F	TTGAGAGAACGTGCGGGCGA	61.7	279	
CTC-2R	AATGCCCGGGATTGGTTGATCG	60.2		
CTC-3F	GCGGTTGCGTGTCCTGTGACCT	64.4	- 153	
CTC-3R	GCAAATCGCCCGCACGTTCTCT	62.8		
CTC-6F	AGTCCTCTAGTACAAACACCCCCA	59.1	201	
CTC-6R	TCGCCCGCACGTTCTCTCAA	61.7	301	
CTC-WF	GAGATTGAGTGTCCTGCGCGCG	62.8	NI/A	
CTC-WR	GCAAATCACACACGGCGCGC	64.5	N/A	

Each primer pair is comprised of one forward and one reverse oligonucleotide, targeted against CTC. Each primer's respective melting temperature is listed, along with each pair's target amplicon length. Primers were named based on the timeline of their design. The CTC-W primers refer to a "worst case scenario" dimerization formation pair, having 6 bp hetero complementarity at their 3' ends.

$$s_p = \sqrt{\frac{(n_1 - 1)s_1^2 + (n_2 - 1)s_2^2}{df}}$$

$$S_{diff} = s_p \sqrt{\frac{1}{n_1} + \frac{1}{n_2}}$$

The test statistic can then be calculated as:

$$\frac{\bar{Y}_1 - \bar{Y}_2 - (\mu_1 - \mu_2)}{S_{diff}}$$

Where \bar{Y}_1 and \bar{Y}_2 are the sample means of both groups. Under the assumption of the null hypothesis, the subtraction of the population means equals 0. Selecting a small type I error of $\alpha = 0.05$, the t-statistic is compared against the corresponding 2-sided rejection region to determine whether to reject or fail to reject the null hypothesis and generate a p-value:

$$rejection\ region = \left[qt\left(\frac{\alpha}{2}, df\right), qt\left(1 - \frac{\alpha}{2}, df\right) \right]$$

Using the calculations above, a 95% confidence interval of the difference in means between two groups can be calculated:

$$(\bar{Y}_1 - \bar{Y}_2 - t_{(1-\frac{\alpha}{2}),df}S_{diff}, \bar{Y}_1 - \bar{Y}_2 + t_{(1-\frac{\alpha}{2}),df}S_{diff})$$

For 95% confidence intervals around a single mean, the previous formula can be re-structured as:

$$(\bar{X}-t_{\left(1-\frac{\alpha}{2}\right),df}\frac{s}{\sqrt{n}},\bar{X}+t_{\left(1-\frac{\alpha}{2}\right),df}\frac{s}{\sqrt{n}})$$

Where \overline{X} is the sample mean, 'n' is the sample size, df = n-1, and 's' is the sample standard deviation.

All data was collected, organized, presented, and analyzed via an originally written python script. Raw data was collected through excel files and imported to the script in order to interpret the output signals seen throughout this chapter. As a result, the combined usage of the

algorithm and statistical analyses helped determine the important quantitative parameters of this POC plasmonic qPCR.

2.3 Results and Discussion

2.3.1 SYTO-16 Optimization

SYTO-16 Concentration Determination

Many qPCR assays involve reporter dyes either placed on probes or as DNA binding agents. The proportionality between amplicon production and dye signal is one main advantage to using a binding dye. SYBR green is a popular choice among these, and although it has reported circumstantial toxicity in conventional PCR assays [102], it has historically shown to be consistently toxic to the plasmonic PCR reactions (data not shown). A substitute was therefore required, and SYTO-16 was selected for its similar excitation and emission spectra of 488 and 518 nm [103], respectively, as well as its ability to strongly fluoresce upon binding. This dye, unlike SYBR green, is hypothesized to bind to the minor grooves of dsDNA, although it is yet to be proven. This assumption is based on the following empirical observations by ThermoFisher [104]:

- It shows some base selectivity.
- It appears to contact the solvent.
- It can be removed from nucleic acids by ethanol precipitation, a characteristic that is not seen in true intercalating dyes.
- It is unaffected by non-ionic detergents.
- It is not quenched by BrdU, meaning it doesn't bind in the same manner as DAPI (minor groove binding dye with a strong affinity for 'T' and 'A' clusters) [105].

In order to understand the dye's agreeableness with the reaction, a concentration vs. toxicity study was done. Based on the research conducted and recommendations by *Gudnason et. al.* (2007) [102], PCR reactions were prepared with final dye concentrations of 2, 3, 4, and 5 μ M, and tested on the POC plasmonic qPCR machine. Once complete, the samples were run through gel electrophoresis to verify product amplification, and the results of this experiment can be seen in **figure 2.1**. The gel electrophoresis image clearly demonstrates that a 5 μ M final dye concentration is toxic to the reaction in a plasmonic setting. The lower concentrations (2, 3, 4 μ M) did not impede on the reaction and returned strong PCR amplicon bands. As such, a final concentration of 4 μ M was selected moving forward to allow for maximal dye binding without introducing toxicity effects.

The dye concentration did not seem to inhibit reactions on the conventional PCR platform but did on the plasmonic system, which implies a cause-effect relationship between the energy input type and the dye's toxicity to the reaction. It is not well understood why the higher dye concentration did not work under the influence of plasmonic heating, although it is well documented that dyes can preferentially bind to GC-rich sequences and/or alter melting temperatures under normal conditions. SYTO-16 has proven to have low inhibitory effects, however it does have medium preferential binding [102]. Other factors that have been discussed are binding tightness to template and binding affinity, which could affect primer binding or polymerase extension from cycle to cycle [106]. Lastly, it is important to consider that the introduction of incident infrared laser light to the sample can cause unforeseen impedances within the reaction as well. A justifiable assumption under this hypothesis, as confirmed by *Noimark et. al. (2016)* [107], would be the generation of reactive oxygen species (ROS) as a result of the reactivity between the dye molecule and the high energy optical input.

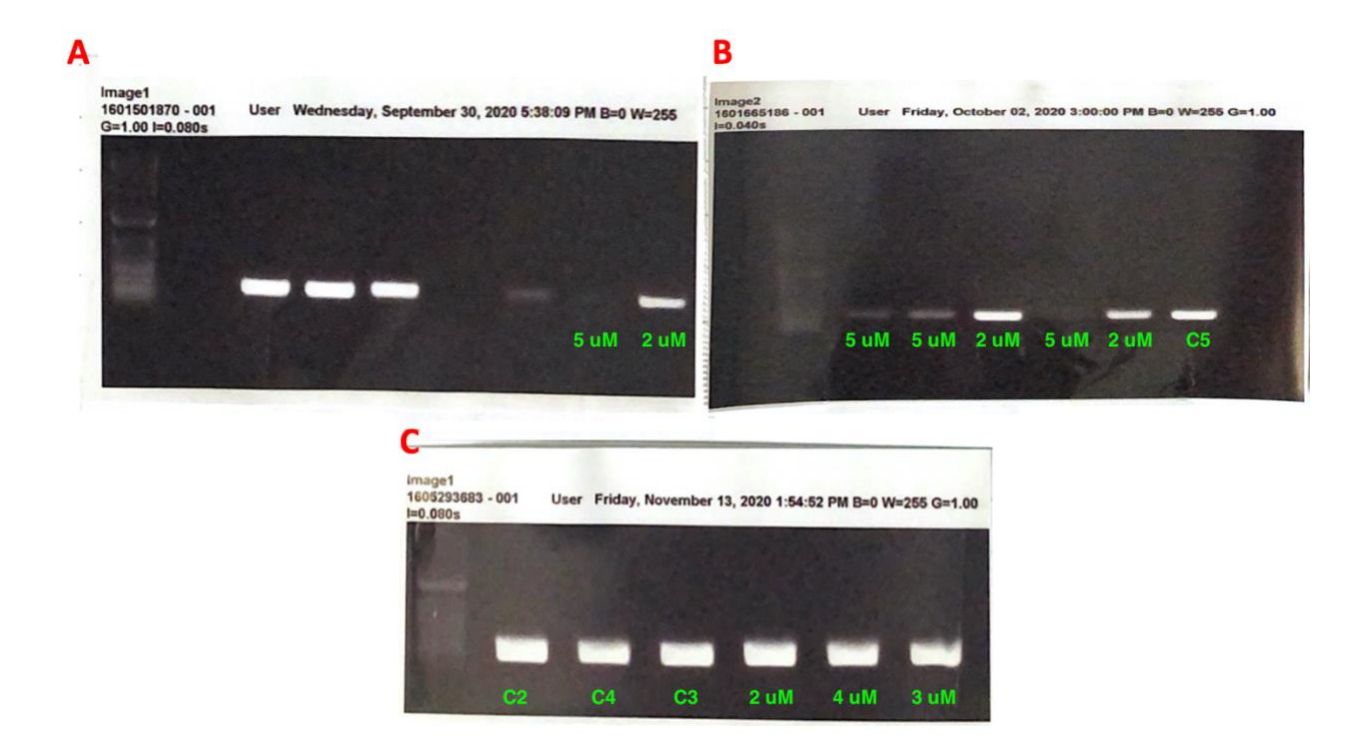


Figure 2.1: Gel electrophoresis images showing PCR amplicon results of samples with varying final concentrations of SYTO-16 dye.

(A) The first 6 bands are irrelevant to the experiment. The last 2 bands demonstrate final dye concentrations of 5 and 2 μ M. The 2 μ M sample shows amplification, while the 5 μ M sample failed. (B) Repeat of experiment (A) with additional repeats. 2x 2 μ M and 5x 5 μ M final dye concentration samples were tested. All 5 μ M show lighter to no amplicon bands, and both 2 μ M bands are strong. The 6th band represents a control of the 5 μ M dye sample amplified in the conventional PCR. (C) 2, 3, and 4 μ M final dye concentration samples were amplified in the POC plasmonic qPCR, and another set in the conventional PCR as a control. All bands are strong and indicate successful amplification.

SYTO-16 Monitoring Point

With the optimal concentration determined, characterizing the dye's functionality inside the POC plasmonic qPCR machine was crucial to explore the aforementioned binding mechanics, as well as understand the appropriate time to record fluorescence readings. PCR was conducted for 30 cycles with 10⁴ starting CTC DNA copies at denaturation, annealing, and elongation stage temperatures of 85, 50, and 68 °C, respectively. Based on prior experimentation in the laboratory (data not shown), the three stages were held for 1, 5, and 1 second(s), respectively, and fluorescence readings were collected at every instance of temperature change (a typical thermocycling profile at this hold time setting is seen in figure 2.2 and can be the assumed protocol for all subsequent experiments). 5 cycles of PCR (23 - 27) after the threshold cycle were then recorded and are presented in **figure 2.3**. This graph demonstrates a hysteresis curve, whereby increasing and decreasing temperature does not return the fluorescence response to its original state – suggesting a time delayed relationship. As seen in this figure, the lowest values occur at denaturation, as expected, and the peak values occur at annealing. A vertical temperature rise can be seen at 50 °C, indicating the temperature variance through the 5 second hold time. The temperature is highest at the end of the hold; therefore, this was deemed the appropriate time to record fluorescence readings.

Considering this dye is thought to bind to the minor grooves of dsDNA, the reduced fluorescence at elongation compared to annealing is hypothesized to be a result of increased rates of unbinding dye (off rates) with temperature increase. As such, since annealing occurs at the lowest temperature and therefore the moments of lowest system energy input, the off rates can logically be assumed to be at their lowest point. This may be the opposite of what one would see with intercalating dyes that are bound by DNA on either side of the molecule.

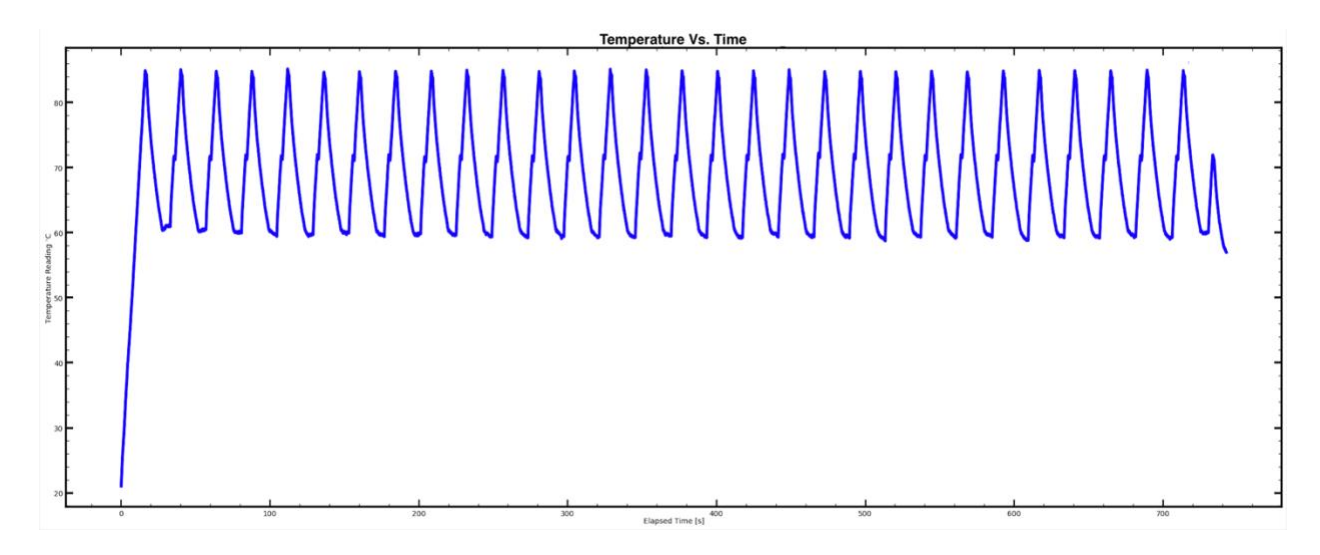


Figure 2.2: Thermocycling profile from one channel of the POC plasmonic qPCR machine.

The heating protocol follows 1-5-1 second(s) holds at denaturation, annealing, and elongation, respectively. Rate of heating is approximately 5°C/second, and cooling is done through forced convection via a fan. This curve demonstrates the ultra-rapid nature of the device having conducted 30 cycles of PCR is roughly 12 minutes.

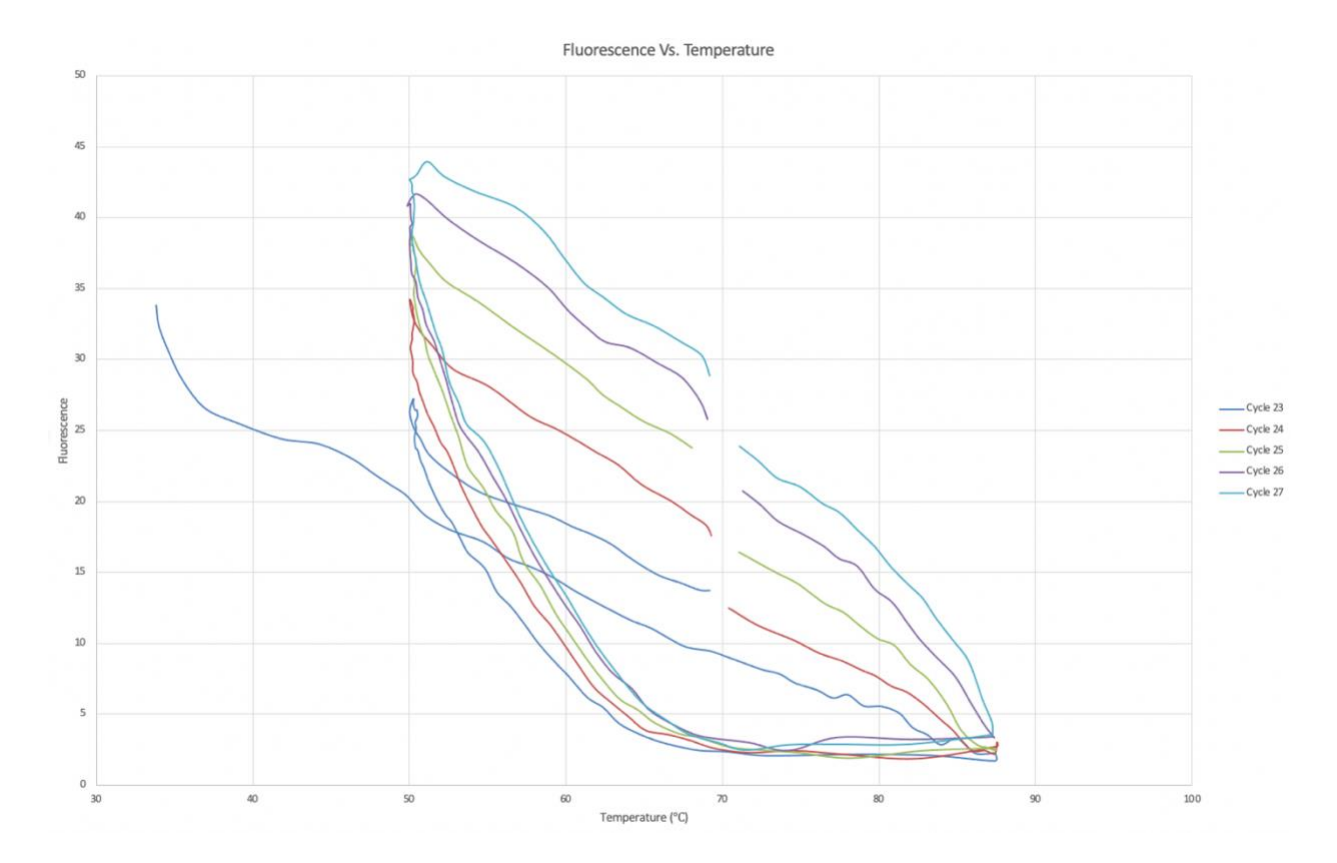


Figure 2.3: Hysteresis curves of fluorescence output vs. temperature across 5 PCR cycles.

One cycle constitutes thermocycling through 85 - 50 - 72 °C for 1 - 5 - 1 second(s), respectively. All 5 cycles are those that make up the linear segment of the fluorescence vs. cycles sigmoid curve, and the fluorescence peaks therefore increase with each cycle.

The behaviour seen at denaturation is expected, as DNA is mostly single stranded at these high temperatures and therefore there are no minor grooves to bind.

2.3.2 Primer Design

The primers within a reaction dictate the section along a genome that is amplified, as well as the amplicon length. In the realm of diagnostics, they should ideally be designed to target a gene that is not prone to mutations, and unique to the pathogen of interest. Unfortunately, designing primers against a desirable gene is not sufficient on its own, as the reaction can still suffer from a phenomenon called primer dimerization (i.e., primer dimer formation). Primer dimers are the result of primers that hybridize to one another, as opposed to the target template, and are extended by the DNA polymerase causing unwanted strand synthesis. Since polymerases extend along DNA strands from the 3' to 5' end, favourable hybridization at the 3' ends of both primers will cause dimerization with higher efficiency. When this occurs at early stages of PCR, and the affinity of one primer for the other is strong, it can reduce reaction efficiency or cause a false positive signal. Since the validation assays in the following experiments rely on a DNA binding dye, dimers cause sigmoidal output signals similar to those of actual target amplification. It was therefore necessary to design a primer set that had a low binding probability at the 3' end (preferably none), as denoted by the change in Gibb's free energy (ΔG).

Another important consideration for primer design is the overall assay speed, and by extension the melting temperature. Reducing the overall change in temperature between denaturation and annealing can save substantial time in each PCR cycle, and this is mostly due to the annealing temperature. At annealing, the closer the sample is to ambient temperature, the slower the rate of convective heat transfer when rapid cooling is desired. It was therefore necessary to avoid lower primer melting temperatures.

CTC was analyzed for primer sequences using the NCBI Primer-BLAST tool. Self 3'complementarity, the ability of a primer to bind to another with the same sequence, was reduced to prevent amplification inefficiencies. The melting temperature was set to 60°C and higher, as cooling rates have been shown to slow at lower values. Once the primers have been generated, the most promising sets were verified for hetero 3' complementarity (binding between the forward and reverse primers at their 3' ends) on IDT's oligo analyzer tool. The primers that demonstrated no 3' binding or the lowest values of free energy changes for this parameter were selected. The CTC-6 primer set (see **table 2.1**) was selected, and its hetero complementarity analysis can be seen in **figure 2.4**. These primers worked exceptionally well at preventing dimer formation and will be further validated in a subsequent section of this chapter.

When primers bind further along their respective 3' ends, the polymerase has more room to extend, and the dimer amplicon lengths therefore increase and bind more dye molecules. In turn, this could cause a false positive sigmoidal curve. Other binding patterns between the primers can contribute to inefficient amplification as the primers get consumed in the early stages of PCR, however they are less likely to generate a measurable fluorescent signal. The primer design ultimately had a major focus on limiting hetero binding at the 3' ends.

Further raising the melting temperature of the primers could also contribute to dimerization prevention, as less time will be spent at the annealing step with faster cooling rates, and therefore there will be less time for primers to bind to one another at the early stages.

Another useful modification could be reducing the primer concentration to prevent self-3' complementarity and the probability of hetero binding.

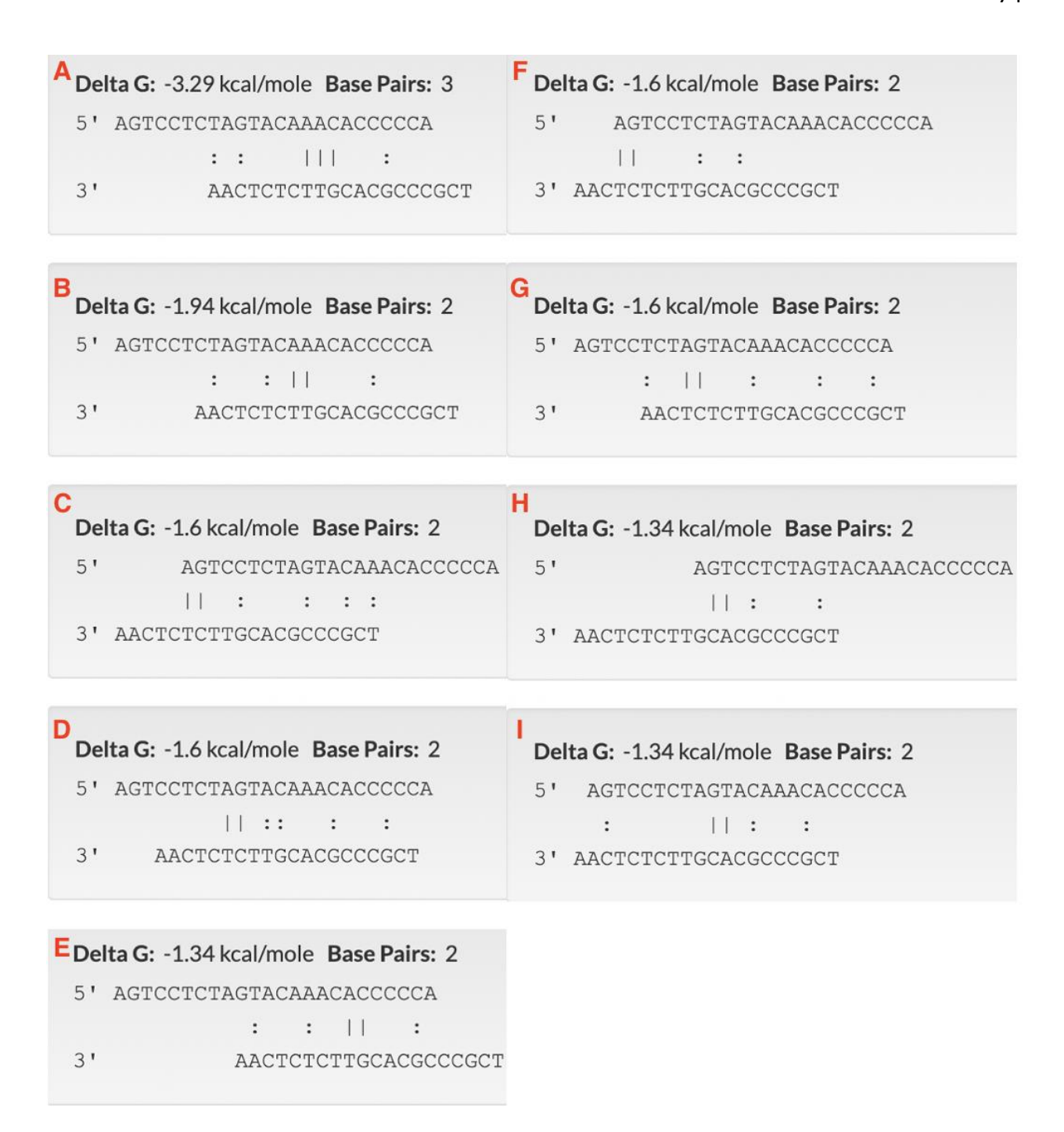


Figure 2.4: Hetero complementary primer dimerization scenarios for CTC-6 primers.

All scenarios demonstrate little to no affinity of the primers towards one another at the 3' ends. **(E)** The only situation presenting opportunity for polymerase extension, although primer dimer size would be very small. The free energy change of -1.34 kcal/mol is negligibly low.

2.3.3 Data Analysis Algorithm

As previously discussed, the POC plasmonic qPCR device uses SYTO-16 as a DNA intercalating dye to monitor amplicon in real time. Depending on the initial DNA copy number, the sigmoidal output signal, developed on a fluorescence vs. cycles plot, will shift to the left or right. At the end of the assay, the raw data will produce the curve, although due to unwanted background electrical noise, the generated data (as seen in **figure 2.5 (a)**) will not be clean. It was therefore necessary to fit a curve through the datapoints to better understand the mathematical parameters surrounding the signal and infer important information from them.

The algorithm shown in **appendix 1** takes raw excel data and fits it with equation 1.3 to generate a sigmoid curve, as shown in **figure 2.5 (b)**. All raw data is normalized by subtracting each point by the average baseline value to correct for discrepancies between channels and return a relative fluorescence gain reading. Additionally, all outlier datapoints within two standard deviations from the baseline are removed for the average calculation. Once a curve is plotted, the Ct value can be determined at the cross section of the linear portion of the sigmoid and the baseline, allowing for an accurate representation of the cycle at which amplicon is observed with certainty. Multiple curves can be fit to one plot, allowing for assessments of precision, as well as serial dilution related validation. As a result, limit of detection, limit of quantitation, and the standard curve can be directly inferred from the combined plotting. The algorithm can detect the coefficient of determination (R^2) describing the goodness of fit between 2 sigmoidal curves as an additional descriptive amplification parameter. Lastly, the algorithm calculates PCR efficiency using the serial dilution plots and the methodology described in *section 1.3.2*.

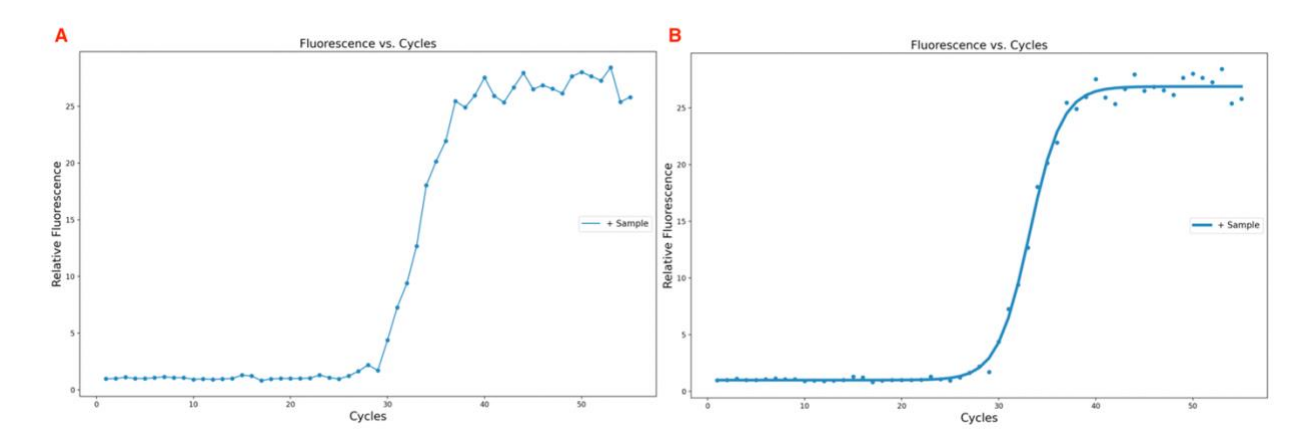


Figure 2.5: Raw relative fluorescence vs. cycles data plot from the POC plasmonic qPCR.

(A) Plot denoting raw datapoints connected linearly. (B) Plot denoting a curve 5-parameter curve fit through the same datapoints seen in (A).

2.3.4 Primer Dimer Characterization and Differentiation

As previously discussed, a cumbersome challenge in PCR presents itself in the form of primer dimerization. This phenomenon occurs when two primers, usually forward and backwards primers, bind together at their respective 3' ends and are subsequently extended by a polymerase creating primer dimers. If there is substantial affinity for one another, a detectable amount of primer dimer amplicon will be generated after many PCR cycles. The amplicon can maximally form an amplicon length measuring the total combined lengths of both primers involved. This phenomenon impacts the overall efficiency of the reaction seeing as primers are used up in an undesirable manner leaving less to amplify the target genetic material. The dimers present an even larger issue when using DNA binding dyes to monitor amplification, since dyes will not discriminate them from target template. While binding fluorescent tags do offer quantitative advantages over probe-based amplification, the formation of this unwanted product raises a justifiable concern for this monitoring method.

From a clinical standpoint, improperly designed primers should not interfere with high initial viral/bacterial load amplification; however, lower detection limits can be heavily affected or made impossible by the formation of dimers. Additionally, their signal can lead to false positive results in true negative samples. Point of care testing requiring the detection of substantially low pathogenic loads are most affected by dimerization, and in order to properly validate the capabilities of the POC plasmonic qPCR, it was necessary to be able to differentiate between output signals generated by primer dimers and true target template through analysis of the fluorescent ceiling, slope of the linear segment of the sigmoidal output fluorescence curve, and threshold cycle. This can also be achieved through melting curve analysis, which is a viable and effective measure of completing the same task; however, this device is geared to function

under time sensitive conditions. Curve analysis can be instantaneously conducted post-PCR, while melting curves are relatively time consuming and impose an additional timely step. In the scope of a POC device, this method of differentiation presents a quick and effective alternative to melting curves on the plasmonic POC qPCR. Additionally, the prototype device is not yet equipped to perform melting curve analysis as the current state of the VCSELs do not allow for slow controlled heating rates, which is one of the limitations of the machine.

Fluorescence Ceiling

The first point of differentiation lies within the fluorescent ceiling (plateau phase) values. This parameter compares the plateau values of template and dimer amplicon and discerns between them with statistical certainty. When designing primers, it is important to ensure that the length of the DNA sequence located between the forward and reverse primers exceeds the length of potential primer dimer formation. The reasoning behind this is that longer amplicon will be able to bind more dye molecules than shorter amplicon, and therefore will generate a larger output signal.

The CTC3 primers were used to assess the relative fluorescence signal gain in the plasmonic POC qPCR machine. 23 positive samples of 10² starting DNA copies and 42 negative no template controls (NTCs) were run consecutively in the POC plasmonic qPCR and their relative fluorescent values obtained via the data analysis algorithm. Relative fluorescence ceiling output values were collected from the positive and NTC (primer dimer producing) samples, and a study to determine statistical significance was conducted in RStudio. The normality assumption was first verified in **figure 2.6** to conduct confidence interval and hypothesis testing. A boxplot

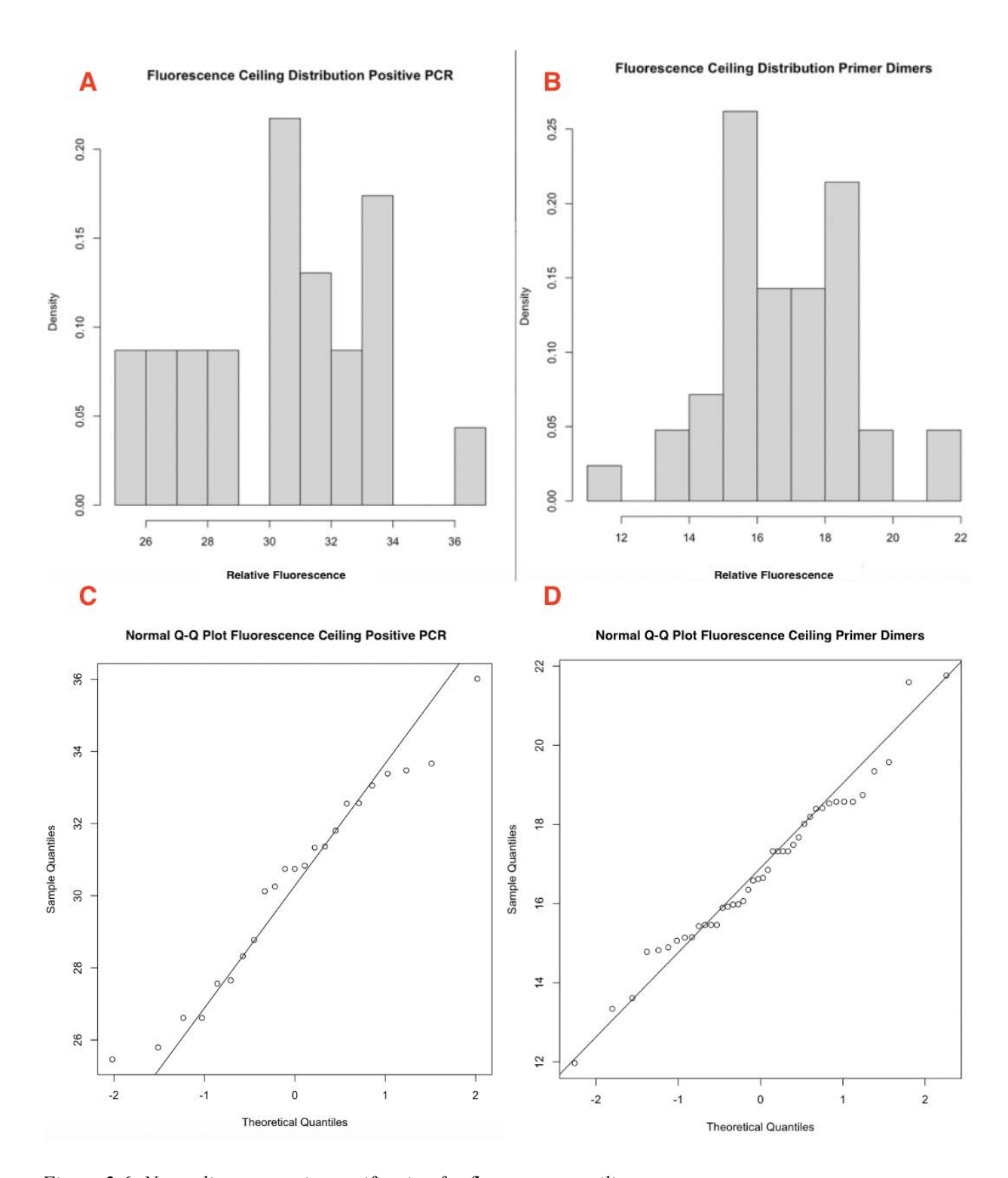


Figure 2.6: Normality assumption verification for fluorescence ceiling.

(A) Histogram of raw relative fluorescence ceiling data for positive samples. (B) Histogram of raw relative fluorescence ceiling data for primer dimers. (C) Quantile-Quantile (Q-Q) plot of relative fluorescence ceiling output for positive samples. (D) Q-Q plot of relative fluorescence ceiling output for primer dimers.

of the positive and primer dimer data as shown in **figure 2.7** was then created to demonstrate the mean fluorescence ceiling values and its deviation among both sample sizes. A 95% confidence interval was constructed around the means and difference in means of both groups, and finally a hypothesis test was done to verify the statistical significance of the results. Considering the small sample size in the NTC group and working under the assumptions of equal variance and normality, the hypothesis test of choice was the t-test.

The boxplot in **figure 2.7** clearly demonstrates a discernible difference between the positive and NTC values. Through the visual inspection of both the histograms and Q-Q plots, it can be seen that the datasets follow a normal distribution, rendering the use of the t-test and confidence interval generation valid. The positive and NTC samples returned mean fluorescence ceiling values of 30.37 and 16.8, respectively. Their standard deviations differ by a factor of 0.8, which is small enough to assume an equal population variance. The 95% confidence interval constructed on the positive mean is [29.13, 31.6], and [16.16, 17.46] on the NTC mean. After conducting the t-test under the assumptions, the R code returned:

```
t = 22.398, df = 63, p-value < 2.2e-16
alternative hypothesis: true difference in means is not equal to 0
95 percent confidence interval:
   12.35257 14.77271
sample estimates:
mean of x mean of y
   30.37478 16.81214</pre>
```

Under the defined calculate rejection region of [-1.998,1.998], the t-statistic value of 22.398 lies well outside the positive bounds. Additionally, the 95% confidence interval of the difference in means is [12.35,14.77].

Boxplot of +/- Sample Fluorescence Ceiling

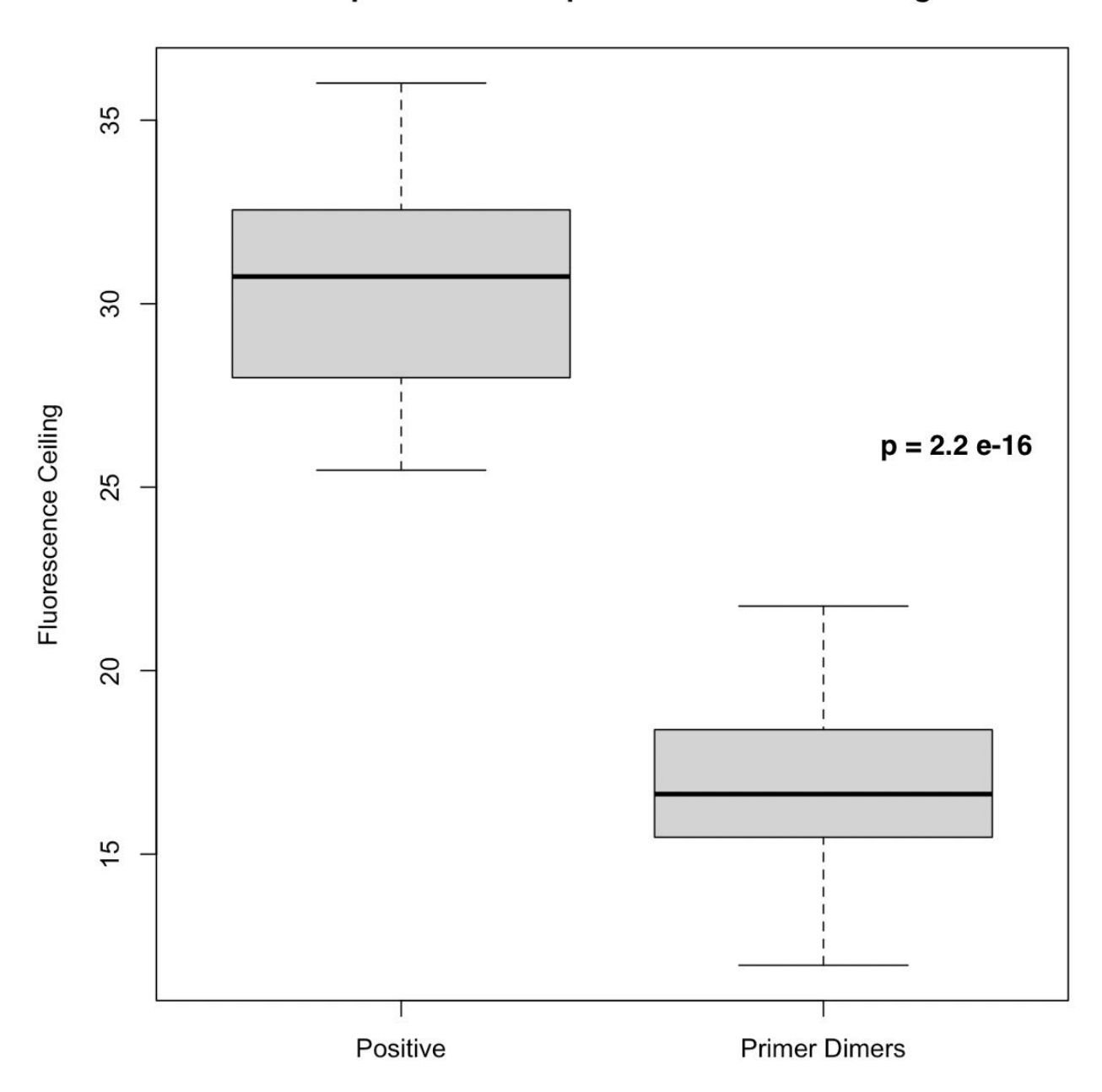


Figure 2.7: Boxplot of the relative fluorescence ceiling for positive samples and primer dimers.

Since the t-statistic lies outside the bounds of the rejection region, the null hypothesis can be rejected, and it can be concluded that there is a difference in the population means of the positive and NTC groups. Additionally, a p-value of $2.2x10^{-16}$ reports that the results of this t-test are statistically significant. This confirms the visual affirmations seen in the boxplot, and therefore this parameter plays a crucial role in discerning between false positive primer dimer amplicon signal and true template signal. As a quantitative measure, the 95% confidence interval of the difference in means for the CTC-3F and CTC-3R primers tells us that the true population difference in means lies within the [12.35,14.77] interval.

Slope of Linear Segment of Sigmoid Curve

Another interesting parameter that was studied was the slope of the linear portion of the generated sigmoid curve. The rationale behind this study is that the rate of fluorescence gain (which rises proportionally with generated amplicon) as a function of time (and thereby 'cycles' by extension) is a good indicator of instantaneous amplification efficiency. A primer's affinity for template in a properly designed reaction should greatly supersede its affinity towards itself or its complementary primer, and therefore it is hypothesized that the formation of dimers should occur with lower efficiency.

The CTC-3F and CTC-3R primers were used to evaluate this parameter. 21 positive samples of 10² starting DNA copies and 36 negative NTC samples were run consecutively in the POC plasmonic qPCR and their relative fluorescence sigmoid curves were generated via the data analysis algorithm. The linear portions of the output sigmoid functions were mathematically defined, and their slopes were calculated. The slopes of each positive and NTC sample were collected and, similarly to the previous parameter, a study to determine statistical significance was conducted in RStudio. To ensure the validity of using a t-test, the normality assumption was

verified using histograms and Q-Q plots (as seen in **figure 2.8**), and the standard deviations were calculated to verify the equal variance assumption. A boxplot was then generated for a visual representation of the disparity between the two groups' mean results and respective distributions. Lastly, a hypothesis test was conducted on the difference in the mean slope values in conjuncture with a 95% confidence interval determination to establish the statistical significance and interpretation of the results.

The boxplot seen in **figure 2.9** denotes discernible differences between the slopes of the two groups. Considering the smaller sample size of the positive group and the satisfaction of all the requirements and assumptions mentioned above, the t-test was selected following the same procedure as the previous parameter. The mean slope values for positive and dimer values are 4.82 and 3.14, respectively. The difference in standard deviations between the samples is 0.15, which is small enough to consider the equal variance assumption. The 95% confidence interval for the individual positive and NTC sample means are [4.51, 5.13] and [2.90, 3.37], respectively. After conducting the t-test in R, the code returned:

```
t = 10.879, df = 55, p-value = 2.506e-15
alternative hypothesis: true difference in means is not equal to 0
95 percent confidence interval:
   1.375006 1.996002
sample estimates:
mean of x mean of y
   4.822810 3.137306
```

Under the defined calculated rejection region of [-2.00, 2.00], the t-statistic lies well outside the positive bounds. Lastly, the 95% confidence interval of the difference in slope means between the 2 groups is [1.375, 1.996].

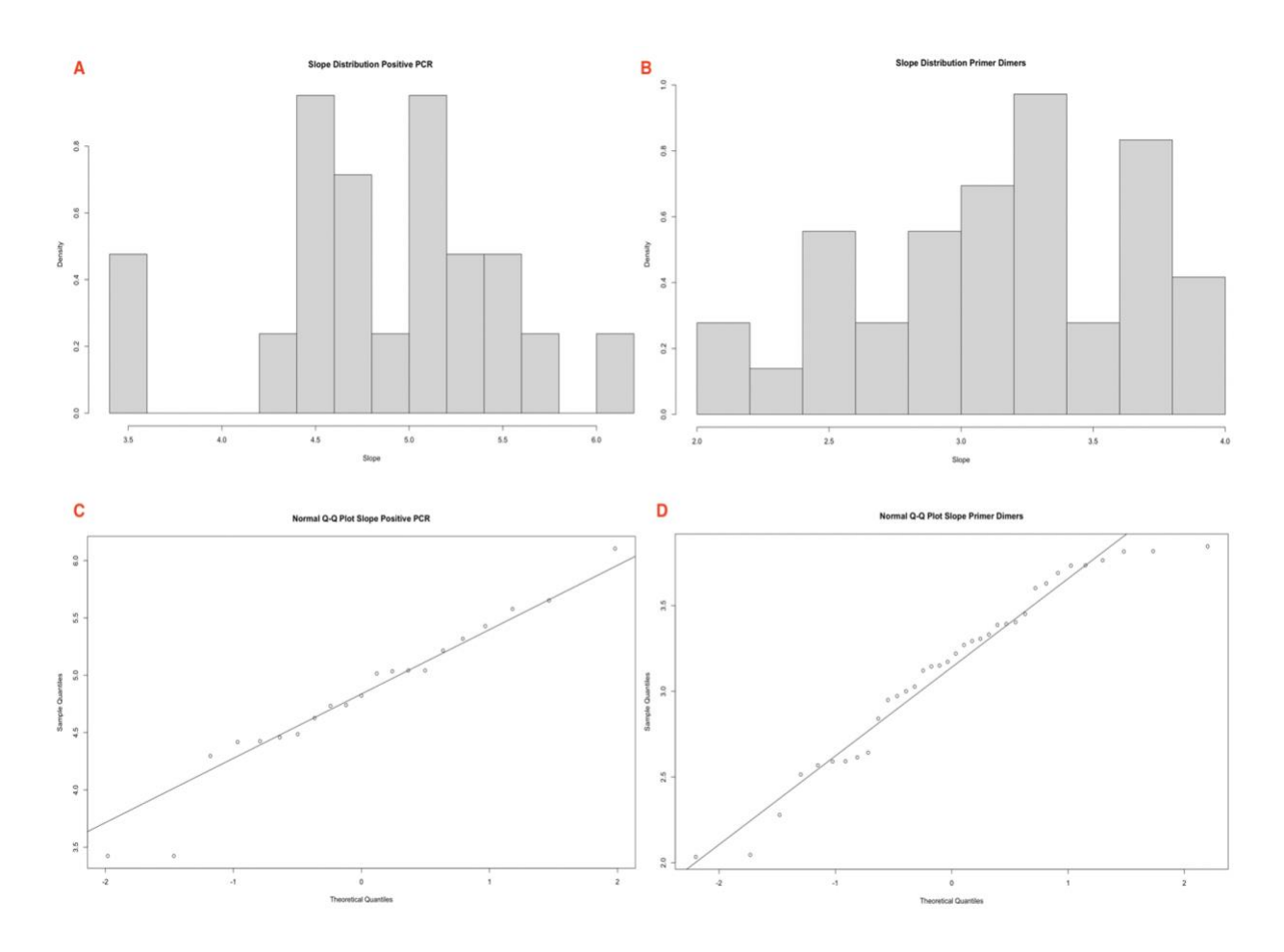


Figure 2.8: Normality assumption verification for the values of the slopes of the linear portion of the output sigmoid fluorescence curve.

- (A) Histogram of linear slope data for positive samples. (B) Histogram of linear slope data for primer dimers.
- (C) Q-Q plot of linear slope for positive samples. (D) Q-Q plot of linear slope for primer dimers.

Boxplot of +/NTC Sample Slopes

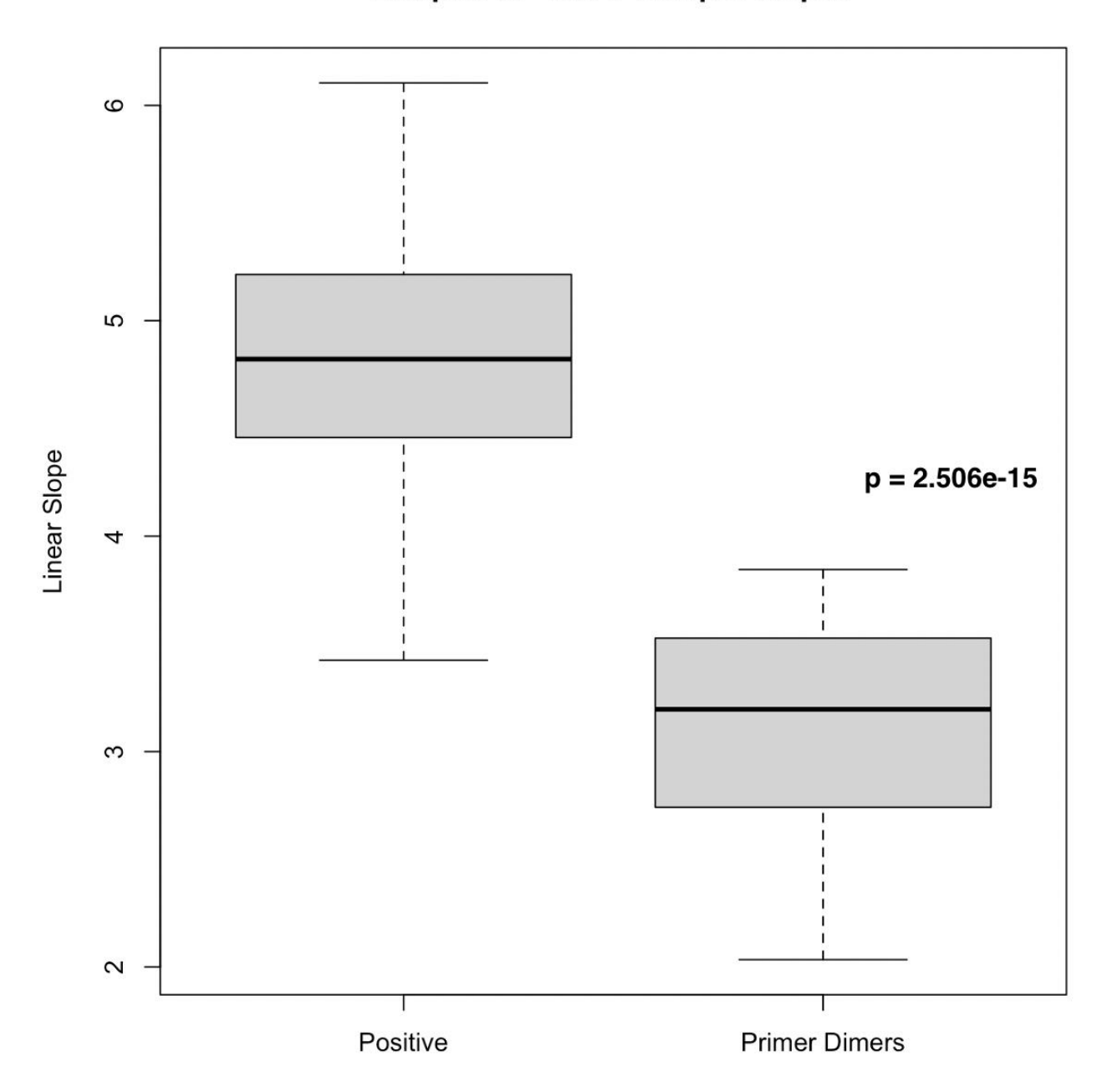


Figure 2.9: Boxplot of the slopes of the linear portion of the output sigmoid fluorescence curve for positive samples and primer dimers.

Since the t-statistic lies outside the bounds of the rejection region, the null hypothesis can be rejected, and it can be concluded that there is a difference in the population means of the positive and NTC groups. Additionally, a p-value of 2.506×10^{-15} indicates that the results of this t-test are statistically significant. This confirms the visual affirmations seen in the boxplot, and therefore this parameter plays a valuable role in discerning between false positive primer dimer amplicon signal and true template signal. As a quantitative measure, the 95% confidence interval of the difference in means for the CTC-3F and CTC-3R primers tells us that the true population difference in means lies within the [1.375, 1.996] interval.

Threshold Cycle

Another important parameter for the characterization of primer dimerization is the Ct value. As the affinity of one primer for another increases, the likelihood of dimer formation increases. Dimers form at the 3' ends of both oligonucleotides, and therefore is the area where caution must be exercised when designing primers. With increased affinity comes more efficient binding, and that is empirically reflected in the Ct value (i.e., the first instance at which amplicon is detectable with statistical certainty). Once primers are designed, a 95% confidence interval around the mean Ct value can be created and therefore infer the point at which signal is likely a false positive.

5 separate primer sequences were designed on the IDT OligoAnalyzer tool at various changes of free energy states for dimer formation at the 3' ends. The 3' hetero complementarity between both primers was the area of interest, as seen in **figure 2.10**, between the primers listed in **table 2.2**. Final concentrations of 0.3 μ M of each of the forward and reverse primers from each set were run in an NTC reaction 8 times. The output fluorescence signal was collected, and the



Figure 2.10: Highest contributing hetero 3' complementarity binding sequences and the respective Gibb's free energy changes (ΔG) of primers (A) CTC-W, (B) CTC-1, (C) CTC-2, (D) CTC-6, and (E, F) CTC-3.

Dotted lines have no impact on Delta G, and solid lines indicate base pair matching that do contribute to the Delta G.

Ct value calculated through the generated algorithm. The Ct values were then inserted into RStudio and a boxplot seen in **figure 2.11** was generated.

The means and standard deviations for the CTC-1, CTC-2, CTC-3, and CTC-W Ct values are 36.21 ± 0.56 , 27.98 ± 0.56 , 36.4 ± 1.09 , and 6.53 ± 0.78 , respectively. The CTC-6 primers were incredibly resistant to dimerization and did not produce enough dimer signals to complement this study. Their analysis can be found in a subsequent section of this chapter.

These studies demonstrate the importance of primer design when dealing with DNA binding dyes in the POC plasmonic qPCR machine. While primer design is an important factor in virtually all qPCR platforms, the ultra-fast nature of this device requires less time to be spent at annealing, and therefore properly designed primers can potentially take advantage of this property and mitigate dimer formation. The previous parameters can be used as a general measure to distinguish between dimers and product; however, this parameter is primer dependent. It is therefore advisable to run multiple repeats of NTC samples to determine its mean Ct value.

The primers that demonstrated high 3' hetero complementarity (CTC-W, CTC-1, CTC-2) all produced dimer signals at varying cycle ranges. Dimer formation (and the ensuing signal) can be caused by numerous factors, such as dimer amplicon length, GC% of the hybridized region, and nucleic acid (or excess primer) contamination, therefore we cannot assume direct proportionality between $-\Delta G$ and Ct value. The CTC-3 primers should not have been as prone to dimerization as they have demonstrated, and this could have been due to one of those factors. Fortunately, any unforeseen and unwanted behaviour from a primer set can be pre-defined and differentiated from true amplicon using all the discussed parameters.

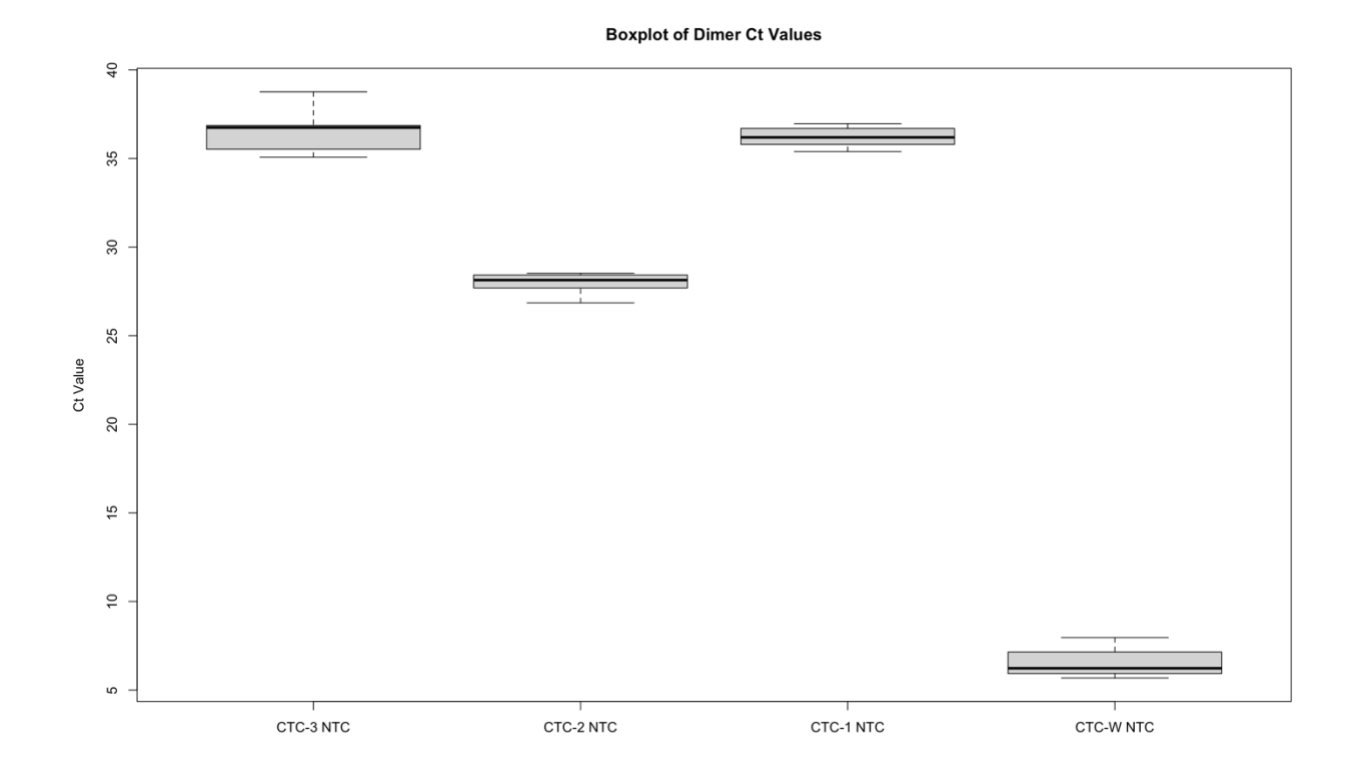


Figure 2.11: Boxplot of the Ct values of 8 NTC samples for 4 separate primer sets.

The CTC-W primers are most prone to dimer formation, followed by CTC-2, CTC-1, and CTC-3.

2.3.5 Limit of Detection, Limit of Quantitation

The LoD and LoQ are important metrics that determine the capabilities of a diagnostics device. They not only give insight into its sensitivity, but also into its potential range of applications. A highly sensitive assay will allow for the diagnosis of pathogens that require monitoring of very low genetic material loads. With respect to the POC plasmonic qPCR, the biological reagent design is of utmost importance to increase the overall sensitivity (i.e., increasing specificity using primers that are unlikely to form dimers), and the prior assessments can be used to accurately study the amplification and diagnosis of CT.

The CTC-6 primers were used in all subsequent assessments to reduce the likelihood of dimer formation and therefore increase the specificity of the assay. Ten-fold serial dilutions of CTC DNA control were made ranging from 10⁴ to 10⁰, as well as an NTC, with roughly 3-5 cryptic plasmids per genomic DNA. Each dilution was amplified 4 times in the POC plasmonic qPCR, and the lowest dilutions returning 4 positive signals were repeated an additional 20 times. The NTC was also repeated 20 times to assess the LoB. **Table 2.3** summaries the results of the LoD assessment, and the graphs in **figures 2.12 and 2.13** demonstrate a serial dilution containing one sample from each dilution conducted on the POC plasmonic qPCR, and the corresponding gel electrophoresis bands, respectively.

As seen in **table 2.3**, the POC plasmonic qPCR device is capable of detecting less than 10 starting DNA copies with 100% certainty, denoting its LoD. The LoQ is a function of the application in question and was found to be within the range of 10¹ starting CTC DNA copies. The 95% confidence interval around the LoD's mean Ct value of 37.07 is [36.75, 37.40], and the 95% confidence interval around the LoQ's mean Ct value of 32.51 is [32.31, 32.75], as seen in

Table 2.3: Summary of LoD Results.

	10 ⁴ DNA Copies / Rx	10 ³ DNA Copies / Rx	10 ² DNA Copies / Rx	10 ¹ DNA Copies / Rx	< 10 ⁰ DNA Copies / Rx	NTC
4x Repeats	4/4	4/4	4/4	4/4	4/4	4/4
20x	N/A	N/A	N/A	20/20	20/20	20/20
Repeats						

Successfully identified positive samples at each 10-fold serial dilution reaction (Rx). Row 1 denotes the initial 4x repeats at each dilution, and row 2 denotes the 20x repeats at the 2 lowest dilutions. NTC repeats assess the LoB of the assay.

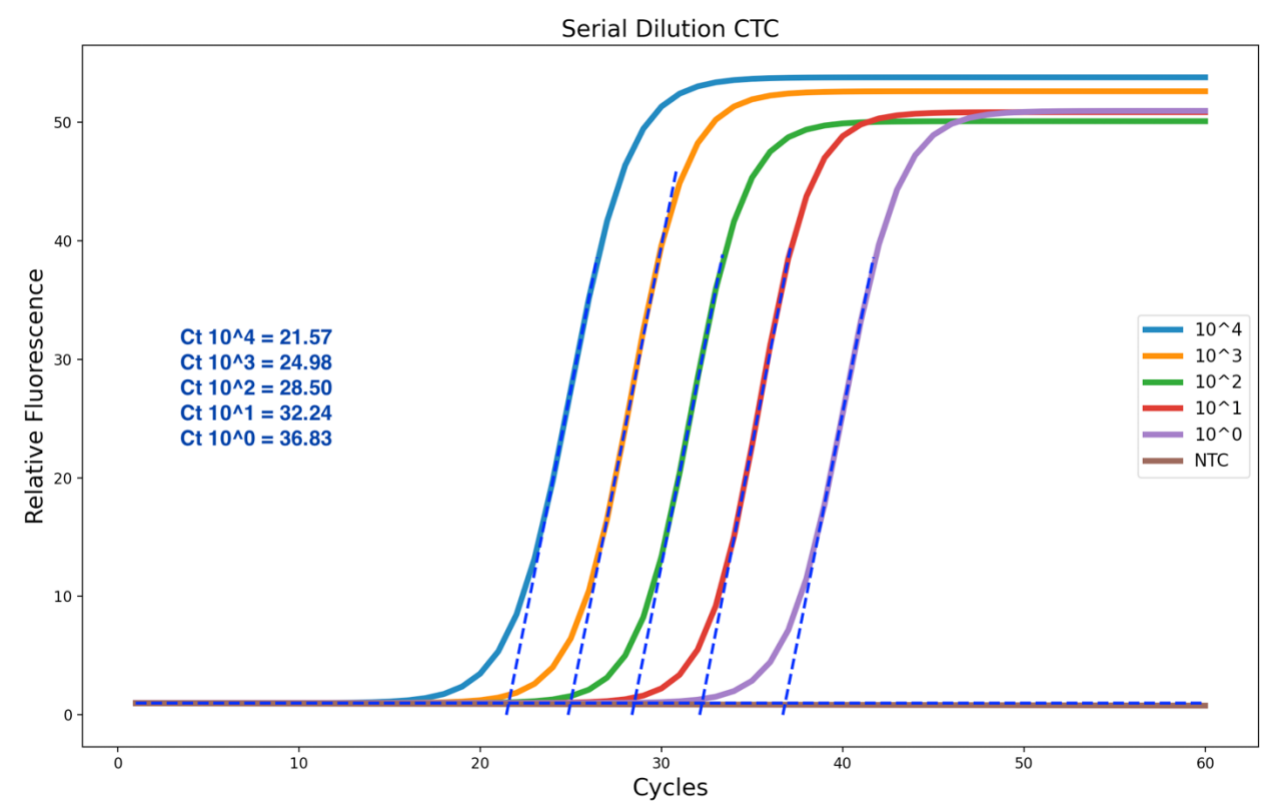


Figure 2.12: 10-fold serial dilution of CTC DNA from 10,000 to < 10 starting DNA copies, and an NTC.

The intersection points between blue diagonal hashed lines and the horizontal hashed line indicate the Ct values and are listed on the left-hand side. Sigmoid curves are in this figure are curve fits through raw datasets.

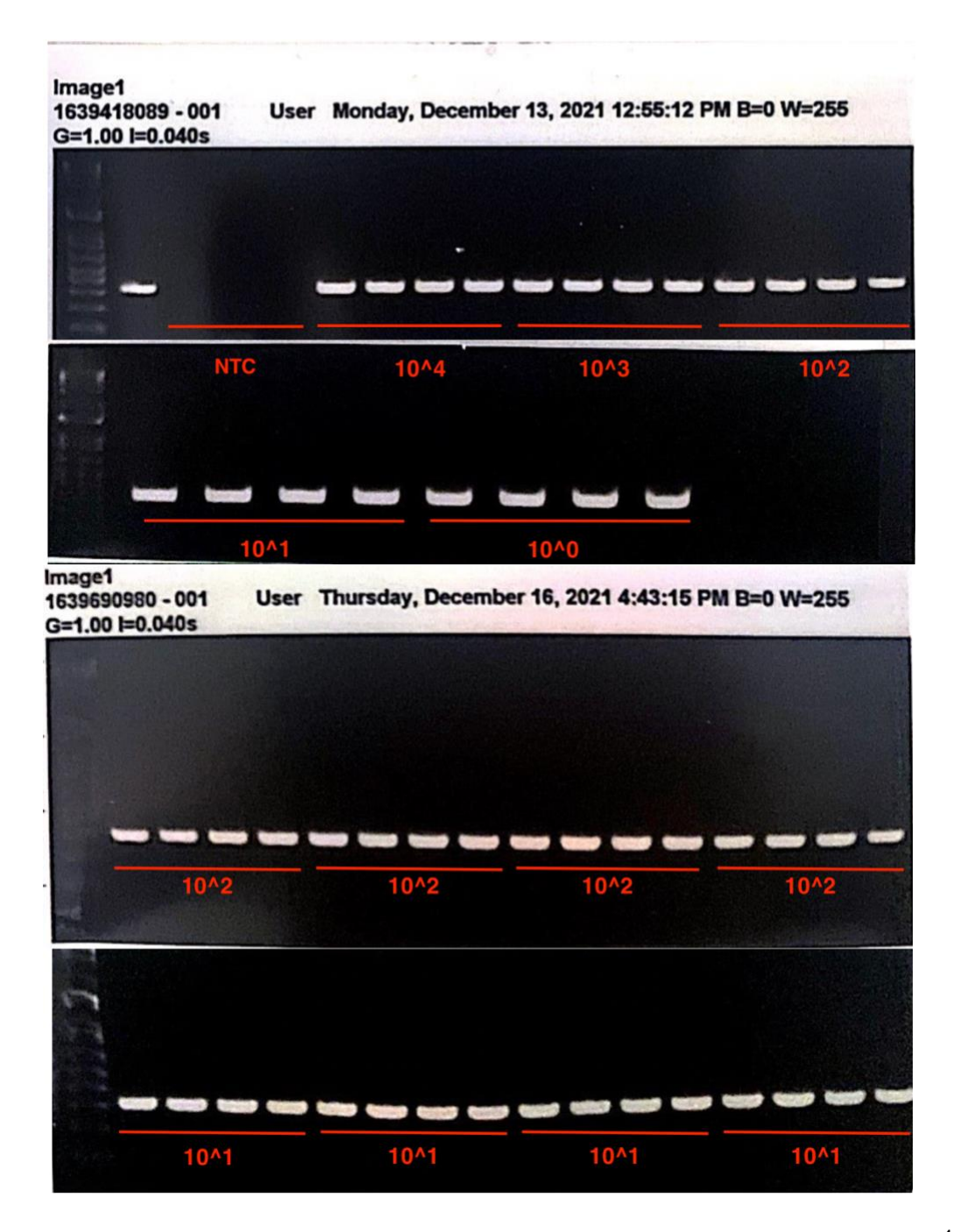


Figure 2.13: Gel electrophoresis image of the 4x repeats from the serial dilutions (NTC, $10^4 - 10^0$ initial DNA copies) in d_2H_2O , and 20x repeats of 10^1 and 10^0 dilutions.

Missing set of 4x 10¹ and 10⁰ were conducted on a separate gel. Generated amplicon length of 301 bp seen on the gel is dictated by CTC-6 primers. First band on gel does not belong to these experiments.

figure 2.14 (b). Additionally, the results presented in this figure give strong insight into the precision of the machine. The standard deviations for the 10^{1} and the 10^{0} dilutions are 0.53 and 0.76, respectively, which denote a very small variation in results generated from run to run and high precision.

The determination of the LoD of an assay is dependent on a linear relationship between the output signal and analyte concentration, i.e., a standard curve. As mentioned in the previous chapter, qPCR uses the Ct value (which is generated by fluorescence signal) as its output signal to generate a standard curve. The outstanding issue is that the Ct value and analyte concentration have a logarithmic relationship, and therefore linearization is necessary. The following standard curve seen in **figure 2.15** was generated in one channel on the POC plasmonic qPCR machine and correlates the Ct value and analyte concentration dilutions on a logarithmic scale. The linearity of the plot suggests a proportionality between fluorescence and DNA copy number, and therefore confirms normality among the signals produced at each dilution.

The first point of discussion focuses on the metrics used to distinguish a positive from a negative. The CTC-6 primers, which are normally highly resistant to primer dimer formation (data shown in a subsequent section in **figure 2.17**), produced a sigmoid response in the absence of target template. The previously discussed primer dimer differentiation parameters were used to analyze this unexpected response and compare it against positive amplicon output signals. A boxplot of the achieved relative fluorescence ceiling values for positive amplicon is presented in **figure 2.14** (a). The normality assumption was then verified using the aforementioned protocols, and a 95% confidence interval on the mean of 48.32 was determined to be [45.94, 50.69]. The false positive dimer signal generated a fluorescence ceiling value of 14.2 and slope of the linear

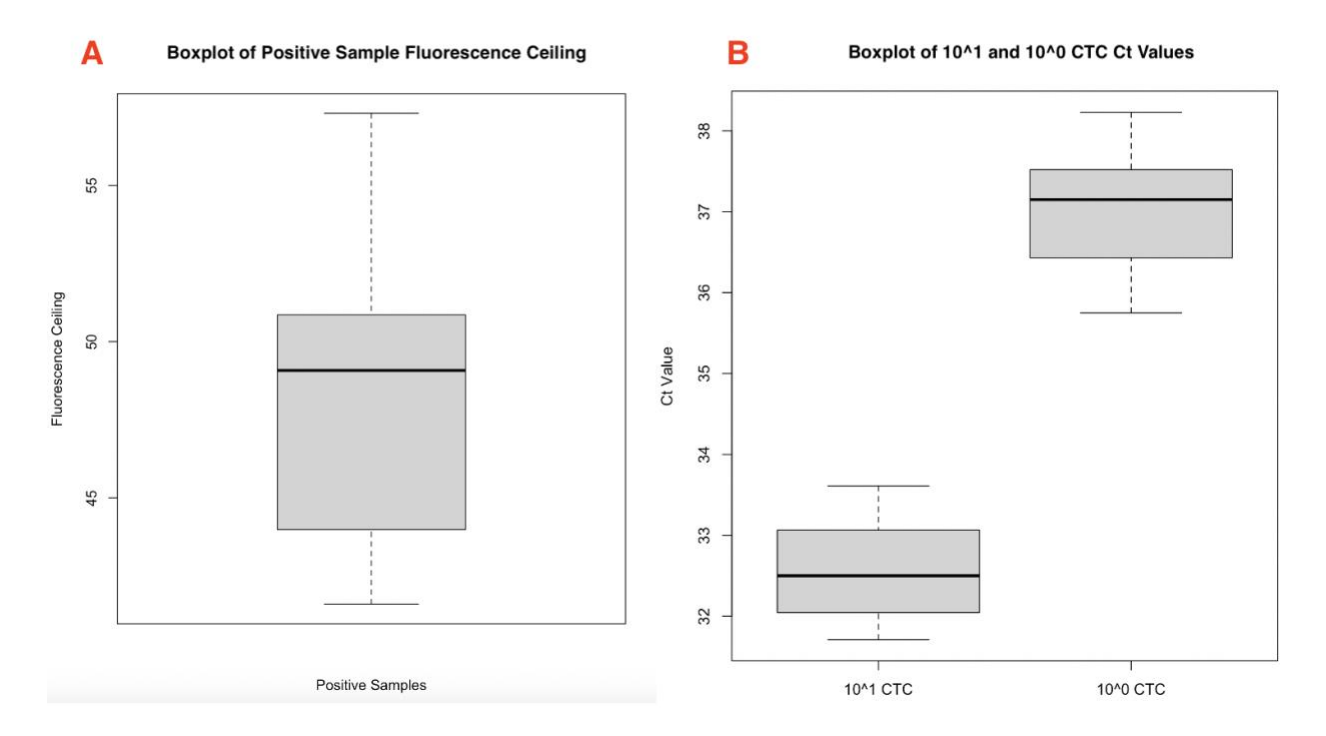


Figure 2.14: Boxplots of ceiling fluorescence and Ct value.

(A) Boxplot of 16 positive generated amplicon (length specified by CTC-6 primers) fluorescence ceilings used as a comparative measure against false positive signal. **(B)** Boxplot of Ct values for the 10¹ and 10⁰ (LoD) starting DNA copies, respectively.

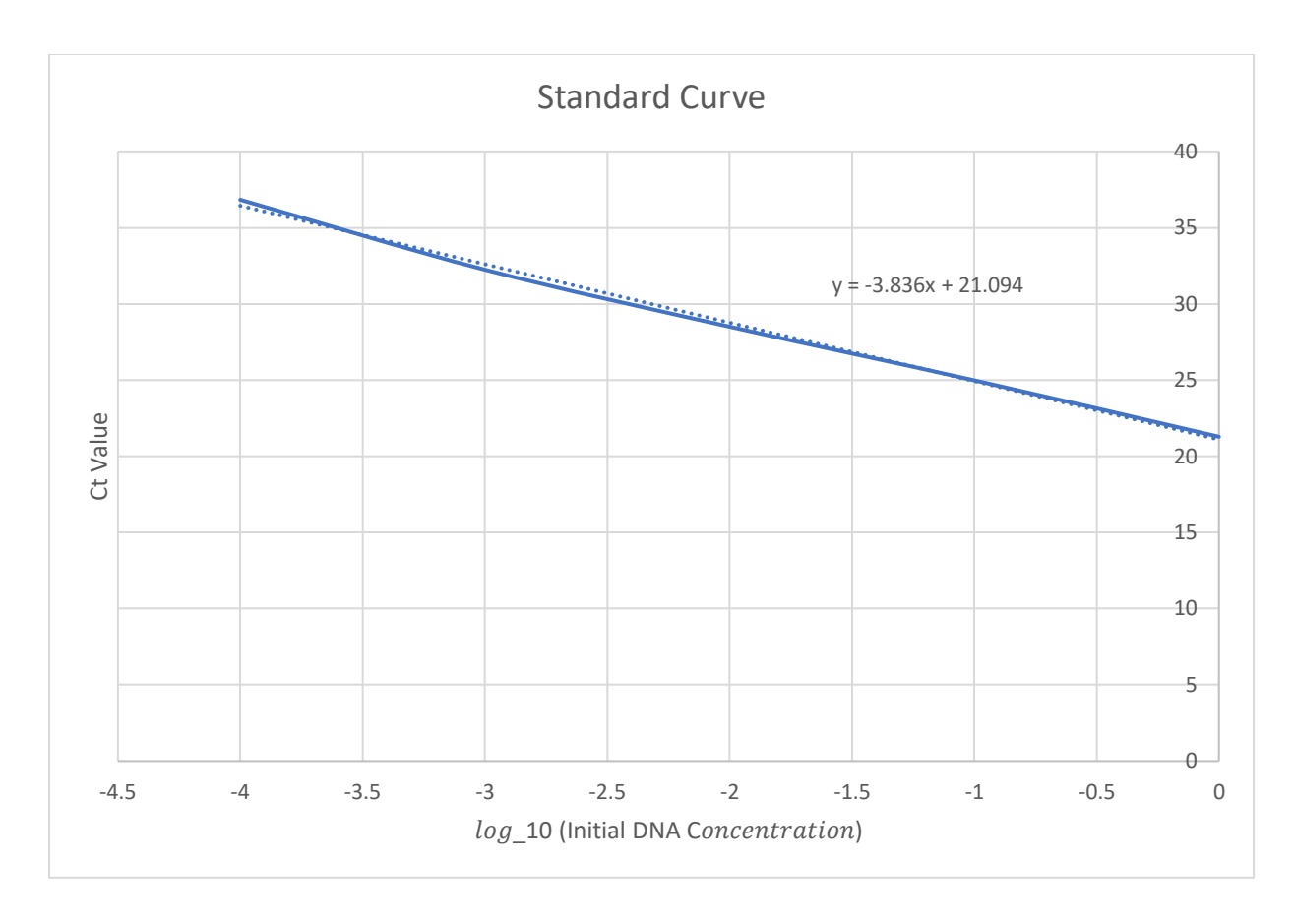


Figure 2.15: Standard curve of \log_{10} (initial DNA concentration) vs. Ct value generated on the POC plasmonic qPCR.

segment of its sigmoid curve of 2.459. The florescence ceiling value falls significantly outside the bounds of the confidence interval for a positive sample using the CTC-6 primers, and the slope value falls within the primer dimer range. The NTC sample that generated a sigmoidal signal was therefore deemed a true negative.

The second point of discussion revolves around the conditions leading to the LoD and LoQ determination. The samples were run on 4 separate channels, and the optical system measurements and outputs in each channel can differ from one another due to electrical noise and calibration differences. As such, the larger than expected range of relative fluorescence ceiling values seen in **figure 2.14** (a) can be explained. The most important information gained from this assay was the impact of primer design on the capabilities of the machine. The CTC-6 primers designed against dimer formation allowed for the detection of incredibly low initial material loads without compromising efficiency. Consequentially, the LoD of this machine can be said to be <10 starting DNA copies with 100% certainty, and its Ct value range is described with 95% confidence.

The LoQ is determined based on the application of the assay. For the purpose of CT testing, a previous study investigating bacterial loads in population-based screening and STI clinics was conducted [108]. Using qPCR to determine CT load, the research suggested a CT load range of $15x10^7$ (on vaginal swabs) to $4.9x10^4$ (in free void urine (FVU)) organisms/mL. Another study conducted by *Blocker et. al.* (2002) used ligase chain reaction to quantify CT elementary bodies in urine samples. The group collected 158 urine samples from women in Madagascar that test positive for CT, and their results found that 63% of samples (majority) ranged from 1086 - 218670 elementary bodies/mL. U Based on these results, we can determine the LoQ to be roughly 10^3 starting DNA copies. Using the lower load limits of both studies and

making a conservative assumption of 5 cryptic plasmids per organism, after aliquoting 11.3 μL of a 2.5% FVU dilution into a 20 μL POC plasmonic qPCR reaction, there are roughly 3460 and 25 plasmids based on the results of the first and second study, respectively. Based on the bacterial loads presented in these thorough studies and the capabilities of the POC plasmonic qPCR, the LoQ is found to be within the range of 10^{1} .

2.3.6 PCR Efficiency

PCR efficiency is a measure of the ratio of actual generated amplicon to the theoretical expected amplicon generation in any given PCR cycle. This is an important characteristic of the POC plasmonic qPCR as it gives insight into whether there are unwanted trade-offs made as a result of excess cycling speed, or if the machine is functioning up to research and clinical diagnostics standards. PCR theoretically amplifies exponentially with a function of $2^{\#cycles}$, although this is never the case in reality. The above equation can be therefore re-written as $(1 + \rho)^{\#cycles}$, and the efficiency coefficient ' ρ ' can be derived.

The procedure to determine the efficiency is derived from section *1.3.2*. The python algorithm selected an arbitrary value of fluorescence intersecting the linear portions of serial dilution sigmoid curves and recorded the corresponding cycle values. These cycle values were then plotted against the log₁₀ (initial DNA concentration), and the standard curve seen in **figure 2.16** was created. A linear trendline was then generated through the data, and the slope was recorded to calculate the efficiency coefficient. Four serial dilutions were run on the POC plasmonic qPCR and their efficiencies were calculated to generate an average value.

Results: Four dilution series were conducted from 10⁴ to 10¹, and their efficiencies were calculated to be 91.90%, 93.37%, 81.4%, and 86.5%, with an average value of 88.3%. With the inclusion of the 10⁰ dilution, the reported efficiencies were 84.15%, 83.35%, 76.35%, and

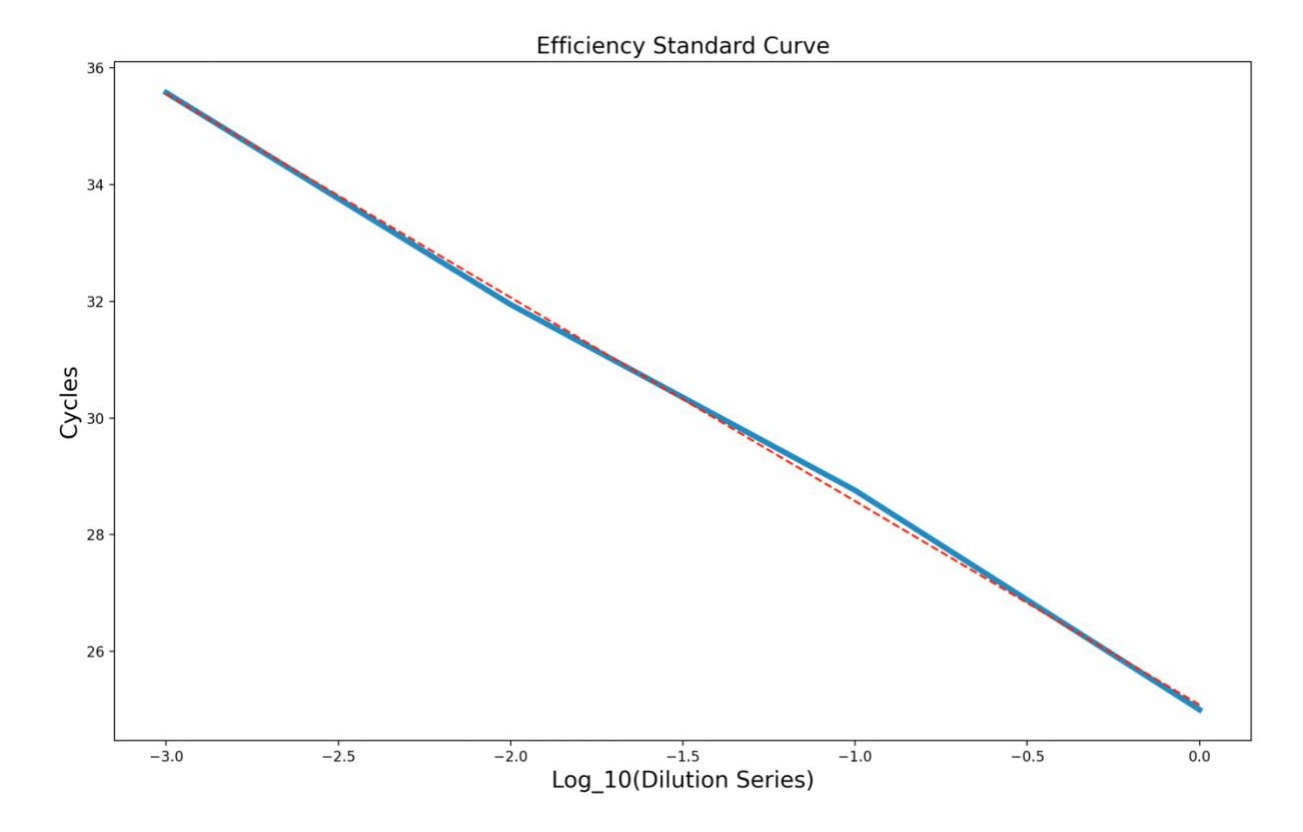


Figure 2.16: Efficiency standard curve.

Logarithmic scale of 10-fold serial dilutions (largest dilution denotes as 1) vs. cycles at arbitrary fluorescence point intersecting the linear segment of each dilution sigmoid curve. Blue line represents the raw data connected linearly, and dashed red line represents the linear curve fit through the raw datapoints.

83.16%, with an average value of 81.75%. To interpret these results, it can be said that the assay creates 88.3% or 81.75% (with and without the inclusion of the 10⁰ dilution, respectively) of the expected final amplicon amount. The gel electrophoresis image in **figure 2.13** confirms the positive amplicon generation of each dilution in the series.

The efficiency values obtained are very promising considering the ultra-rapid nature of the machine, essentially indicating that there are negligible trade-offs made for the assay's speed. The dilutions were done on separate channels, and this could explain the discrepancies between the 4 sets of values. In the specific machine used for analysis, channel 3 seems to be slightly more inefficient than the other channels, and as previously mentioned, this can be attributed to the fact that each channel is equipped with individual monitoring systems that can be uniquely affected by noise or calibrated differently from one another. Lastly, the incorporation of the 10^o dilution lowered the overall efficiencies in every channel. This can be attributed to the fact that the effectiveness of the initial cycles of PCR may be slightly compromised due to the incredibly low template number in the sample.

2.3.7 Sensitivity and Specificity

Sensitivity and specificity are important benchmark tests when validating a novel diagnostic device to ensure its successful translation into clinical settings, as well as its ability to properly diagnose positive and negative samples. The sensitivity and specificity tests use a "gold standard" assay to confidently verify positive and negative samples, respectively, and those samples are then tested on the device in question. Using equations 1.13 and 1.14, the sensitivity and specificity can be calculated.

The gold standard reference test used to validate the sensitivity was an Eppendorf conventional Peltier block PCR machine. 80 samples spiked with CTC control DNA (60 in

 d_2H_2O and 20 in urine diluted to 2.5%) were tested in the reference machine, and again in the POC plasmonic qPCR. An additional 30 NTC samples (26 in d_2H_2O and 4 in urine diluted to 2%) were run through the same protocol to determine specificity. CTC-6 primers were used for their reduced affinity for dimer formation. The gel electrophoresis images of each sample were then collected, as well as their fluorescent outputs.

The results of the sensitivity and specificity tests are summarized in **table 2.4** and organized according to **figure 1.11**. The calculated sensitivity and specificity are both 100%. **Figures 2.13, 2.17, and 2.18**, demonstrate the gel electrophoresis results for the 60 positive samples in d_2H_2O , the relative fluorescence curves of those same 60 samples and 26 NTC samples in d_2H_2O , and the gel electrophoresis and relative fluorescence curves of the 20 positive and 4 NTC clinical samples, respectively.

The sensitivity and specificity are near perfect based on the assays performed. This level is attainable due to the nature of the primer design, allowing for the discrimination between a 10^0 sample and an NTC by ensuring a low affinity for dimerization. In the instances where dimer formation does present itself, the studies conducted previously provide excellent benchmarks against which the signal can be deemed a false positive.

2.3.8 Clinical Sample Validation

The LoD and efficiency assessments were conducted with d_2H_2O as the dilution medium, although the POC plasmonic qPCR is a device aimed at being utilized in a clinical setting. It was therefore crucial to assess its abilities using clinic media as opposed to d_2H_2O and verify whether amplification was possible to a comparable extent. This would facilitate sample preparation (i.e., by removing DNA extraction steps) and save time to allow for quicker on the spot test-to-result turnover. A troublesome issue that could arise with the use of clinical media is

Table 2.4: Summary of Sensitivity and Specificity Results.

	Gold Standard	Gold Standard	Total
	Reference Test (+)	Reference Test (-)	
POC Plasmonic	TP = 80	FP = 0	80
qPCR (+)			
POC Plasmonic	FN = 0	TN = 30	30
qPCR (-)			
Total	80	30	110

Summary of the sensitivity and specificity assessments for 110 total samples. Gold standard reference test refers to positive and negative samples verified through an Eppendorf conventional PCR machine. TP = True Positive, FP = False Positive, FN = False Negative, TN = True Negative.

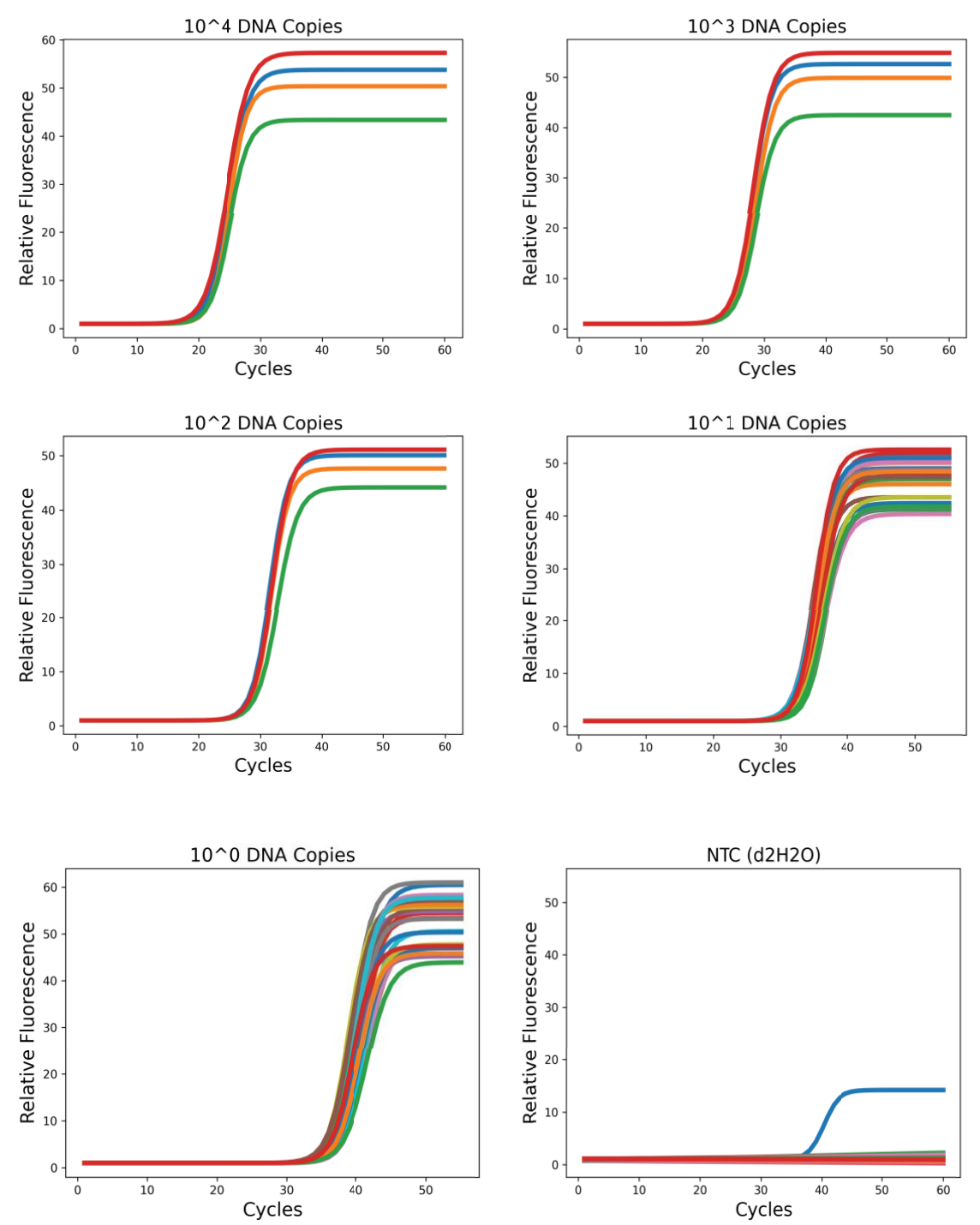


Figure 2.17: Relative fluorescence curves of 60 positive CTC DNA and 26 NTC samples in d_2H_2O .

Positive samples were tested at 5 different dilutions from $(10^4 \text{ to } 10^0)$, plotted individually, and confirmed positive by conventional PCR. 10^4 , 10^3 , and 10^2 dilutions were repeated 4 times, and 10^1 and 10^0 were repeated 24 times. NTC samples were run for 60 cycles, of which one produced a false positive (primer dimer) signal.

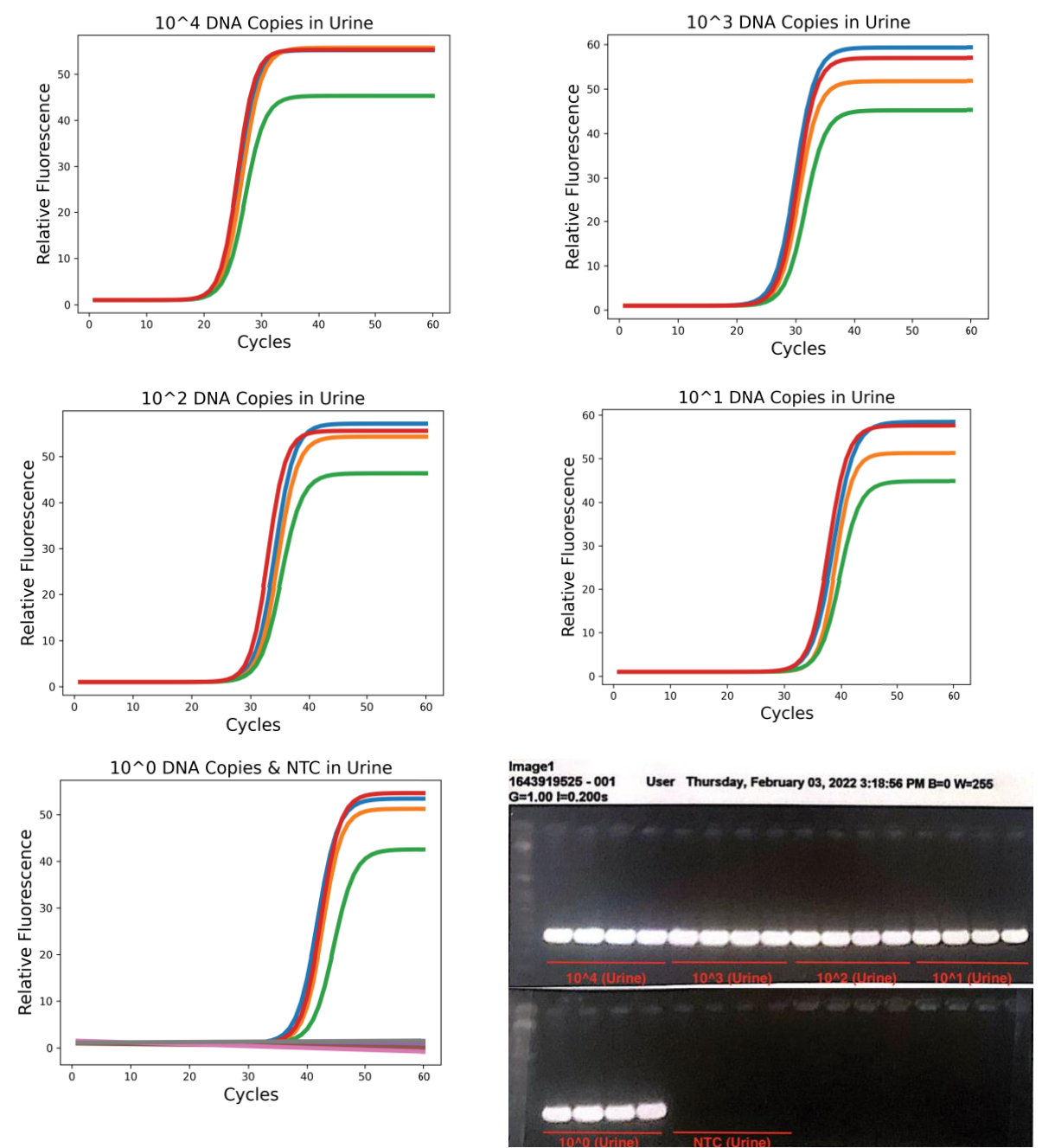


Figure 2.18: Relative fluorescence curves of 20 negative clinical urine samples spiked with 10-fold serial CTC DNA dilutions from $10^4 - 10^0$ copies, 4 NTC samples, and their corresponding gel electrophoresis results.

Each graph represents 4 repeats of each dilution, and the NTC fluorescence curves were combined the 10¹ dilutions.

the risk of PCR inhibitory substances that can exist within samples, and therefore determining the appropriate dilution factor is of utmost importance.

Clinical urine that tested negative for CT by conventional PCR was diluted to 20%, 10%, 5%, and 2.5%, and spiked with 10^4 positive CTC DNA. Each dilution replaced the 11.3 μ L of d_2H_2O normally used for a 20 μ L reaction. 4 repeats of each were tested on the POC plasmonic qPCR using CTC-6 primers, and their fluorescent output signals collected and verified via gel electrophoresis.

The electrophoresis image from the spiked urine samples can be seen in **figure 2.19**. Any urine dilution more concentrated than 5% yielded a failed PCR. The 5% dilution returned signal, although the reaction was heavily affected. The 2.5% final dilution allowed for DNA amplification and was used for a serial dilution as seen in **figure 2.18**.

The data presented shows that a dilution between 0-5% is the window of functionality. The first sample in the 5% final dilution shows band sizes that do not coincide with the expected amplicon length dictated by the CTC-6 primers, and therefore appear to be non-specific amplification along with a primer dimer signal. The reasoning behind this is unknown, but urine can contain many compounds that affect amplification. The 10% and 20% final dilutions are far too large and did not generate any amplicon. The final dilution of the urine used in **figure 2.18** was 2.5% and demonstrated amplification capabilities similar to that of d_2H_2O dilutions. The serial dilutions of 2.5% urine showed the ability to detect < 10 DNA copies. Notably, the presence of urine delayed Ct values among the samples and proved to return results that are less consistent and therefore less quantitative.

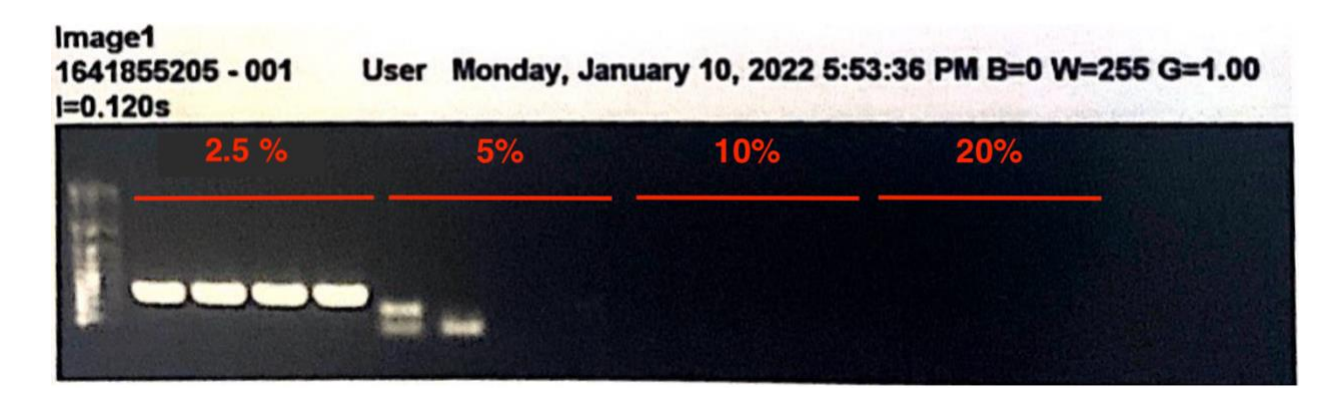


Figure 2.19: Gel electrophoresis image of final urine concentration dilutions.

4 repeats of control, 5%, 20% and 20% final dilutions are shown.

Chapter 3

3.1 Diagnosis at the Point of Care

3.1.1 Defining Point of Care

The 4-channel POC plasmonic qPCR is a device that is meant to be used at the point of care. This concept was repeatedly discussed throughout this thesis; however, it is important to understand what makes a diagnostic device truly "POC" and how it fits within its criteria. The most notable definition is described by *James. H. Nichols, PhD (2007) [109]*, who defines POC testing as "laboratory diagnostic testing performed at or near the site where clinical care is delivered". He discusses the ever-evolving world of patient care where physicians face pressure to see an increased number of patients. Under this definition, treatment can be conducted in a faster manner through the elimination of centralized testing centers, and the number of patients seen can be facilitated. Many POC devices use a wide array of small amounts of direct clinical analyte for testing, ridding of the need for extensive pre-analytic work such as genetic material extraction steps.

The POC plasmonic qPCR machine aims at improving upon this definition with increased assay sensitivity and specificity over traditional POC devices. There currently exists very few POC PCR machines in circulation; however, many POC devices are currently in used across a wide array of applications. More recently, throughout the SARS-CoV-2 pandemic, rapid antigen and nucleic acid detection tests received EUA by the FDA [110, 111]. These assays fit within the confines of the definition above since they are easily accessible, generate results rapidly, and are conducted outside of centralized locations (often at the homes of patients). The issue with many of these tests is that they are highly insensitive, with the rapid antigen test

owning a sensitivity of roughly 65-67%, and do not truly offer the quality seen in testing laboratories [112, 113]. With the introduction of the POC plasmonic qPCR, the definition of POC is being further expanded to include highly sensitive and specific rapid testing at the site of clinical care.

3.1.2 Value of PCR as a Point of Care Tool

As mentioned, the POC plasmonic qPCR sets to improve upon the current definition of POC. Many POC devices are designed to detect specific analytes; however, this PCR machine is highly adaptable to diagnose a wide variety of pathogens. *Chlamydia trachomatis* was selected as the pathogen of interest within this thesis as the template to validate the performance of the device because of the vast applicability to the world of STI diagnostics.

Within the clinical setting of STI diagnostics, many patients are screened against several pathogens and wait multiple days before discovering their results. Physicians often prescribe broad-spectrum antibiotics before an official diagnosis to prevent further infection, which contributes to the continually increasing issue of microbial resistance. Consequently, patients who ultimately test negative were given antibiotics unnecessarily, and patients who test positive were given a treatment that was not specific to their infection. A POC diagnostic device can greatly assist physicians in these clinics to make accurate and personalized treatment plans without having to wait for time consuming result generation from centralized laboratories. As a result, more patients can be tested, and broad-spectrum antibiotics can be eliminated as a treatment option.

Beyond STI clinics, POC diagnostics have proven to be necessary for a wide array of other infectious diseases. Most notably, the SARS-CoV-2 pandemic has demonstrated a massive demand for testing and the severe consequences of lengthy test to result turnover times.

Throughout the beginning of the pandemic, PCR received EUA by the FDA, although the inconvenience of centralized testing locations and the inherently time-consuming nature of the assay made it so that demand could not be kept up with. Consequentially, testing was often limited to those who presented themselves with symptoms and many infectious asymptomatic patients went undiagnosed or did not seek testing. These limitations directly contributed to the rapid rate of transmission and encouraged the initial propagation of the virus. A POC qPCR device would have been of great use throughout the entirety of the pandemic, allowing patients to discover their results within a short time after testing, and take appropriate and immediate quarantine measures to avoid compromising public health.

3.2 Point of Care Diagnostic Tests

POC devices have been in circulation for years, although they've gained popularity since the beginning of the SARS-CoV-2 pandemic. There are a wide variety of them for an array of different applications to improve patient care efficiency and treatment plans; however, some offer substantial advantages over others, such as increased sensitivity and specificity, rapid test speed, simplicity, and reduced costs. The following technologies are a few of the many available devices in circulation today that highlight the important aspects of POC and share common goals with the POC plasmonic qPCR machine:

POC Rapid Antigen Test

As previously discussed, rapid antigen tests have received EUA by the FDA throughout the SARS-CoV-2 pandemic. These tests use cost effective and quick lateral flow assays, where a direct clinical swab sample is suspended in an extraction solution and the virus antigen proteins are released. A portion of this solution is then applied to a test strip that is prepared with SARS-

CoV-2-antigen-specific antibodies bound by luminescent indicators, and as the antigens migrate through the strip, their interactions with antibodies create positive-indicating colours [114].

These tests encompass an important POC characterization – testing at the patient's bedside. With rapidly increasing demand for PCR testing and the evolving nature of the virus and pandemic, immediate result generation outside of both centralized testing locations and clinics were offered. One vital caveat that accompanies antigen testing is the low sensitivity that they provide. Assays that are not sensitive will only positively detect analyte if there is a large abundance of it present in the measured sample. With respect to the SARS-CoV-2 antigen test, only those individuals with very high viral loads (and therefore most likely symptomatic) benefit from these rapid tests, meaning a large portion of the asymptomatic infected community falsely test negative. This is referred to as a "rule-in" test, indicating that it cannot be singularly used as a test to rule out infection, however a positive result is most likely indicative of infection [115]. As such, these tests are mainly used to identify patients that are infectious (can transmit the virus), and act as compliments to the PCR assays located in centralized laboratories which are far more sensitive albeit time consuming. Figure 3.1 demonstrates the drastic LoD differences between the rapid antigen test and other more sensitive tests given EUA, as well as their effectiveness in clinical settings [116]. Noticeably, the Sofia2 antigen test has an LoD at least 10,000 times higher than the more sensitive EUA tests. Additionally, at an LoD value this high, this device is only expected to be able to detect ~31% of clinical cases – reaffirming its major disadvantage.

While low sensitivity is a substantial limitation, there are still many benefits to using these tests. Firstly, those that are symptomatic and are positively diagnosed can be confident in the accuracy of their result, thereby preventing uncertainty and further compromising public

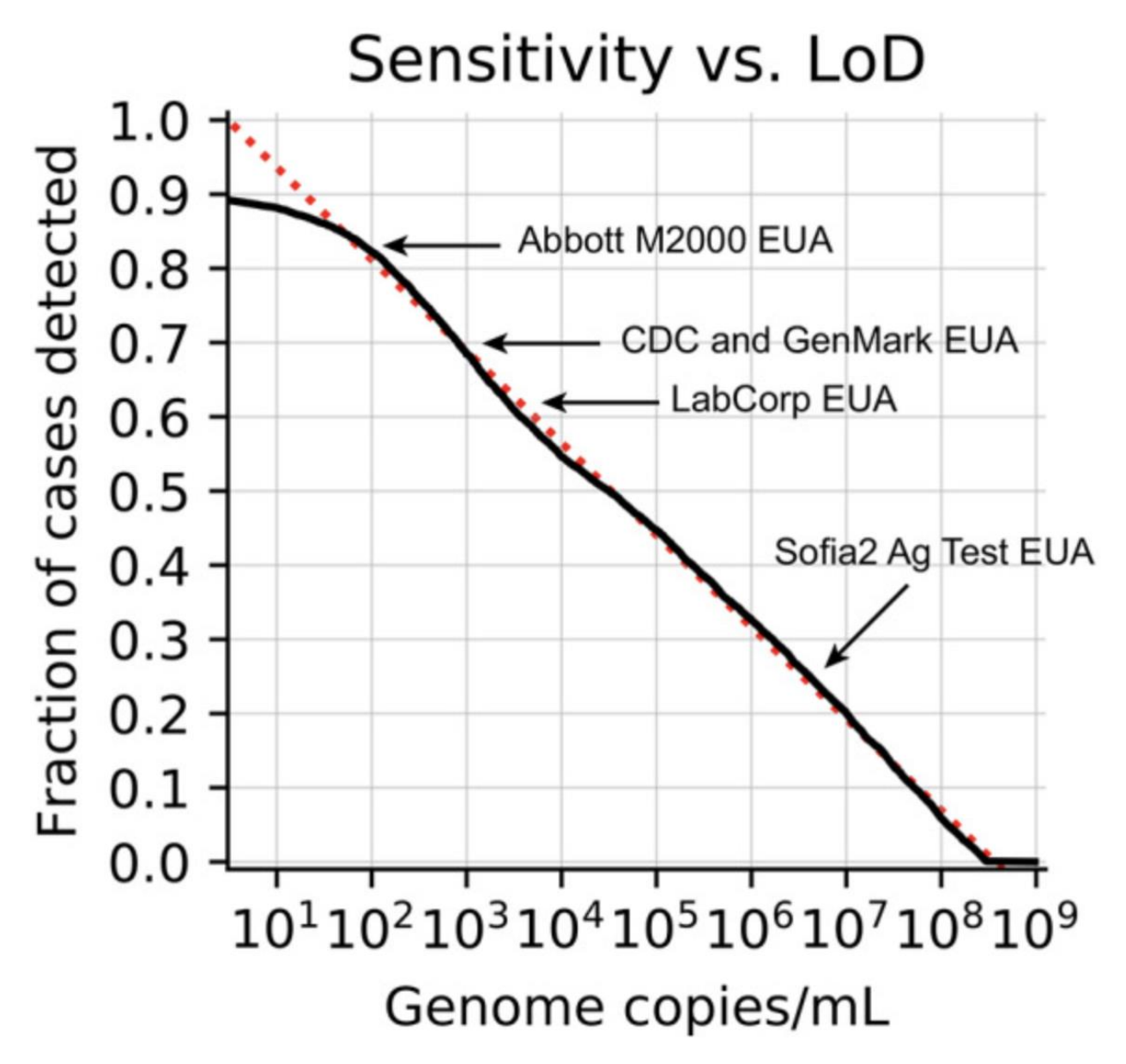


Figure 3.1: Graphic depicting fraction of clinical cases detected vs. LoD (genome copies/mL). Intersection points along the axes indicate the expected fraction of clinical cases a device will detect at its given LoD. Solid line represents actual correlation, dotted line represents trendline. 5 EUA SARS-CoV-2 detection assays are shown, where the Abbott M2000, CDC, GenMark and LabCorp EUA assays are PCR technologies, and the Sofia2 Test is an antigen test.

health. Secondly, post diagnosis, infection monitoring is possible as a result of the test accessibility. In accordance with the capabilities and limitations of the test, the CDC released a decision matrix flowchart in 2020 to allow the public to better understand how to interpret their test results and what subsequent actions to take (as seen in **figure 3.2**) [117]. This flowchart is continuously modified with the evolution of the pandemic and its implementation varies within different governmental bodies. The general idea is that the symptomatic positive diagnosis is detected with high certainty and does not require further validation; however, positive antigen tests from asymptomatic individuals require additional PCR testing to rule out the rare false positive result. If an individual is symptomatic and obtains a negative result rapid test, the sensitivity is too unreliable to rule out infection and a PCR test is recommended. Additionally, any negative results obtained while asymptomatic are considered low risk and judgment should be used when deciding on how to proceed.

POC Isothermal Nucleic Acid Amplification Test

A POC isothermal nucleic acid amplification test is one that amplifies genetic material from a low to high copy number at a constant temperature at the point of care (i.e., LAMP. See section 1.2.1). The Abbott ID Now [118] is a rapid molecular diagnostic test that utilizes isothermal nucleic acid amplification technology targeting the RNA-dependent RNA polymerase gene. The device conducts a qualitative POC assay that claims to detect positive and negative results in as little as 5 and 13 minutes, respectively. The machine's size is relatively small, measuring 20.7 cm width x 14.5 cm height x 19.4 cm depth, allowing for portability and therefore near patient testing.

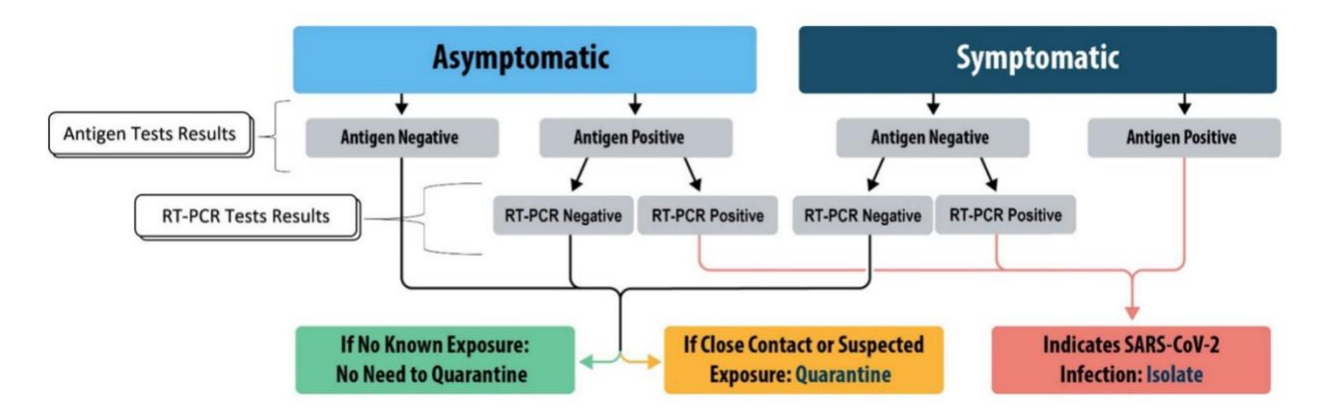


Figure 3.2: Antigen test decision matrix flowchart.

Flowchart describes courses of action during the SARS-CoV-2 pandemic if a symptomatic or asymptomatic patient has tested positive from a rapid antigen test.

The ID Now fits the criteria for POC, considering its portable frame and rapid nature. In addition to this, the machine takes direct patient samples (i.e., nasopharyngeal and oropharyngeal swabs) with little preparation time, rendering the total testing time much shorter than traditional amplification systems. The major concern with this device is the general lack of sensitivity found amongst various groups who conducted performance assessment studies, contradicting the claims of the manufacturer. Abbott announced very sensitive SARS-CoV-2 diagnostic results and an LoD of 125 genome equivalents/mL, however a machine performance assessment study conducted by Zhen et. al. (2020) [119] found that this was inaccurate by a factor of roughly 100, obtaining a value of 20,000 copies/mL. Basu et. al. (2020) [120] conducted separate sensitivity studies using the more time consuming Cepheid Xpert Xpress SARS-CoV-2 diagnostic assay as a reference test and found that while the ID Now had strong positive percent agreement (PPA) with the reference test at samples with high viral loads, the PPA was very poor at lower dilutions. This study also found the device to be highly specific, similar to the rapid antigen test, with a negative percent agreement (NPA) of 98.6%. A third study conducted by Smithgall et. al. [121] had explored the PPA of both of these devices against the Cobas Roche assay and found that the ID Now and Xpert Xpress had 73.9% and 98.9% PPA values, respectively. Evidently, the ID Now suffers from sensitivity issues similar to the rapid antigen test, and while it appears to be more capable at detecting lower viral loads, it should not be used as a singular test to rule out infection.

POC RT-PCR Test

The Cobas Liat is a POC device that conducts rapid RT-PCR in roughly 20 minutes, introducing a commonly used sensitive assay into the point of care. This device has shown very promising results through various studies, although there are concerns surrounding the validity of

the reported successful results. A study conducted by *Hansen et. al. (2021)* [122] reported excellent PPA and NPA values of 100% and 97.4%, respectively, with the reference Roche cobas 68/8800 SARS-CoV-2 test. Additionally, they found its LoD to be 0.012 median tissue culture infectious dose (TCID₅₀) per mL, which equates to roughly 48 RNA copies/mL. Several months later, *Blackall et. al. (2021)* [123] responded to an FDA issued alert concerning an alarming false positive rate among the Liat device tests with a study of their own. They reported false positive rates far higher than those denoted in the study by *Hansen et. al.*; however, they claimed that the utility and accessibility of the device provide benefits useful enough to outweigh the cons of this malfunction.

The Cobas Liat device is an important step in the direction of sensitive POC testing; however, there are numerous underlying issues to be improved upon. In addition to the large false positive rate, the Ct values of low viral load detection (>30) were larger than expected compared to other molecular assays [124], in turn creating an undesirable balance between testing time and sensitivity. The device itself is quite heavy for a small POC device, weighing 8.3 lbs, and comes with a relatively large power supply that can hinder its abilities concerning portability and functioning as a self-powered device [125]. Lastly, the device is only capable of analyzing one sample at a time, and therefore cannot run simultaneous controls to distinguish between false negative and true negative results.

3.3 Future of POC plasmonic qPCR

The POC concepts seen throughout the various technologies are all important characteristics that the POC plasmonic qPCR machine encompasses and attempts to further improve on. While the Cobas Liat is similar in function, the plasmonic device realized the importance of energy efficiency and true portability. The power consumption of the machine is

low enough to reduce the power supply size and is therefore truly transferable among any setting. The work within this thesis demonstrates its incredible speed, sensitivity, specificity, and utility in a wide range of applications. There are four channels within the machine for multiple clinical samples and/or internal controls, all kept within a light and 3-D printed frame.

The POC plasmonic qPCR is the future of point of care diagnostics. The emergence of the SARS-CoV-2 pandemic highlighted the great need for such devices, and a new era of highly precise and sensitive equipment used at the site of clinical care is well under way. Physicians will be able to provide more accurate care for a larger number of patients, and pandemics can be more easily contained with the ability to accurately test asymptomatic patients. Beyond the world of rapid diagnostics, this device proves to be a valuable research tool that can cut amplification time and improve result generation efficiency within laboratories. The POC plasmonic qPCR is an ideal point of care device for the future of diagnostic medicine, and it will do the community a large and impactful service.

References

- 1. The History of PCR (RU 9577). 2004 [cited 2021 May 15]; Available from: http://siarchives.si.edu/research/videohistory_catalog9577.html.
- 2. Mo, Y., *Probing the nature of hydrogen bonds in DNA base pairs.* J Mol Model, 2006. **12**(5): p. 665-72.
- 3. Crick, F., Central dogma of molecular biology. Nature, 1970. **227**(5258): p. 561-3.
- 4. Sinden, R.R., DNA Structure and Function. 1994: Gulf Professional Publishing.
- 5. Brock, T.D. and H. Freeze, *Thermus aquaticus gen. n. and sp. n., a nonsporulating extreme thermophile.* J Bacteriol, 1969. **98**(1): p. 289-97.
- 6. Chien, A., D.B. Edgar, and J.M. Trela, *Deoxyribonucleic acid polymerase from the extreme thermophile Thermus aquaticus*. J Bacteriol, 1976. **127**(3): p. 1550-7.
- 7. Saiki, R.K., et al., *Primer-directed enzymatic amplification of DNA with a thermostable DNA polymerase.* Science, 1988. **239**(4839): p. 487-91.
- 8. Dias, N. and C.A. Stein, *Antisense oligonucleotides: basic concepts and mechanisms.* Mol Cancer Ther, 2002. **1**(5): p. 347-55.
- 9. Garibyan, L. and N. Avashia, *Polymerase chain reaction*. J Invest Dermatol, 2013. **133**(3): p. 1-4.
- 10. Lorenz, T.C., *Polymerase chain reaction: basic protocol plus troubleshooting and optimization strategies.* J Vis Exp, 2012(63): p. e3998.
- 11. Goldberg, A. *A Brief History of PCR and Its Derivatives*. 2019; Available from: https://blog.labtag.com/a-brief-history-of-pcr-and-its-derivatives/.
- 12. Rychlik, W., W.J. Spencer, and R.E. Rhoads, *Optimization of the annealing temperature* for DNA amplification in vitro. Nucleic Acids Res, 1990. **18**(21): p. 6409-12.
- 13. Blaber, M. *Polymerase Chain Reaction (PCR) and Cloning of PCR Products*. 2021 [cited 2021 12-27-2021]; Available from:

 <a href="https://bio.libretexts.org/Bookshelves/Biochemistry/Supplemental Modules (Biochemistry)/3. Biotechnology 1/3.3%3A Polymerase Chain Reaction (PCR) and Cloning of PCR Products.
- 14. Khalsa, G. *PCR* (polymerase chain reaction). ASU Ask A Biologist 2010; Available from: https://askabiologist.asu.edu/pcr-polymerase-chain-reaction.
- 15. Haddad, F. and K.M. Baldwin, *Reverse transcription of the ribonucleic acid: the first step in RT-PCR assay.* Methods Mol Biol, 2010. **630**: p. 261-70.
- 17. Qiu, X. and J. Yuan, *Temperature control for PCR thermocyclers based on peltier-effect thermoelectric.* Conf Proc IEEE Eng Med Biol Soc, 2005. **2005**: p. 7509-12.

- 18. Weier, H.U. and J.W. Gray, *A programmable system to perform the polymerase chain reaction*. DNA, 1988. **7**(6): p. 441-7.
- 19. Ashcroft, N.W. and N.D. Mermin, *Solid State Physics*. 1976, Saunders College, Philadelphia.
- 20. Uchida, K.I., et al., *Observation of anisotropic magneto-Peltier effect in nickel.* Nature, 2018. **558**(7708): p. 95-99.
- 21. Kondepudi, D. and I. Prigogine, *Modern Thermodynamics: From Heat Engines to Dissipative Structures*. 1998, Chichester: Wiley.
- 22. Kryndushkin, D.S., et al., *Yeast [PSI+] prion aggregates are formed by small Sup35 polymers fragmented by Hsp104*. J Biol Chem, 2003. **278**(49): p. 49636-43.
- 23. Borst, P., *Ethidium DNA agarose gel electrophoresis: how it started.* IUBMB Life, 2005. **57**(11): p. 745-7.
- 24. Sabnis, R.W., *Handbook of Biological Dyes and Stains: Synthesis and Industrial Application*. 2010: Wiley.
- 25. P. Quillardet, M.H., *Ethidium bromide and safety readers suggest alternative solutions.* Trends in Genetics, 1988: p. 89-90.
- 26. Tran, N.A.M., *Universal Point of Care Biosensor using Ultrafast Plasmonic Polymerase Chain Reaction*, in *Department of Electrical Engineering*. 2018, McGill University.
- 27. Bastien, P., G.W. Procop, and U. Reischl, *Quantitative real-time PCR is not more sensitive than "conventional" PCR.* J Clin Microbiol, 2008. **46**(6): p. 1897-900.
- 28. Dragan, A.I., et al., *SYBR Green I: fluorescence properties and interaction with DNA*. J Fluoresc, 2012. **22**(4): p. 1189-99.
- 29. Cosa, G., et al., *Photophysical properties of fluorescent DNA-dyes bound to single- and double-stranded DNA in aqueous buffered solution.* Photochem Photobiol, 2001. **73**(6): p. 585-99.
- 30. Wittwer, C.T., et al., *Continuous fluorescence monitoring of rapid cycle DNA amplification*. Biotechniques, 1997. **22**(1): p. 130-1, 134-8.
- 31. Brunstein, J. *Interpretation of qPCR curve shapes*. 2015 [cited 2021 21 December]; Available from: https://www.mlo-online.com/home/article/13008268/interpretation-of-qpcr-curve-shapes.
- 32. *qPCR Checklist: Steps to Better Results*. 2017 [cited 2021 Dec 21]; Available from: https://www.biocompare.com/Bench-Tips/343854-qPCR-Checklist-Steps-to-Better-Results/.
- 33. Jansson, L. and J. Hedman, *Challenging the proposed causes of the PCR plateau phase.* Biomol Detect Quantif, 2019. **17**: p. 100082.
- 34. TaqMan vs. SYBR Chemistry for Real-Time PCR. Available from: https://www.thermofisher.com/ca/en/home/life-science/pcr/real-time-pcr/real-time-pcr/real-time-pcr-basics/taqman-vs-sybr-chemistry-real-time-pcr.html.
- 35. Tajadini, M., M. Panjehpour, and S.H. Javanmard, *Comparison of SYBR Green and TaqMan methods in quantitative real-time polymerase chain reaction analysis of four adenosine receptor subtypes.* Adv Biomed Res, 2014. **3**: p. 85.
- 36. Spiess, A.N., C. Feig, and C. Ritz, *Highly accurate sigmoidal fitting of real-time PCR data by introducing a parameter for asymmetry.* BMC Bioinformatics, 2008. **9**: p. 221.

- 37. Olson, N.D. and J.B. Morrow, *DNA extract characterization process for microbial detection methods development and validation*. BMC Res Notes, 2012. **5**: p. 668.
- 38. Hilario, E.C., et al., *An Improved Method of Predicting Extinction Coefficients for the Determination of Protein Concentration*. PDA J Pharm Sci Technol, 2017. **71**(2): p. 127-135.
- 39. Hsieh, H.B. and M.A. Kneissl, *LED or laser enabled real-time PCR system and spectrophotometer*, USPTO, Editor. 2006, Palo Altho Research Center Inc: United States. p. 13.
- 40. Fakruddin, M., et al., *Nucleic acid amplification: Alternative methods of polymerase chain reaction.* J Pharm Bioallied Sci, 2013. **5**(4): p. 245-52.
- 41. Notomi, T., et al., *Loop-mediated isothermal amplification of DNA*. Nucleic Acids Res, 2000. **28**(12): p. E63.
- 42. Nagamine, K., T. Hase, and T. Notomi, *Accelerated reaction by loop-mediated isothermal amplification using loop primers*. Mol Cell Probes, 2002. **16**(3): p. 223-9.
- 43. Keikha, M., *LAMP Method as One of the Best Candidates for Replacing with PCR Method.* Malays J Med Sci, 2018. **25**(1): p. 121-123.
- 44. An, L., et al., Characterization of a thermostable UvrD helicase and its participation in helicase-dependent amplification. J Biol Chem, 2005. **280**(32): p. 28952-8.
- 45. Vincent, M., Y. Xu, and H. Kong, *Helicase-dependent isothermal DNA amplification*. EMBO Rep, 2004. **5**(8): p. 795-800.
- 46. Jeong, Y.J., K. Park, and D.E. Kim, *Isothermal DNA amplification in vitro: the helicase-dependent amplification system.* Cell Mol Life Sci, 2009. **66**(20): p. 3325-36.
- 47. Zhang, D.Y., et al., *Amplification of target-specific, ligation-dependent circular probe.* Gene, 1998. **211**(2): p. 277-85.
- 48. Beals, T.P., et al., A mechanism for ramified rolling circle amplification. BMC Mol Biol, 2010. **11**: p. 94.
- 49. Hsuih, T.C., et al., *Novel, ligation-dependent PCR assay for detection of hepatitis C in serum.* J Clin Microbiol, 1996. **34**(3): p. 501-7.
- 50. Barany, F., Genetic disease detection and DNA amplification using cloned thermostable ligase. Proc Natl Acad Sci U S A, 1991. **88**(1): p. 189-93.
- 51. Wiedmann, M., et al., *Ligase chain reaction (LCR)--overview and applications*. PCR Methods Appl, 1994. **3**(4): p. S51-64.
- 52. Armbruster, D.A. and T. Pry, *Limit of blank, limit of detection and limit of quantitation.* Clin Biochem Rev, 2008. **29 Suppl 1**: p. S49-52.
- 53. Protocols for Determination of Limits of Detection and Limits of Quantitation, Approved Guideline. CLSI document EP17. 2004, Wayne, PA USA: Clinical and Laboratory Standards Institute.
- 54. Forootan, A., et al., *Methods to determine limit of detection and limit of quantification in quantitative real-time PCR (qPCR)*. Biomol Detect Quantif, 2017. **12**: p. 1-6.
- 55. Theodorsson, E., *Limit of detection, limit of quantification and limit of blank*. European Federation of Clinical Chemistry and Laboratory Medicine.
- 56. Fung, B., et al., *Direct Comparison of SARS-CoV-2 Analytical Limits of Detection across Seven Molecular Assays.* J Clin Microbiol, 2020. **58**(9).

- 57. Alvarez, M.J., et al., *Model based analysis of real-time PCR data from DNA binding dye protocols.* BMC Bioinformatics, 2007. **8**: p. 85.
- 58. Lalam, N., *Estimation of the reaction efficiency in polymerase chain reaction.* J Theor Biol, 2006. **242**(4): p. 947-53.
- 59. Svec, D., et al., How good is a PCR efficiency estimate: Recommendations for precise and robust qPCR efficiency assessments. Biomol Detect Quantif, 2015. **3**: p. 9-16.
- 60. Amplification Efficiency of TaqMan Gene Expression Assays. 2006: Applied Biosystems.
- 61. Generating Standard Curve to analyse the reaction optimization Real Time qPCR, Calculating PCR Efficiency. 2012, Bio-Resource: Technology in Science.
- 62. Ramesh Raghavachari, W.T., *Genomics and Proteomics Technologies (Proceedings of Spie)*. 2001: Society of Photo Optical.
- 63. Evrard, A., N. Boulle, and G.s. Lutfalla, *Nanoscience: Nanobiotechnology and Nanobiology*, ed. P. Boisseau and M. Lahmani. 2009: Springer Science & Business Media.
- 64. Parikh, R., et al., *Understanding and using sensitivity, specificity and predictive values.* Indian J Ophthalmol, 2008. **56**(1): p. 45-50.
- 65. Trevethan, R., Sensitivity, Specificity, and Predictive Values: Foundations, Pliabilities, and Pitfalls in Research and Practice. Front Public Health, 2017. **5**: p. 307.
- 66. Halliday, D., R. Resnick, and J. Walker, *Fundamentals of Physics part 2*. 7 ed. 2005: John Wiley & Sons Ltd.
- 67. Huang, X., S. Neretina, and M.A. El-Sayed, *Gold nanorods: from synthesis and properties to biological and biomedical applications*. Adv Mater, 2009. **21**(48): p. 4880-4910.
- 68. Kelly, K.L., et al., The Journal of Physical Chemistry B, 2003. **107**(3): p. 668-677.
- 69. Homola, J., S.S. Yee, and G. Gauglitz, *Surface plasmon resonance sensors: review.* Sensors and Actuators B: Chemical, 1999. **54**(1-2): p. 3-15.
- 70. Nguyen, H.H., et al., *Surface plasmon resonance: a versatile technique for biosensor applications.* Sensors (Basel), 2015. **15**(5): p. 10481-510.
- 71. Willets, K.A. and R.P. Van Duyne, *Localized surface plasmon resonance spectroscopy and sensing*. Annu Rev Phys Chem, 2007. **58**: p. 267-97.
- 72. Rao, W., et al., *Comparison of photoluminescence quantum yield of single gold nanobipyramids and gold nanorods.* ACS Nano, 2015. **9**(3): p. 2783-91.
- 73. Kim, M., J.H. Lee, and J.M. Nam, *Plasmonic Photothermal Nanoparticles for Biomedical Applications*. Adv Sci (Weinh), 2019. **6**(17): p. 1900471.
- 74. Link, S. and M.A. El-Sayed, *Shape and Size Dependence of Radiative, Non-Radiative and Photothermal Properties of Gold Nanocrystals.* International Reviews in Physical Chemistry, 2000. **19**(3): p. 409-453.
- 75. Amendola, V., et al., *Surface plasmon resonance in gold nanoparticles: a review.* J Phys Condens Matter, 2017. **29**(20): p. 203002.
- 76. Polo, E., et al., *Colloidal bioplasmonics*. nanotoday, 2018. **20**: p. 58-73.
- 77. Kim, M., et al., Dealloyed Intra-Nanogap Particles with Highly Robust, Quantifiable Surface-Enhanced Raman Scattering Signals for Biosensing and Bioimaging Applications. ACS Cent Sci, 2018. **4**(2): p. 277-287.
- 78. Lim, D.K., et al., *Highly uniform and reproducible surface-enhanced Raman scattering from DNA-tailorable nanoparticles with 1-nm interior gap.* Nat Nanotechnol, 2011. **6**(7): p. 452-60.

- 79. Puchkova, A., et al., *DNA Origami Nanoantennas with over 5000-fold Fluorescence Enhancement and Single-Molecule Detection at 25 muM.* Nano Lett, 2015. **15**(12): p. 8354-9.
- 80. Ament, I., et al., Single unlabeled protein detection on individual plasmonic nanoparticles. Nano Lett, 2012. **12**(2): p. 1092-5.
- 81. Cole, L.E., et al., *Gold nanoparticles as contrast agents in x-ray imaging and computed tomography.* Nanomedicine (Lond), 2015. **10**(2): p. 321-41.
- 82. Qiu, L., et al., Single Gold Nanorod Detection Using Confocal Light Absorption and Scattering Spectroscopy. IEEE Journal of Selected Topics in Quantum Electronics, 2007. **13**(6): p. 1730-1738.
- 83. Baffou, G., *GOLD NANOPARTICLES as nanosources of heat.* Photonic Devices and Applications, 2018: p. 42-47.
- 84. Evenhuis, C.J. and P.R. Haddad, *Joule heating effects and the experimental determination of temperature during CE.* Electrophoresis, 2009. **30**(5): p. 897-909.
- 85. Jain, P.K., et al., *Calculated absorption and scattering properties of gold nanoparticles of different size, shape, and composition: applications in biological imaging and biomedicine.* J Phys Chem B, 2006. **110**(14): p. 7238-48.
- 86. Mohammadyousef, P., et al., *Plasmonic and label-free real-time quantitative PCR for point-of-care diagnostics*. Analyst, 2021. **146**(18): p. 5619-5630.
- 87. Huhmer, A.F. and J.P. Landers, *Noncontact infrared-mediated thermocycling for effective polymerase chain reaction amplification of DNA in nanoliter volumes.* Anal Chem, 2000. **72**(21): p. 5507-12.
- 88. Pak, N., et al., *Plug-and-play, infrared, laser-mediated PCR in a microfluidic chip.* Biomed Microdevices, 2012. **14**(2): p. 427-33.
- 89. Jia, J., et al., *Graphene enhances the specificity of the polymerase chain reaction*. Small, 2012. **8**(13): p. 2011-5.
- 90. Rehman, A., et al., *Metal Nanoparticles Assisted Polymerase Chain Reaction for Strain Typing of Salmonella Typhi*. Royal Society of Chemistry, 2010.
- 91. Tong, W., et al., Enhancing the specificity and efficiency of polymerase chain reaction using polyethyleneimine-based derivatives and hybrid nanocomposites. Int J Nanomedicine, 2012. **7**: p. 1069-78.
- 92. Li, H., et al., *Nanoparticle PCR: nanogold-assisted PCR with enhanced specificity.* Angew Chem Int Ed Engl, 2005. **44**(32): p. 5100-3.
- 93. Li, M., et al., Enhancing the efficiency of a PCR using gold nanoparticles. Nucleiv Acids Research, 2005. **33**: p. 10.
- 94. Roche, P.J., et al., *Demonstration of a plasmonic thermocycler for the amplification of human androgen receptor DNA*. Analyst, 2012. **137**(19): p. 4475-81.
- 95. Kim, J., et al., *Gold Nanorod-based Photo-PCR System for One-Step, Rapid Detection of Bacteria.* Nanotheranostics, 2017. **1**(2): p. 178-185.
- 96. Roche, P.J.R., et al., *Real time plasmonic qPCR: how fast is ultra-fast? 30 cycles in 54 seconds.* Analyst, 2017. **142**(10): p. 1746-1755.
- 97. Son, J.H., et al., *Ultrafast photonic PCR*. Light: Science & Applications, 2015. **4**(7): p. e280-e280.
- 98. Son, J.H., et al., *Rapid Optical Cavity PCR*. Adv Healthc Mater, 2016. **5**(1): p. 167-74.

- 99. Fair, R.J. and Y. Tor, *Antibiotics and bacterial resistance in the 21st century.* Perspect Medicin Chem, 2014. **6**: p. 25-64.
- 100. Doron, S. and L.E. Davidson, *Antimicrobial stewardship*. Mayo Clin Proc, 2011. **86**(11): p. 1113-23.
- 101. Trifiro, M., A. Kirk, and M. Paliouras, *Plasmonic PCR The Next Generation in Point-of-Care Diagnostics*. 2017, GenomeCanada, GenomeQuébec. p. 59.
- 102. Gudnason, H., et al., Comparison of multiple DNA dyes for real-time PCR: effects of dye concentration and sequence composition on DNA amplification and melting temperature. Nucleic Acids Res, 2007. **35**(19): p. e127.
- 103. Eischeid, A.C., *SYTO dyes and EvaGreen outperform SYBR Green in real-time PCR.* BMC Res Notes, 2011. **4**: p. 263.
- 104. STYO 16 Green Fluorescent Nucleic Acid Stain 1 mM Solution in DMSO. Available from:

 https://www.thermofisher.com/order/catalog/product/S7578?ef_id=CjwKCAiAsYyRBhA
 CEiwAkJFKovBrgcPySCCJ1cdQJ0SSdA1z93NSW3ETAPjYFW344XYuZkeDoY3h4xoC KcQAv
 D_BwE:G:s&s_kwcid=AL!3652!3!447292198730!!!g!!&cid=bid_pca_iva_r01_co_cp1359
 pjt0000_bid00000_0se_gaw_dy_pur_con&gclid=CjwKCAiAsYyRBhACEiwAkJFKovBrgcPy
 SCCJ1cdQJ0SSdA1z93NSW3ETAPjYFW344XYuZkeDoY3h4xoC KcQAvD_BwE.
- 105. Chazotte, B., *Labeling nuclear DNA using DAPI*. Cold Spring Harb Protoc, 2011. **2011**(1): p. pdb prot5556.
- 106. Quyen, T.L., et al., Classification of Multiple DNA Dyes Based on Inhibition Effects on Real-Time Loop-Mediated Isothermal Amplification (LAMP): Prospect for Point of Care Setting. Front Microbiol, 2019. **10**: p. 2234.
- 107. Noimark, S., et al., Comparative study of singlet oxygen production by photosensitiser dyes encapsulated in silicone: towards rational design of anti-microbial surfaces. Phys Chem Chem Phys, 2016. **18**(40): p. 28101-28109.
- 108. Dirks, J.A., et al., *Chlamydia trachomatis load in population-based screening and STI-clinics: implications for screening policy*. PLoS One, 2015. **10**(3): p. e0121433.
- 109. Nichols, J.H., *Point of care testing*. Clin Lab Med, 2007. **27**(4): p. 893-908, viii.
- 110. FDA. Coronavirus (COVID-19) Update: FDA Issues first Emergency Use Authorization for Point of Care Diagnostic. 2020; Available from: https://www.fda.gov/news-events/press-announcements/coronavirus-covid-19-update-fda-issues-first-emergency-use-authorization-point-care-diagnostic.
- 111. FDA. *In Vitro Diagnostics EUAs Antigen Diagnostic Tests for SARS-CoV-2*. 2020; Available from: https://www.fda.gov/medical-devices/coronavirus-disease-2019-covid-19-emergency-use-authorizations-medical-devices/in-vitro-diagnostics-euas-antigen-diagnostic-tests-sars-cov-2.
- 112. De Marinis, Y., et al., *Detection of SARS-CoV-2 by rapid antigen tests on saliva in hospitalized patients with COVID-19.* Infect Ecol Epidemiol, 2021. **11**(1): p. 1993535.
- 113. Jegerlehner, S., et al., *Diagnostic accuracy of a SARS-CoV-2 rapid antigen test in real-life clinical settings.* Int J Infect Dis, 2021. **109**: p. 118-122.
- 114. *Understanding COVID-19 Antigen Tests*. 2021: National Collaborating Centre for Infectious Diseases. p. 4.
- 115. Lee, W.C., Selecting diagnostic tests for ruling out or ruling in disease: the use of the Kullback-Leibler distance. Int J Epidemiol, 1999. **28**(3): p. 521-5.

- 116. Arnaout, R., et al., SARS-CoV2 Testing: The Limit of Detection Matters. bioRxiv, 2020.
- 117. CDC. CDC. Interim Guidance for Antigen Testing for SARS-CoV-2. Centers Dis Control Prev. 2020; Available from: https://www.cdc.gov/coronavirus/2019-ncov/lab/resources/antigen-tests-guidelines.html
- 118. *ID NOW COVID-19*. 2020; Available from: https://www.globalpointofcare.abbott/en/product-details/id-now-covid-19.html.
- 119. Zhen, W., et al., Clinical Evaluation of Three Sample-to-Answer Platforms for Detection of SARS-CoV-2. J Clin Microbiol, 2020. **58**(8).
- 120. Basu, A., et al., Performance of Abbott ID Now COVID-19 Rapid Nucleic Acid Amplification Test Using Nasopharyngeal Swabs Transported in Viral Transport Media and Dry Nasal Swabs in a New York City Academic Institution. J Clin Microbiol, 2020. 58(8).
- 121. Smithgall, M.C., et al., *Comparison of Cepheid Xpert Xpress and Abbott ID Now to Roche cobas for the Rapid Detection of SARS-CoV-2.* J Clin Virol, 2020. **128**: p. 104428.
- 122. Hansen, G., et al., Clinical Performance of the Point-of-Care cobas Liat for Detection of SARS-CoV-2 in 20 Minutes: a Multicenter Study. J Clin Microbiol, 2021. **59**(2).
- 123. Blackall, D., et al., Performance Characteristics of the Roche Diagnostics cobas Liat PCR System as a COVID-19 Screening Tool for Hospital Admissions in a Regional Health Care Delivery System. J Clin Microbiol, 2021. **59**(10): p. e0127821.
- 124. Akashi, Y., et al., Clinical Performance of the cobas Liat SARS-CoV-2 & Influenza AB for the Detection of SARS-CoV-2 in Nasal Samples. medRxiv, 2022.
- 125. cobas Liat system Operator's Manual. Vol. 7.2. 2017, Roche.

Appendix I

```
import numpy as np
import pandas as pd
from matplotlib import pyplot as plt
from numpy import arange
from scipy.optimize import curve_fit
#Variable Toggles
page = 'Sheet1'
df = pd.read_excel("Data.xlsx", page)
number_of_datasets = 5
curve_fit_toggle = 1
scatterplot_toggle = 1
ct\_toggle = 1
efficiency_toggle = 0
normalize_by_division = 0
normalize_by_subtraction = 1
# Plot Design
line\_width = 4
scatter_dot_size = 25
ct_line_width = 2
x_fontsize = 16
y_fontsize = 16
title_fontsize = 16
legend_fontsize = 12
# Initialized Variables
x = df.iloc[:, 0]
avg\_tot = 0
avg\_final\_tot = 0
c1 = 0
dilution = 1 \\
Lx = len(x)
list1 = [] * Lx
list2 = [] * Lx
x_list = [] * Lx
y_list = [] * Lx
list3 = [] * Lx
list4 = [] * Lx
list5 = [] * Lx
list6 = [] * Lx
list9 = [] * number_of_datasets
list10 = [] * number_of_datasets
# Functions
def sigmoid(x, L, x0, k, b, f):
  y = b + ((L-b)/(1+np.exp(-k*(x-x0)))**f)
  return y
def NTC(x, a, b):
  y = (a^*x)+b
  return y
def second_deriv(x, L, x0, k, b, f):
  y = (f^*(b-L)^*(k^{**}2)^*(np.exp(k^*(x-x0))-f)) \ / \ (((np.exp(-k^*(x-x0))+1)^{**}f)^*((np.exp(k^*(x-x0))+1)^{**}2))
  return y
```

```
def slope(y2, y1, x2, x1):
        a = (y2 - y1) / (x2 - x1)
        return a
def horiz(x, y, a):
        h = (-y + (a^*x))/a
        return h
def tangent(x, h, a):
       y = a^*(x-h)
        return y
def ct_calc(y, h, a):
        x = (y/a)+h
        return x
def line(x, b):
       y = (0^*x) + b
        return y
def efficiency(a_eff):
        rho = ((10 ** (-1/a_eff)) - 1) * 100
        return rho
def efficiency_line(x, a, b):
       y = (a^*x) + b
        return y
# Code Body
for d in range(1, number_of_datasets+1):
       x = df.iloc[0:Lx, 0]
        df.iloc[0:Lx, d] = df.iloc[0:Lx, d].fillna(0)
       for i in range(0, Lx):
                if df.iloc[i, d] == 0:
                        df.iloc[i, d] = df.iloc[(i-1), d]
                else:
                        continue
        stdev_tot = df.iloc[0:6, d].std()
       for i in range(0, 6):
                avg\_tot = avg\_tot + abs((df.iloc[i, d]))
       avg\_tot = avg\_tot/6
       for i in range(0, 6):
                if \; ((abs(df.iloc[i,\;d])) > (avg\_tot + (2 * stdev\_tot))) \; | \; ((abs(df.iloc[i,\;d])) < (avg\_tot - (2 * stdev\_tot))) : \; | \; ((abs(df.iloc[i,\;d])) < (avg\_tot - (2 * stdev\_tot))) : \; | \; ((abs(df.iloc[i,\;d])) < (avg\_tot - (2 * stdev\_tot))) : \; | \; ((abs(df.iloc[i,\;d])) < (avg\_tot - (2 * stdev\_tot))) : \; | \; ((abs(df.iloc[i,\;d])) < (avg\_tot - (2 * stdev\_tot))) : \; | \; ((abs(df.iloc[i,\;d])) < (avg\_tot - (2 * stdev\_tot))) : \; | \; ((abs(df.iloc[i,\;d])) < (avg\_tot - (2 * stdev\_tot))) : \; | \; ((abs(df.iloc[i,\;d])) < (avg\_tot - (2 * stdev\_tot))) : \; | \; ((abs(df.iloc[i,\;d])) < (avg\_tot - (2 * stdev\_tot))) : \; | \; ((abs(df.iloc[i,\;d])) < (avg\_tot - (2 * stdev\_tot))) : \; | \; ((abs(df.iloc[i,\;d])) < (avg\_tot - (2 * stdev\_tot))) : \; | \; ((abs(df.iloc[i,\;d])) < (avg\_tot - (2 * stdev\_tot))) : \; | \; ((abs(df.iloc[i,\;d])) < (avg\_tot - (2 * stdev\_tot))) : \; | \; ((abs(df.iloc[i,\;d])) < (avg\_tot - (2 * stdev\_tot))) : \; | \; ((abs(df.iloc[i,\;d])) < (avg\_tot - (2 * stdev\_tot))) : \; | \; ((abs(df.iloc[i,\;d])) < (avg\_tot - (2 * stdev\_tot))) : \; | \; ((abs(df.iloc[i,\;d])) < (avg\_tot - (2 * stdev\_tot))) : \; | \; ((abs(df.iloc[i,\;d])) < (avg\_tot - (2 * stdev\_tot))) : \; | \; ((abs(df.iloc[i,\;d])) < (avg\_tot - (2 * stdev\_tot))) : \; | \; ((abs(df.iloc[i,\;d])) < (avg\_tot - (2 * stdev\_tot))) : \; | \; ((abs(df.iloc[i,\;d])) < (avg\_tot - (2 * stdev\_tot)) : \; | \; ((abs(df.iloc[i,\;d])) < (avg\_tot - (2 * stdev\_tot)) : \; | \; ((abs(df.iloc[i,\;d])) < (avg\_tot - (2 * stdev\_tot)) : \; | \; ((abs(df.iloc[i,\;d])) < (avg\_tot - (2 * stdev\_tot)) : \; | \; ((abs(df.iloc[i,\;d])) < (avg\_tot - (2 * stdev\_tot)) : \; | \; ((abs(df.iloc[i,\;d])) < (avg\_tot - (2 * stdev\_tot)) : \; | \; ((abs(df.iloc[i,\;d])) < (avg\_tot - (2 * stdev\_tot)) : \; | \; ((abs(df.iloc[i,\;d])) < (avg\_tot - (2 * stdev\_tot)) : \; | \; ((abs(df.iloc[i,\;d])) < (avg\_tot - (2 * stdev\_tot)) : \; | \; ((abs(df.iloc[i,\;d])) < (avg\_tot - (2 * stdev\_tot)) : \; | \; ((abs(df.iloc[i,\;d])) < (avg\_tot - (2 * stdev\_tot)) : \; | \; ((abs(df.iloc[i,\;d])) < (avg\_tot - (2 * stdev\_tot)) : \; | \; ((abs(df.iloc[i,\;d])) < (avg\_tot - (2 * 
                        avg\_final\_tot = ((avg\_tot * (6-c1)) - abs(df.iloc[i, d])) / (6 - (c1+1))
                        c1 = c1 + 1
                else:
                        continue
        if avg_final_tot == 0:
                avg\_final\_tot = avg\_tot
        df.iloc[0, d] = avg_final_tot
```

```
if normalize_by_division:
  for i in range(0, Lx):
     df.iloc[i, d] = abs(df.iloc[i, d]) / avg_final_tot
if normalize_by_subtraction:
  for i in range(0, Lx):
     df.iloc[i, d] = abs(df.iloc[i, d]) - (avg_final_tot - 1)
y = df.iloc[0:Lx, d]
if d == 1:
  p0 = [max(y), np.median(x), 1, min(y), 1]
  popt, _ = curve_fit(sigmoid, x, y, p0, method='dogbox')
  L, x0_tot, k, b, f = popt
p0\_tot = [max(y), np.median(x), 1, min(y), 1]
if (y[Lx-1] > (3+y[0])):
  popt_tot, _ = curve_fit(sigmoid, x, y, p0_tot, method='dogbox')
else:
  popt_ntc, _ = curve_fit(NTC, x, y)
  a_ntc, b_ntc = popt_ntc
  x_{ine} = arange(np.min(x), np.max(x)+1, 1)
  y_line_ntc = NTC(x_line_ntc, a_ntc, b_ntc)
  list1.append(x_line_ntc)
  list2.append(y_line_ntc)
L\_tot, \ x0\_tot, \ k\_tot, \ b\_tot, \ f\_tot = popt\_tot
x_{line} = arange(np.min(x), np.max(x)+1, 1)
y_line = sigmoid(x_line, L_tot, x0_tot, k_tot, b_tot, f_tot)
subtract_factor = y_line[0] - 1
y_line = y_line-subtract_factor
y = y - subtract_factor
if (y[Lx-1] > (3+y[0])):
  list1.append(x line)
  list2.append(y_line)
x_list.append(x)
y_list.append(y)
avg\_tot = 0
avg_final_tot = 0
c1 = 0
linear_points_tot = [] * Lx
breaker\_tot = 0
# R^2 Value - Sigmoidal Curve Matching
y_line_shift = sigmoid(x_line, L, x0, k_tot, b_tot)
residuals_tot = y_line_shift - sigmoid(x, L, x0, k, b)
ss_res = np.sum(residuals_tot ** 2)
ss_tot = np.sum((y_line_shift - np.mean(y_line_shift)) ** 2)
r_squared = round(1 - (ss_res / ss_tot), 5)
if r_squared < 0:</pre>
```

```
r_squared = 0
   # Ct Value Calculation
  if ct_toggle & (y[Lx-1] > (3+y[0])):
     for i in range(1, Lx+1):
        if breaker_tot == 1:
          break
        second\_d\_tot = second\_deriv(x\_line[i], L\_tot, x0\_tot, k\_tot, b\_tot, f\_tot)
        if float(second_d_tot) < 0:</pre>
          linear_points_tot.append(i-1)
          linear_points_tot.append(i)
          linear_points_tot.append(i+1)
          breaker_tot += 1
        else:
          continue
     count_tot = len(linear_points_tot)
     slope_tot = slope(y_line[linear_points_tot[count_tot-2]], y_line[linear_points_tot[0]-1],
                 linear_points_tot[count_tot-1], linear_points_tot[0])
     horiz_shift_tot = horiz(linear_points_tot[0], y_line[(linear_points_tot[0]-1)], slope_tot)
     x\_tangent\_tot = arange(np.min(horiz\_shift\_tot), \ np.max(linear\_points\_tot[count\_tot-1]) + 1, \ 1)
     y_tangent_tot = tangent(x_tangent_tot, horiz_shift_tot, slope_tot)
     list3.append(x_tangent_tot)
     list4.append(y_tangent_tot)
     ct_tot = round(ct_calc(y_line[0], horiz_shift_tot, slope_tot), 2)
     y_{ine} grapher: int = line(x_{ine}, 1)
   # PCR Efficiency Calculation
  if efficiency_toggle & (y[Lx-1] > (3+y[0])):
     if d == 1:
        fluo_point = round(y_line[linear_points_tot[2]], 3)
     for i in range(1, Lx+1):
        if y_line[i] > fluo_point:
          y1 = y_line[i-1]
          y2 = fluo_point
          y3 = y_{line[i]}
          x1 = i
          x3 = i+1
          break
     x2 = (((y2 - y1) * (x3 - x1)) / (y3 - y1)) + x1
     list9.append(np.log10(dilution))
     list10.append(x2)
     dilution = dilution/10
  # Data Plotting
for f in range(0, number_of_datasets):
  if curve_fit_toggle:
     plt.plot(list1[f],\ list2[f],\ linewidth=line\_width,\ label=df.columns[f+1])
  if scatterplot_toggle:
     plt.scatter(x_list[f], y_list[f], s=scatter_dot_size)
for e in range(0, len(list3)):
  if ct_toggle:
     plt.plot(list3[e], list4[e], '--', color='blue', linewidth=ct_line_width)
if ct_toggle:
  plt.plot(x_line, y_line_grapher, '--', color='blue', linewidth=ct_line_width)
```

```
plt.xlabel('Cycles', fontsize=x_fontsize)
plt.ylabel('Relative Fluorescence', fontsize=y_fontsize)
plt.title(page, fontsize=title_fontsize)
plt.legend(loc="right", fontsize=legend_fontsize)
plt.show()
\label{eq:condition}  \begin{tabular}{ll} \begin{tabular}{ll} if efficiency\_toggle & (y[Lx-1] > (3+y[0])): \\ popt\_eff, $\_= curve\_fit(efficiency\_line, \ list9, \ list10) \\ \end{tabular}
   a_eff, b_eff = popt_eff
   x_{line} = arange(np.min(list9), 1, 1)
  y_line_eff = efficiency_line(x_line_eff, a_eff, b_eff)
   plt.plot(list9, list10, linewidth=line_width)
plt.plot(x_line_eff, y_line_eff, '--', color = 'red')
   plt.xlabel('Log_10(Dilution Series)', fontsize=x_fontsize)
   plt.ylabel('Cycles', fontsize=y_fontsize)
   plt.title("Efficiency Standard Curve", fontsize=title_fontsize)
   print("slope", a_eff)
   print("Efficiency =", round(efficiency(a_eff),3), "%")
plt.show()
```